Plasma etch characteristics of nitrogen trifluoride gas mixtures.

NOTE TO USERS

Plasma Etch Characteristics of Nitrogen Trifluoride Gas Mixtures

A Dissertation
Presented to the Graduate Committee
of Lehigh University
in Candidacy for the Degree of
Doctor in Philosophy
In
Chemistry

by
John A. Barkanic

May 24, 2004
Lehigh University
Bethlehem, PA

Certificate of Approval

This dissertation is approved and recommended for acceptance in partial fulfillment of the requirements for the degree of Doctor of Philosophy.

APRIL 30, 2004
date

Professor in Charge

Accepted:

APRIL 30, 2004
date

Special Committee directing the doctoral work of John A. Barkanic

Chairman: Dr. James Roberts

Dr. Gary Simmons

Dr. Natalie Foster

Dr. Ralph J. Jaccodine

Acknowledgements

The pursuit of a PhD is a substantial undertaking. There is a commitment in time and energy required that very few could appreciate. I owe a debt of gratitude to those people who played an instrumental role in my pursuit of this honorable distinction.

I would like to thank Dr. James Roberts for the initial encouragement some eight years ago and his continued support throughout the entire degree. He played an inspirational role as a guidance counselor and represents one the best teachers I've had in my considerable tenure as a student. I also need to extend thanks to Dr. Ralph Jaccodine for his mentorial role. Over the last twenty years I've come to know Dr. Jaccodine as a giving individual. He has genuinely influenced my life as a result of his actions. I sincerely thank him for all he has done for me over the years.

Further, considerable involvement of other staff and faculty members at Lehigh University has been very much appreciated. The

support of Drs. Kraihanzel, Larsen, Foster, Simmons and Ferguson through the many technical challenges presented in the last eight years has been greatly appreciated. I thank Dr. Alfred Miller for his help with surface analysis science and the use of the XPS equipment and David Ackland for his help with the scanning electron microscope. In the Sherman Fairchild Laboratory, I owe thanks to Dr. Floyd Miller and Ray Filozof for their support in using the Integrated Circuit Laboratory.

I would like to sincerely thank Regina Mattai for being there. She is one of the very few people I confided in during my years of study. Finally, I would to thank my parents for their continued and unyielding support through any and all activities. Through this somewhat turbulent period of education and growth I have often drawn the confidence and strength to continue from their words. Their constancy and support have been a real inspiration in my life. Often, their encouragement is the only thing that kept me going. It is to them, my Mother and Father, that I dedicate this thesis.

Table of Contents

List of Tables

List of Figures

Abstract

Semiconductor manufacturing involves a complex series of sequential pattern transfer processes. The design rules needed to successfully manufacture advanced gigabit microdevices must include plasma processes with a high degree of etch anisotropy and high reaction selectivity of over-layered materials. Even with the continued tightening of anisotropy and selectivity requirements, little has been published regarding the interdependence of these important etch characteristics. The main objective of this research was to develop and define the parametric dependencies of silicon to silicon dioxide reaction selectivity and silicon etch anisotropy.

Plasma etching was investigated using NF_3 mixtures to generate a low-pressure reactive plasma. Nitrogen trifluoride was mixed with combinations of argon, CF_2Cl_2 or chlorine. Plasma pressure, power density and chemical composition were varied. Silicon and silicon dioxide reaction rates and silicon to silicon dioxide reaction selectivity were established. The etch anisotropy obtained from a patterning process was also investigated

For mixtures of NF_3 in argon, reaction selectivity was found to be highest under processing conditions that minimize cationic bombardment of the surfaces. Selectivity approaching 90:1 was obtained for a plasma of 25% NF_3 in argon at 250 watts power and 800 millitorr. Reaction selectivity was also found to be a function of concentration and pressure. Mixtures of NF_3, CF_2Cl_2 and argon were investigated. In general, silicon to silicon dioxide reaction selectivity was lower for gas mixtures containing CF_2Cl_2. The highest selectivity of 50:1 was obtained for conditions of low power and high pressure.

Anisotropy trends were established using mixtures of NF_3 in argon. Over the range of power and pressure investigated, anisotropic etch profiles in silicon could not be obtained. For mixtures of NF_3, CF_2Cl_2 and argon, the anisotropy improved as the degree of ion bombardment increased. Anisotropic profiles in etched silicon were obtained using 62% CF_2Cl_2, 25% NF_3 in argon at high power and low pressure. The use of a polymer forming chemistry with NF_3 provides a method for improving etch anisotropy while keeping the reaction selectivity at levels of approximately 20:1.

1. Introduction

1.1 Semiconductor Industry

Change in semiconductor device manufacturing is a result of many factors. The most prominent factor is the pursuit of higher levels of integration on a chip. Benefits include increased signal processing speed, more complex functional ability of the circuit and reduced material costs (1). The semiconductor industry's Technology Roadmap (2) was prepared to guide developmental activities industry-wide. The Roadmap contains suggestions for each technological area associated with the manufacturing process. Two important requirements outlined in the Technology Roadmap are addressed in this dissertation. Etch anisotropy and reaction selectivity are critical complementary parameters that must be balanced to achieve a successful pattern transfer. The main objective of this research is to better develop the corollaries between plasma chemistry, reaction selectivity and etch anisotropy.

An introduction to the current state of the industry is presented in Chapter 1. Aspects that impact plasma pattern transfer technology are reviewed. Issues that are likely to affect future trends are discussed. In Chapter 2, the current state of the literature is reviewed. The review covers approximately twenty-five years of developmental and scientific research in plasma processing of electronic materials. A description of the experimental protocol used for this investigation is presented in Chapter 3. The samples, preparation, experimental matrix, etch reactor and analytical equipment are described. In Chapter 4, the experimental findings are presented. Silicon and silicon dioxide etching and reaction selectivity are discussed in Chapter 4, Sections 4.1, 4.2 and 4.3. Anisotropy data are presented separately in Sections 4.4 and 4.5. Nitrogen trifluoride plasmas are discussed first and the effects of additives to the plasma are presented subsequently. Chapter 5 and 6 represent a statement of conclusions based on the work and an analysis of future research opportunities, respectively.

Regarding integration, Moore's Law (3) is most notable. The law was used to predict a doubling of device density, the number of transistors per square inch of integrated circuit, every year. The original prediction was made in the mid 1960's and was reasonably accurate through the early 1990's.

In recent years, the growth rate in component density has slowed. Moore (4) suggested that a more accurate growth rate would be a doubling of circuit density every eighteen months. Moore further suggested that the pace would continue to slow for successive generations of microprocessors. Plasma etching and pattern transfer technology are playing a large role in defining the geometric limitations of device technology.

A second industrial pursuit is realizing cost improvements using economy of scale (5). This economic theory equates the benefit of producing and selling larger volumes of product with the ability to provide the goods at a lower cost and price per unit.

The main motivation is to reduce the overall manufacturing cost, thereby reducing the product price and expanding market opportunities.

The upfront cost of integrated circuit research and development has skyrocketed over the past decade. An increase in production volume means the upfront costs can be amortized over more manufactured units. The amortized expenditure, when considered as a component of the total unit cost, is very low. The high cost of process development, along with the escalating cost of capital equipment, can only be afforded through economy of scale manufacturing.

To take advantage of economy of scale manufacturing, the focus of industrial research is on increasing the diameter of the silicon wafers (1). For example, a wafer with a 150 mm diameter has 177 cm^2 of surface area on which to build microchips. By doubling the silicon wafer diameter to 300 mm, the available area increases

by 300% to 707 cm^2. If yields are maintained constant, the increased surface area results in a substantial increase in manufacturing throughput. Intel, IBM and TMSC Corporation are among the first putting 300 mm wafers into production (6,7).

An additional driving force for change in process technology is yield enhancement. The impact of even a 1% increase in operating yield can be substantial. Assuming a plant has ten thousand 150 mm wafer starts per month, obtains a 35% yield of acceptable product and has a product price of $35.00 per 400 mm^2 die, a 1% increase in yield will increase revenue by $2 million.

Perhaps the industry's most formidable challenge is the escalating cost of building manufacturing capacity (8). The estimates for building a new facility to make 0.25-micron integrated circuits are about a $2 billion investment. The next generation device technology will likely use a 0.18-micron critical dimension, and it will cost over $3 billion to construct the plant. Considering

these initial costs, it will become increasingly important to use only high yield, high uniformity pattern transfer processes.

The environmental impact of the manufacturing process is the fourth issue driving technological change. A typical integrated circuit fabrication process can involve over 500 individual steps (9). The large number of processing steps requires the use of a wide variety of chemistry. Invariably, waste is produced. The chemicals used in the manufacturing process include acids, bases, solvents, metals, water and a host of reactive gaseous materials. Reducing the overall environmental impact of the processes is a main concern facing the industry today.

Any technology that provides a means to move toward higher integration, larger wafer diameter, increased yields or reduced environmental impact will be welcomed by semiconductor manufacturers.

1.2 Plasma Processing

Manufacturing a semiconductor microdevice requires a series of sequential steps whereby thin films of electronic material are deposited and patterned. The patterning process, using plasma chemistry, is the main area of interest in this research. Plasma or low-pressure gaseous discharge chemistry has found wide acceptance as a fabrication process for making microelectronic devices (10). The use of plasma chemistry is common for patterning a wide variety of electronic materials. One of the main driving forces associated with its use is the ability to define extremely small geometries. A pattern that is less than one micron in width can be reliably produced, with controlled shape and anisotropy, using plasma chemistry.

In a typical patterning application, electronic materials are layered as thin films on top of each other. Silicon on a thin film of silicon dioxide is a common device configuration. A masking material is used to define a region in the upper thin film of silicon

using subtractive pattern transfer. Etching proceeds on areas of silicon that are not protected by the mask. As the etching proceeds to completion, the under-lying thin film of silicon dioxide is exposed. Because etching proceeds non-uniformly across the surface of the wafer, some regions of the upper silicon film are completely removed before other regions. The etching process, at this point, must slow considerably so the under-lying SiO_2 film remains intact. In other words, reaction selectivity needs to be high for a successful process.

Although liquid etching chemistry has been used in the past, the industry has slowly displaced the technology (11,12). Pattern delineation using a buffered acid tends to undercut the pattern mask. Acid etching increases the line width or size of the patterned image and reduces the effective use of die area available for devices. This major drawback of liquid etching has made plasma processing the cornerstone for manufacturing advanced semiconductor integrated circuits.

Throughput increases have largely been accomplished by increasing the diameter of the silicon wafer (1). The use of larger diameter wafer technology has resulted in considerable challenges for plasma processing. There are two key processing areas that require substantial improvements: uniformity and reaction selectivity.

Uniformity of the process and reaction selectivity are complementary parameters. A balance in uniformity and selectivity is often required to obtain a successful high yield process. If a thin film to be patterned on the surface of a wafer were completely flat, without variation in thickness, the required reaction selectivity would be low. The selectivity is the ratio of reaction rates for different materials exposed to the plasma. For example, a one-micron thick film deposited with a uniformity of +/- 1% may be successfully patterned with plasma chemistry providing 2:1 reaction selectivity. However, if the film thickness is reduced to 0.1 micron and the uniformity of the film thickness is +/- 10%, the required reaction selectivity would need to be increased substantially. In this

case, a reaction selectivity of 20:1 may be needed to obtain a successful pattern transfer. As a result of the device technology requiring thinner films across larger areas, the plasma technologies of the future will need to have higher reaction selectivity and increased process uniformity (13).

Another method for increasing throughput in production is to reduce the time required for individual steps. A typical pattern transfer operation could take anywhere from 1 to 5 minutes per wafer (14). As a result, any increase in the reaction rate associated with a pattern transfer process is welcome. Plasma processes for the next generation of devices may need to be an order of magnitude faster (15). The reason for this is two fold. First, an increasing number of layers must be processed on a single wafer as a result of the increasing degree of integration. Second, the larger diameter wafers provide a larger loading effect in the chamber (16). The additional load substantially reduces the reaction rate of conventional plasma etch chemistry.

Plasma chemistry used in the future will be designed to increase good die yield (17). One mode of yield loss is poor uniformity and reaction selectivity. Another mode of yield loss is caused by contamination introduced into the process, such as particulate or metallic contamination.

The particle count in the work area has always been an issue in controlling contamination (18). Semiconductor manufacturers put forth considerable effort to reduce airborne particulate matter to extremely low levels. For example, a class 1 clean room is typically used for fabricating 1-megabit devices. Such an environment contains less than one particle of one-micrometer diameter per cubic feet of air. A room designed to meet these standards can cost over $10 million.

Many plasma chemistries incorporate the use of halocarbon compounds as feed gases. These chemistries are predominant throughout the industry and can be found in almost all manufacturing facilities worldwide (19). The use of fluorocarbons,

however, has sparked interest in the mechanisms associated with particle formation inside a piece of equipment (20,21).

Device performance properties have been well correlated with metallic contamination in wet chemical etching. Levels of metallic impurities, as low as 0.50 parts per billion, have a detrimental impact on device performance (22). As a result, feed gases typically used in plasma processing are purified to reduce the level of metallic impurities. As device geometries scale to smaller dimensions, this area of concern becomes increasingly more critical.

The industry would benefit from a shift to low ion energy etch chemistry (23,24). As ion energies or ion concentrations increase, the level of surface bombardment increases. The result is an increase in defects generated in the surface of the material being processed. There is positive correlation between the level of ion bombardment and the integrity of the thin film interface. From a plasma chemistry perspective, the use of gases that are corrosive or

that require the use of high ion energies to achieve the desired etch result are increasingly less desirable.

Etch anisotropy is a major requirement for this and future generations of devices (1,10). Anisotropy and reaction selectivity are complementary parameters. Typically, as anisotropy improves in a pattern transfer process, reaction selectivity degrades. As integration levels on a single chip increase, the line widths and device dimensions must shrink. The plasma etch characteristic needed to obtain higher device density is anisotropy, the ability to define a pattern without loss of dimensional control due to mask undercut. In other words, the profile of the geometry patterned needs to be vertical. The ability to pattern a material in a vertical direction without compromising reaction selectivity is a major challenge facing the industry.

A wide variety of process chemistry is used in microchip fabrication. Each process has a defined set of parameters to control to achieve the desired effect. For example, if a complete process had

300 individual steps and each step was completed with a 99% yield, the overall statistical yield for the entire process would be 4.9%. A complete understanding of how process variables independently and synergistically affect the response or outcome is becoming crucial as the wafer diameter increases and device geometry becomes smaller.

Chemometrics is a relatively young scientific discipline that involves statistical mathematics and quantitative analytical chemistry (25). Its genesis is a result of modern-day computer technology. As computer processing developed, the collection of qualitative and quantitative data expanded. Concomitantly, the need for quantitative analysis of the data expanded the use of statistical mathematics. Using statistical metrics in plasma processing is immensely valuable for controlling influential parameters.

1.3 Environmental Issues

The gases that are typically used in the pattern transfer operation often contain halogen atoms (26). Indeed, fluorinated, chlorinated and brominated compounds constitute the majority of the gases used in this application. Unfortunately, these compounds can be harmful to the environment, particularly regarding global warming. The development of new etchant gas mixtures must begin with considering the environmental impact of the chemistry. While new process chemistries must be developed to meet the needs of the semiconductor industry, they should be optimized to have a minimal environmental footprint.

In 1988, Hansen and co-workers (27) published the results of initial predictions developed using a three-dimensional atmospheric global climate model. In the model, several climate-forcing scenarios including time-dependent emissions of greenhouse gases and naturally occurring climate-forcing events, such as volcanoes, were taken into consideration. The model was used to predict the global-

mean temperature change as a function of time through the year 2019. Best and worst case scenarios were considered and global warming was predicted to occur over the next several decades.

More recently, Hansen and co-workers at NASA (28) published the measured global-mean surface temperatures on the NASA web site. They presented global-mean temperatures and five-year global-mean temperatures through the end of calendar year 2000. The data are presented graphically in Figure 1.3.1. A global warming trend is indicated starting in the mid-1970's. Hansen also published the collected temperature data on his NASA web site (29). The data are presented in the form of a graphical animation. Advancing through the animation, from 1970 through 1999, global warming trends are apparent.

Hansen and co-workers (30) have brought another significant source of global warming to the forefront of debate. They believe that "rapid warming in recent decades has been driven mainly by non-CO_2 greenhouse gases." This is a significant statement from a

leading authority on global warming and warrants immediate attention.

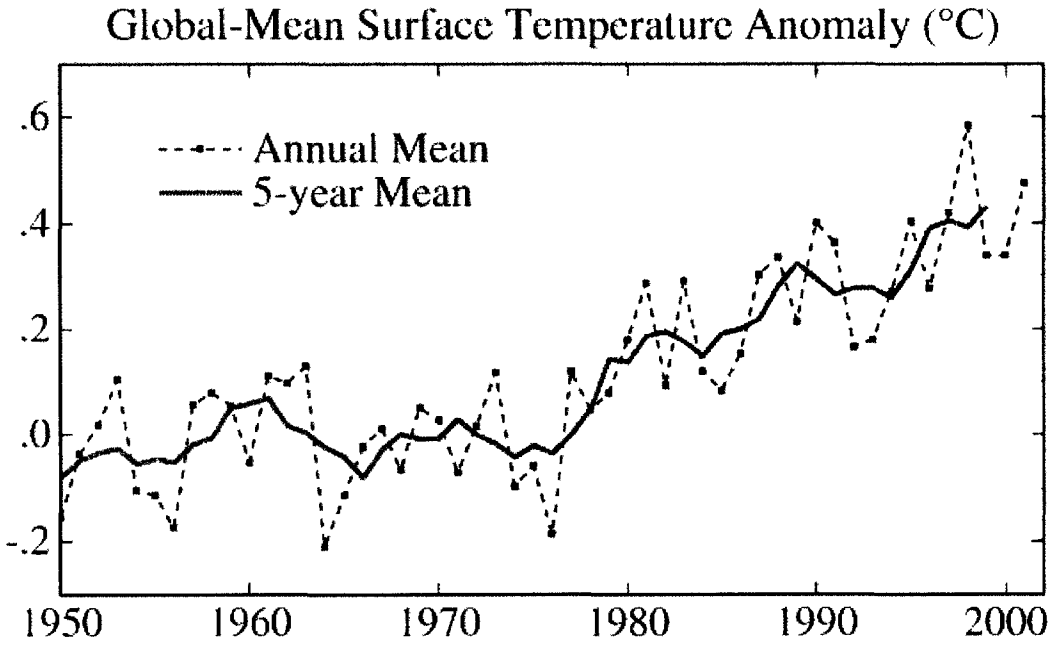

Figure 1.3.1. Global-Mean Surface Temperature (28)

Sulfur hexafluoride, a common etchant for silicon, has a significant global warming potential relative to carbon dioxide (CO_2 = 1). In a recent investigation, the atmospheric lifetime of sulfur hexafluoride was studied (31). The researchers found sulfur hexafluoride to be one of the most potent greenhouse gases once

vented to the atmosphere. Sulfur hexafluoride has a 100-year global warming potential estimated at 22,200 (CO_2 = 1) and an atmospheric lifetime estimated at 3,200 years (32). Another etchant gas, CF_3CF_2Cl, has an atmospheric lifetime estimated at 1,700 years and a global warming potential of 11,200.

Use of semiconductor etchant gas is growing at an environmentally alarming rate, 150% over the last decade (33). On an industry-wide basis, the potential for greenhouse gas emission is estimated at 7.4 teragrams of carbon dioxide equivalents. For the semiconductor industry, discussions regarding non-carbon dioxide based greenhouse gases have been focused on the widespread use of plasmas. In Sematech's 2000 Annual Report (1), climate change mitigation is targeted as a major priority for the industry. The focus area map for the environmental, health and safety group specifies the identification of chemicals with low global warming potential as part of the five-year strategy.

2. Background

2.1 Radiofrequency Plasma

Manufacturing a semiconductor microdevice requires sequential steps whereby thin films of conductors and insulators are deposited and patterned (10). Plasma or low-pressure gaseous discharge chemistry has found wide acceptance for this patterning application. Plasma chemistry, unlike wet chemical etching, can produce patterns of very small, sub-micron dimensions. As design rules for next generation devices tighten, plasma processes must etch materials with higher reaction selectivity and less mask undercut. The research discussed in this dissertation addresses plasma chemistry and the effects on etch selectivity and anisotropy.

Subtractive pattern transfer is used in the industry for defining regions of electronic material on a substrate. One measure of the quality of the image transfer is etch bias (10). It represents a quantitative means of determining the extent to which the initial pattern has lost definition. Figure 2.1.1 is an illustration of etch bias (B), the difference between the lateral dimension of the mask

and the lateral dimension of the etched image. A zero etch bias has zero percent mask under-cut and a perfect pattern transfer. The dimension of the mask is equal to the dimension of the etched image. As device dimensions continue to shrink, pattern transfer requirements tighten and zero etch bias becomes essential (2).

$$B = d_m - d_f$$

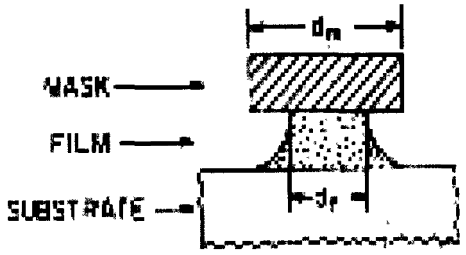

Figure 2.1.1. Etch bias (10)

Radiofrequency plasma chemistry (1) is commonly carried out at pressures between 100 millitorr and 1 torr. Power inputs vary between 100 and 1,000 watts (power density varies between 0.023

to 0.230 watt per cm^2 of electrode area). Depending on the nature of the plasma feed gases, these operating parameters could provide etch profiles that vary from isotropic to anisotropic.

Figure 2.1.2 is a schematic illustration of profiles etched in silicon that are isotropic and anisotropic (10). For plasma conditions and chemistry providing isotropic etch profiles, the mask is undercut. This means the lateral etch rate is equal to the vertical etch rate of the material. Anisotropic etch profiles are vertical. These profiles are highly desirable because there is minimal loss of pattern definition and minimal mask undercut. The reaction proceeds in the vertical direction with no reaction laterally.

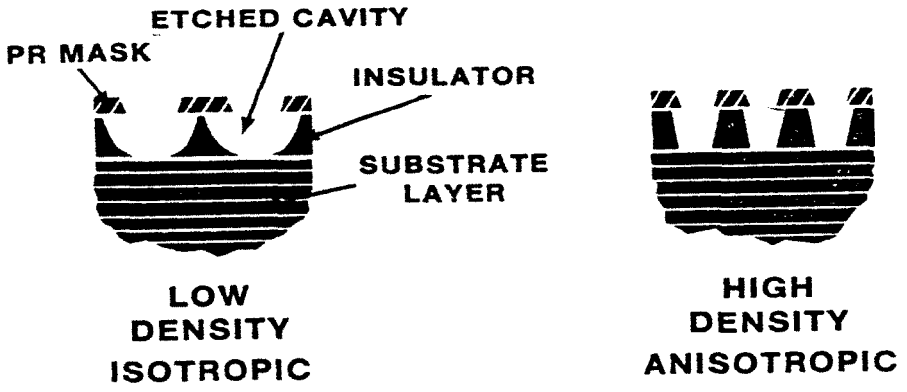

Figure 2.1.2. Isotropic versus anisotropic etch profiles (10).

The earliest published applications using low-pressure discharge chemistry in the microelectronics industry were for ashing photoresist (38). In the application, molecular oxygen was used in a plasma state to oxidize the photoresist. The ashing process generated carbon dioxide and water as reaction products until all the photoresist was removed from the surface. Subsequently, plasma technology was adopted for more advanced pattern transfer processing.

Plasma is a reactive state of matter that consists of electrons, anions, cations, excited state and neutral species. A plasma predominately consists of molecular fragments of the compounds used as feed gases. Many reactive species that form in a plasma are a result of electron-molecule collision reactions (39). Electrons are accelerated in the radiofrequency field and gain momentum as they oscillate. Electron motion in the plasma follows the applied ac voltage as it swings through it's sinusoidal cycle.

Gases used for plasma etching are typically halogenated and non-reactive at room temperature (10). When the gases are placed in an electric field, they dissociate, ionize and form a plasma (39). Typically, the applied field is a radiofrequency, 13.56 megahertz being the most common. The Federal Communication Commission has approved this operating frequency for industrial applications. Plasmas have also been generated for pattern transfer and cleaning applications using kilohertz and microwave frequency fields (11).

The electrical properties and voltage distribution of the plasma are important parameters. They control the degree of ion bombardment of the surface being treated. To understand profile control and anisotropy, it is important to understand the electrical characteristics of the plasma.

A typical voltage distribution between two parallel plate electrodes is shown in Figure 2.1.3 (40). The radiofrequency voltage oscillates at a frequency of 13.56 megahertz. The voltages shown are time-averaged values. The alternating current power

supply shown in the diagram is capacitively coupled to the load through tunable or variable capacitors. The capacitors are adjusted to maximize load coupling efficiency and minimize reflected power.

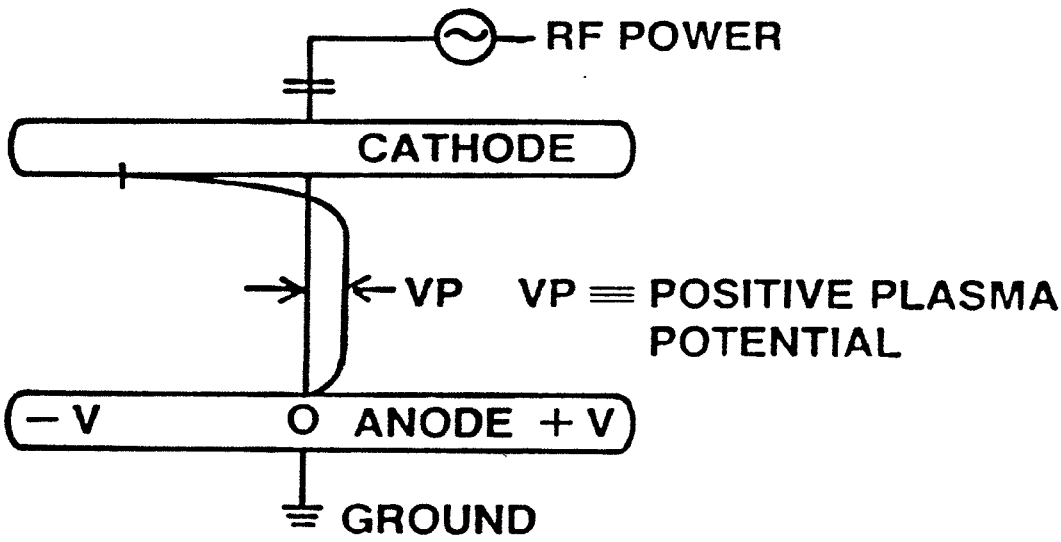

Figure 2.1.3. Voltage distribution in a radio frequency parallel plate reactor (40).

As illustrated in Figure 2.1.3, the cathode develops a negative bias voltage. The potential of the plasma, V_p, is shown as positive. The positive value of the plasma potential is indicative of a high relative concentration of positive ions in the plasma state. Electrons present in the plasma have great mobility and move quickly towards grounded surfaces (39). Positive ions, in general, have lower

mobility in the plasma field and tend to oscillate in the space between the electrodes. The time averaged plasma potential is normally in the range of 50 to 100 volts.

Electron collisions with halogenated gases result in ions, neutrals and excited states being formed, which then interact with the material being patterned. Plasma states are noted for their characteristic colors resulting from photon emissions of excited state species (11). The use of visible light emission has become a common diagnostic method and is routinely used to determine the end-point of the reaction. For example, the reaction of difluorosilyl radicals with fluorine atoms produces a trifluorosilyl excited state. The excited state emits photonic energy with a maximum intensity at a wavelength of 632 nanometers.

$$SiF_2 + F \rightarrow SiF_3^*$$

$$SiF_3^* \rightarrow SiF_3 + h\nu$$

Monatomic fluorine has also been used for plasma diagnostics and end-point determination. Peak emission intensity occurs at 704 nanometers.

$$F + e^- \rightarrow F^* + e^-$$

$$F^* \rightarrow F + h\nu$$

A simple molecular ionization reaction proceeds:

$$Ar + e^- \rightarrow Ar^+ + 2\,e^-$$

Molecular ionization with dissociation, also called dissociative ionization, can also proceed:

$$NF_3 + e^- \rightarrow NF_2^+ + F\cdot + 2\,e^-$$

For this reaction, the electron energy must exceed the N-F bond energy of the NF_3 molecule, 247 kJ/mol. Dissociation energies for

several neutral species commonly found in radio frequency plasmas are listed in Table 2.1.1 (41).

Table 2.1.1

Dissociation Energies for Neutral Species (41)

	Dissociation Energy (kjoule/mole)	Products
NF_3	247	$\cdot NF_2 + F\cdot$
$\cdot NF_2$	243	$\cdot NF + F\cdot$
CF_4	544	$\cdot CF_3 + F\cdot$
$\cdot CF_3$	364	$\cdot CF_2 + F\cdot$

2.2 Silicon Etching

When silicon is exposed to a plasma, it reacts and a volatile reaction product is formed which is then pumped away using a vacuum pump:

$$Si\ (solid) + 4\ F^{\cdot} \rightarrow SiF_4\ (gas)$$

Ion and electron loss mechanisms also weaken the plasma. These processes reduce the concentration of electrons and make it more difficult to sustain a plasma state. For example, dissociative electron attachment proceeds:

$$NF_3 + e^- \rightarrow NF_2 + F^-$$

Electron loss has been problematic for plasmas using SF_6 as the feed gas. Sulfur hexafluoride has a high electronegativity and electron attachment reactions occur very rapidly (42).

$$SF_6 + e^- \rightarrow SF_6^-$$

In addition, dissociative electron attachment can produce SF_5^- via:

$$SF_6 + e^- \rightarrow SF_5^- + F$$

Ion currents generated from SF_6^- and SF_5^- are shown in Figure 2.2.1 as a function of electron accelerating voltage (42). At low energy, between 0 and 0.1 electron-volts, electrons are scavenged from the plasma to form anionic sulfur hexafluoride very efficiently.

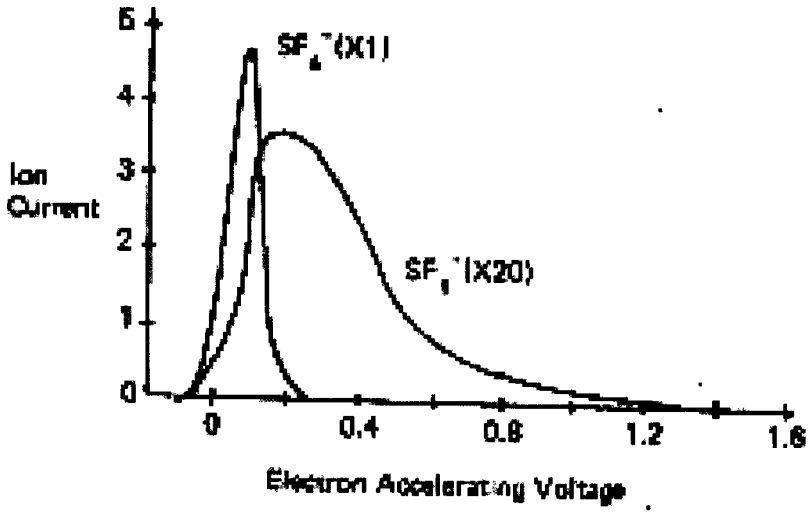

Figure 2.2.1 Ion Currents for SF_6 Plasma (42).

Further, since monatomic fluorine has a high electronegativity, these atoms are likely to participate in rapid electron attachment reactions:

$$F\cdot + e^- \rightarrow F^-$$

Other electron loss mechanisms to be considered include surface recombination on the metal reactor walls or electrodes. All of these electron loss reactions reduce electron density in the plasma. A low electron density results in a low cation density and the potential for isotropic etch profiles.

Selectivity of the plasma reaction is also a critical requirement for manufacturing microdevice structures. The etch selectivity (S) is the ratio of the reaction rates ($R_{silicon}$, $R_{silicon\ dioxide}$) between two different electronic materials (10).

$$S = \frac{R_{silicon}}{R_{silicon\ dioxide}}$$

A successful etch process must have minimal reactivity for the under lying silicon dioxide film and provide a pattern that has not lost definition. Providing pattern anisotropy at the expense of reaction selectivity is not acceptable.

The plasma used in pattern transfer applications is a low temperature, non-equilibrium plasma (43). It is classified as a weakly ionized plasma having ion concentrations on the order of 10^{-4} or 100 ppm. The bulk of the plasma is at room temperature. However, the electron temperatures can exceed 20,000 Kelvin. The dynamics of the etching process consist of those typical for gas-solid heterogeneous reactions. However, the reactions are coupled with a more complex component of radiation-enhanced chemistry.

To better understand the chemistry, the two phenomena have been investigated separately. Chuang (44) studied silicon etching using xenon difluoride gas. Xenon difluoride dissociatively chemisorbs on the surface of silicon. X-ray photoelectron spectroscopy (XPS) was used to identify silicon difluoride on the surface of silicon. No evidence of silicon tetrafluoride bonding was noted.

Flamm et al. (45) used monatomic fluorine to etch silicon spontaneously in the absence of a plasma. The reaction proceeded favorably at room temperature. Silicon <100> was exposed to fluorine atoms at 298 Kelvin. The etch rate proceeded at approximately 250 nanometers per minute.

Studies have also been done investigating the radiation enhancement component of plasma chemistry. Gerlach-Meyer et al. (46) have etched the surface of silicon using xenon difluoride combined with a beam of inert ions incident normal to the surface. They studied argon, helium and neon and reported the yields of silicon atoms per incident ion. Yields varied with incident ion energy and the inert gas. Yields as high as 25 atoms per incident ion were reported using cationic neon and xenon difluoride. Coburn et al. (47) studied the effects of ion enhanced chemistry and found etch rates of silicon increased by a factor of 10 with and without radiation enhancement.

Heterogeneous gas solid chemistry involves a series of sequential steps for a reaction to proceed favorably (48). The first step required is the diffusion of reactive species to the surface. In this step, a concentration gradient of reactant exists between the bulk gas phase and the solid surface. The chemical potential necessary for the species to diffuse to the surface is provided by the concentration gradient.

The species must chemisorb on the surface of the solid. Many factors in the plasma potentially impact chemisorption. For example, low sticking coefficient, steric hindrance, surface saturation, high surface energy and ionic bombardment all influence chemisorption.

A chemical transformation to form an intermediate or product occurs. The molecule desorbs from the surface of the solid and diffuses back into the bulk plasma phase. Any one of these sequential steps may be rate limiting. Which step limits the etch rate

depends on the operating conditions of the plasma and the type of chemistry employed.

A substantial portion of the energy associated with ionic bombardment of the surface is thermalized (49). As a result, surface temperature increases significantly. Donnelly reported measuring surface temperatures as high as 100 °C when surfaces were exposed to low-frequency plasma (49). Also, because the reaction thermodynamics are exothermic, a substantial amount of heat is generated as the fluorination reaction proceeds.

$$Si + 4F \rightarrow SiF_4$$

A rate expression for etching silicon with fluorine atoms has been suggested by Flamm et al. (50). In this study, fluorine atoms were generated from molecular fluorine, and the temperature of the silicon was varied. Rate constants and activation energies were established:

$$R_{Si} = AT^{0.5} n_f e^{-\frac{x}{kT}}$$

The term T is the temperature in Kelvin, n_f is the fluorine atom density, k is the Boltzman constant, A = 2.91 x 10^{-12} and x = 0.108 electron-volt activation energy.

Considering the dependence of etch rate on temperature, the lack of adequate or uniform heat removal may lead to poor etch uniformity across the diameter of a wafer. A number of other factors could potentially influence the rate of heat removal, surface temperature and the reaction rate including wafer contact quality with the cooled electrode, the area being etched, the dopant type and concentration, and the uniformity of dopant atom distribution.

2.3 Silicon Dioxide Etch Chemistry

Flamm et al. (51) used molecular fluorine as a source gas and measured the reactivity of fluorine atoms with silicon dioxide. Monatomic fluorine etches SiO_2 spontaneously at room temperature

in the absence of surface ion bombardment. The reaction proceeded slowly, relative to that of silicon, at approximately 6 nm/min.

As a result of the large number of layers on a microchip that are silicon dioxide, a selective oxide etch process was needed in the industry (52). Selective etching of silicon dioxide over silicon was achieved using fluorocarbon gases (53). A plasma of carbon tetrafluoride mixed with molecular hydrogen was proposed and tested. The proposed reactions are:

$$CF_4 + H_2 \rightarrow CF_2 + 2\,HF$$

$$CF_4 \rightarrow CF_2 + 2\,F$$

The difluorocarbene reacts with silicon dioxide readily forming gaseous by-products.

$$CF_2 + SiO_2 \rightarrow SiO_2\text{-}CF_2(s)$$

$$M + e^- \rightarrow M^+ + 2\,e^-$$

$$SiO_2\text{-}CF_2(s) + M^+ \rightarrow SiO(s) + M^+ + CF_2O$$

The cation M^+ imparts energy to the surface of the silicon dioxide through ion bombardment. The impact energy is sufficient to break the silicon-oxygen bond of the intermediate complex. Silicon dioxide can also react with monatomic fluorine to form volatile reaction products.

$$2\ F\cdot + SiO_2 \rightarrow SiF_2 + O_2$$

Over the past two decades, most of the research has been done on selective silicon dioxide etching. As a result, most of the chemistry investigated used fluorocarbon-based plasmas.

Langan et al. (54) studied the reactivity of difluorocarbene with silicon dioxide surfaces. In this work, XPS was used to identify CF_2 adsorbed to the surface. The difluorocarbene did not dissociate or react with the silicon dioxide. Langan further demonstrated that difluorocarbene only reacts with silicon dioxide in the presence of simultaneous ion bombardment.

The reactivity of CF_3 toward silicon dioxide has also been investigated (55). McFeely et al. used XPS surface analysis to determine that CF_3 adsorbs to the SiO_2 surface, but not dissociatively. They further concluded that the CF_3 was chemically bonded to oxygen atoms through a carbon-oxygen bond. Joyce (56) also found the CF_3 adsorbs on silicon dioxide but does not dissociate. Evidence of carbon-oxygen and carbon-silicon bonding was found in the XPS analysis.

Recently, Ho et al. (57) modeled the etching of silicon dioxide using C_2F_6 and CHF_3 plasmas. The model was divided into two categories: gas phase kinetics and surface reactions. The gas phase plasma reactions involve 28 different species and a total of 132 different reactions. The surface chemistry involves 85 reactions with 6 species. Concentrations of difluorocarbene were measured in the gas phase using laser-induced fluorescence. The concentration of difluorocarbene decreased as the input power to the plasma increased.

2.4 Radiation Enhanced Anisotropy

Anisotropic profiles are commonly obtained using two different mechanisms (11). The first method uses directional cationic bombardment to assist anisotropy. The second method discussed Section 2.5, uses plasma polymerization to protect the sidewall of the feature. There are several different approaches to using ion bombardment for obtaining etch anisotropy. These approaches include reactive ion etching, low-frequency (kHz) plasma etching, ion milling, multi-frequency plasma, super-imposed dc biasing and magnetic field enhanced plasmas (11).

In the ion assisted technique, regardless of the approach used, etch rate enhancement is achieved by ion bombardment of the material being patterned and the induced physical damage on the surface (58). This occurs mostly when high power density and low-pressure plasmas are used. Under these conditions, the ions maintain normal directionality as they are accelerated through the sheath and bombard the surfaces.

The plasma potential has a positive correlation with the degree of cationic bombardment on surfaces positioned on the ground electrode. Positive ions are extracted from the plasma and accelerated toward the ground electrode. The impact energy of the ion is important in determining several critical etch characteristics. Etch rate, reaction selectivity and etch anisotropy all depend on the degree of radiation enhancement provided by the impinging ions.

Operating parameters, such as power input, pressure and gas composition, affect ion densities and the electrical/chemical properties of the plasma state. The higher the plasma potential, the higher the degree of ion bombardment and the more likely anisotropic profiles will be etched.

The substrate can also be positioned on the cathode. The coupling of radiofrequency power to the electrode holding the substrate is referred to as reactive ion etching (59). Low pressures, ranging between 10 and 100 millitorr, are typically used in the

process. The cathode takes on a negative bias and cations in the bulk plasma are extracted and accelerated towards the cathode. Using this electrode configuration, the cations develop a kinetic energy that is proportional to the plasma potential plus the negative bias on the cathode. The process is not commonly used today. The low pressures required for the process result in reaction rates that are unacceptably low (11).

Anisotropic profiles in single crystal silicon can be obtained by manipulating the systemic variables of the plasma. Varying input power to the plasma is often used to control the etch profile (60, 61). An increase in power density, ρ, results in stronger field intensity across the electrodes.

$$\rho = \frac{\text{input power (watts)}}{\text{electrode area (cm}^2\text{)}}$$

At high power, the plasma potential becomes more positive. An increased depletion of electrons occurs in the plasma and a higher concentration of positively charged species results. As the

plasma potential is increased, the acceleration rate of cations drawn toward the surface being etched increases. A higher degree of ionic bombardment and a more anisotropic profile result.

Plasma pressure also impacts etch anisotropy. An increase in pressure increases the number density of molecules in the plasma state and increases the collision frequency. In high-pressure plasmas of approximately one torr, collisionless transport of ions to the surface becomes difficult. As pressure is reduced, the collision frequency reduces correspondingly and uninterrupted transport to the surface becomes more probable. At high pressure, cations may have inelastic collisions that can redirect their path toward the sidewall of the feature being patterned.

The frequency of the power applied to the electrode has also been varied as an operating parameter (62). The voltage distribution in a plasma is a time-averaged voltage. The physical effect of an oscillating radiofrequency field on a cation is important. The ion accelerates in one direction, then decelerates. As the field

reverses, the ion accelerates in the other direction, then decelerates. This process is continuous and is affected by the operating frequency.

At high radiofrequencies (13.56 megahertz), cations of larger mass can be trapped in the volume of the plasma. The cations of small mass are more mobile in the high frequency field and are more likely to interact with the material being patterned.

When the radiofrequency is reduced, cations oscillate at a slower rate. Larger mass ions respond to field changes and are more likely to participate in the etching reaction. Bruce (62) has shown that etch rate and anisotropy are increased by operating at lower frequency (kHz). Unfortunately, low frequency plasmas generate substantial surface damage and have low reaction selectivity. Therefore, low frequency plasmas will have limited use in patterning advanced microdevices (11).

Other approaches to radiation enhanced anisotropy, such ion milling, multi-frequency plasma and dc substrate biasing, also suffer from poor reaction selectivity (11). As a result, these techniques will find limited use in future device patterning applications. The use of magnetic confinement of the plasma does have potential for future device patterning (11). In this method, the loss of electrons is minimized by B-field confinement. Cation density in the plasma can be tailored by varying the B-field intensity, providing an additional degree of process flexibility.

2.5 Plasma Polymerization

A second common method for obtaining anisotropic profiles is the use of polymer passivation chemistry (63,64,65). In this method, the plasma sustains a concentration of reactive neutral species that form a deposit on the surface. Typically, these are chlorofluorocarbon species formed through electron collision reactions:

$$CF_2Cl_2 + e^- \rightarrow (CF_2Cl_2^-)^*$$

$$(CF_2Cl_2^-)^* \rightarrow \cdot CClF_2 + Cl^-$$

$$\cdot CClF_2 + e^- \rightarrow :CF_2 + Cl^-$$

$$n :CF_2 \rightarrow (CF_2)_n$$

Halogen atoms are electronegative and electron attachment reactions are likely to occur in the plasma. On electron impact, dichlorodifluoromethane is raised to an excited state. For small molecules, stabilization is usually obtained through dissociation. The carbon-chlorine bond has a bond energy of 3.3 electron-volts compared to 4.8 electron-volts for a carbon-fluorine bond. As a result, the reaction usually proceeds via dissociative electron attachment, breaking the carbon-chlorine bond and forming anionic chlorine. The chlorodifluoromethyl radical formed is very reactive due to the one unpaired electron. The radical can react in the gas phase or deposit on surfaces forming polymeric material. Chlorodifluoromethane can also participate in electron collision reactions forming difluorocarbene and anionic chlorine. The difluorocarbene can also participate in gas phase reactions or deposit on surfaces forming polymeric material.

A halocarbon film forms on the sidewalls of the material being patterned and protects it from etching in a horizontal direction.

Under the proper operating conditions, etching is allowed to proceed in the vertical direction. Cationic bombardment clears the deposited film and exposes the electronic material to be etched.

Both Flamm (63) and Millard et al. (65) discussed the importance of having "unsaturated" species in the plasma to promote polymer film deposition. They established a strong positive correlation between the concentration of difluorocarbene and the rate of polymer film deposition.

Plumb and Ryan (66) established rate coefficients for different gas phase reactions in a plasma polymerization process. They studied the reactions:

$$CF_3 + F \xrightarrow{k_1} CF_4$$

$$CF_2 + F \xrightarrow{k_2} CF_3$$

The rate coefficients were established for different gas densities. They found $k_1 >> k_2$ by approximately two orders of magnitude. The trifluoromethyl radicals are depleted relatively quickly. The difluorocarbene species react more slowly with monatomic fluorine, providing higher gas phase concentrations. The reaction to form a polymer film proceeds:

$$n\ CF_2 \rightarrow (CF_2)_n$$

forming protection from sidewall etching.

Recently, Cunge et al. (67) etched silicon anisotropically using a high density plasma. Mixtures of HBr, Cl_2 and O_2 were used in the study and ion fluxes were monitored using Mass spectrometry. The authors identified a significant portion of the ion flux as $SiBr_xCl_y$. In the formula, x and y are between 0 and 2 and $x + y > 0$. The authors suggest the products of the reaction and the feed gas composition both play a role in developing anisotropic profiles in silicon.

2.6 Negative Ion Formation

A number of studies have been conducted regarding negative ions in the plasma state. Electron loss through anion formation indirectly reduces the cation population in the plasma, making anisotropic etching more difficult. Anions are short-lived in the plasma and are less likely to play a significant role in the heterogeneous reaction (68). The positive plasma potential contains a minimum negative ion population. The low anion density prevents or at least minimizes interaction with negatively biased or grounded surfaces.

A study of negative ion formation in a dichlorodifluormethane plasma was carried out by Stoffels et al. (69). They investigated mixtures of CF_2Cl_2 with argon in a capacitively coupled radio frequency plasma. The dominant negative ion in the plasma was Cl^-. The density of anionic monatomic chlorine was nearly 100 times that of the plasma electrons. Dissociative electron attachment was proposed as the dominant pathway for the formation of Cl^-. The

authors proposed that an electron attachment process is most likely to occur when using an electronegative etch gas such as CF_2Cl_2.

$$CF_2Cl_2 + e^- \rightarrow (CF_2Cl_2^-)^*$$

As a result, an excited state intermediate is formed which must stabilize. For small molecules, the stabilization usually occurs through dissociation.

$$(CF_2Cl_2^-)^* \rightarrow CF_2Cl\cdot + Cl^-$$

Stoffels et al. (70) measured the electron density in admixtures of CF_2Cl_2 in argon. The work was done in a parallel plate radiofrequency reactor operating at 50 watts, 30 standard cm^3/min. flow and 200 millitorr pressure. The measured electron density is shown in Figure 2.6.1 as a function of increasing volume percent CF_2Cl_2. Data are shown for experiments with and without silicon present in the reactor.

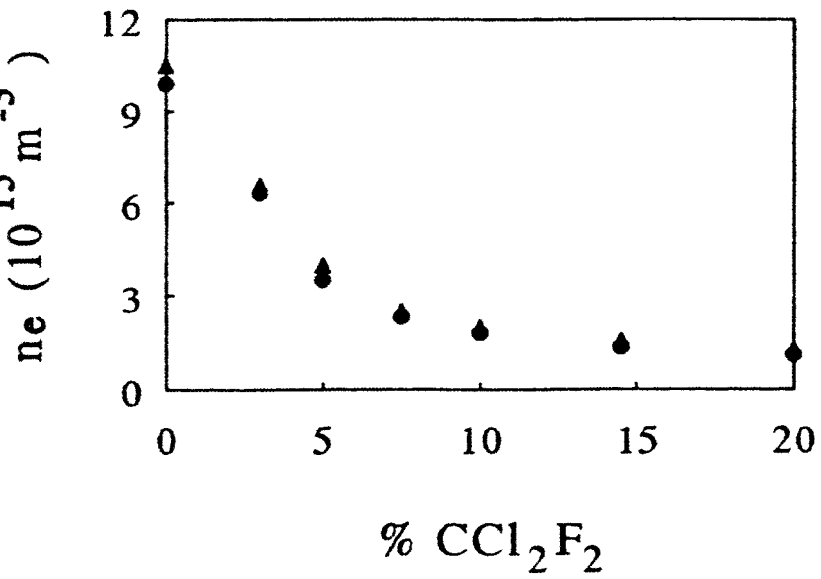

Figure 2.6.1. Electron density as a function of vol. % CF_2Cl_2 (70).

2.7 Nitrogen Trifluoride Plasmas

The earliest reported experimentation using NF_3 as a plasma source gas was by Eisele (71). He studied NF_3 plasma etching of silicon and thermally grown silicon dioxide. Silicon etch rates greater than 1 μm/min. and selectivity of 50:1 compared to thermal SiO_2 were reported. As a plasma source gas, NF_3 has been used when high etch rates or high reaction selectivity are required. However,

NF_3 has had limited use in patterning when anisotropic profiles are needed (19). The research presented in this dissertation uses NF_3 as a source of monatomic fluorine for etching silicon. Polymer forming gas additives were used to improve etch anisotropy and maintain high etch rates and reaction selectivity.

Barkanic et al. (72) investigated mixtures of NF_3 in both argon and helium diluent gases. Single crystal silicon was etched using plasma etching and reactive ion etching electrode configurations. Figure 2.7.1 is an illustration of the etch rate dependence of silicon as a function of volumetric percent NF_3. As the concentration of NF_3 in diluent gas increases, the etch rate of silicon increases. Higher power density coupled into the plasma also resulted in an increased reaction rate.

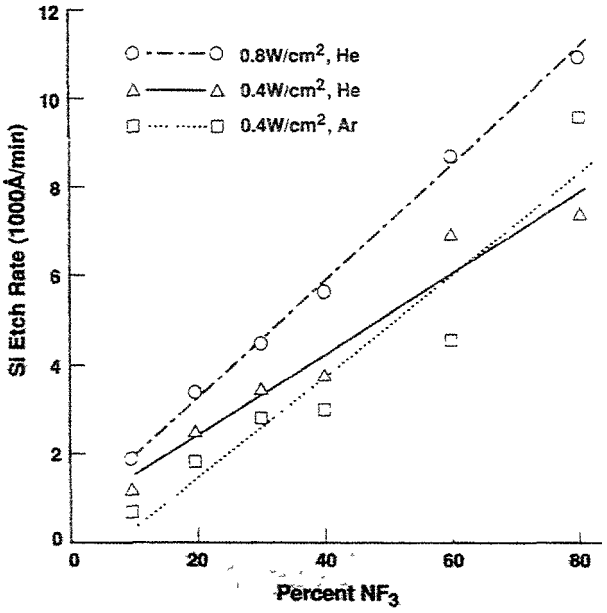

Figure 2.7.1 Silicon Etch Rate as a Function of % NF_3 (72).

Korman et al. (73) and Bower (74) used a low frequency 380 kHz generator to study NF_3 plasma effects on polycrystalline silicon. Korman focused on loading effects and etch rate uniformity as a function of gas flow rate. Bower reported isotropic etching of silicon using mixtures of NF_3 and CCl_4. Etch rates of silicon as high as 1.5 μm/min. were reported.

Barkanic et al. (75) reported analytical data regarding the dissociation of NF_3 in a plasma environment. In this work, a

quadrupole mass spectrometer was used to analyze the effluent stream of the plasma reactor. Table 2.7.1 contains the mass spectral signals for an NF_3 plasma as a function of power density. Peak identification, assigned mass to charge ratio and current signal for two power densities are shown. As plasma power density is increased, there is an increase in the dissociation of the source gas, NF_3.

Table 2.7.1 Mass Spectral Signals for NF_3 Discharge (75).

		Signal (picoamp)	
Peak ID	Mass/Charge	0.2 W/cm^2	0.4W/cm^2
NF_3^+	71	16	2.4
NF_2^+	52	108	16.2
NF^+	33	80	26.0

Several investigators (76, 77) studied the mechanism for NF_3 dissociation in a gas discharge. Donnelly et al. (76) suggested the

dissociation process occurs predominately through electron collision reactions. A proposed mechanism is:

$$NF_3 + e^- \rightarrow NF_2 + F^-$$

followed by a rapid electron detachment reaction:

$$F^- + e^- \rightarrow F\cdot + 2\,e^-$$

Further dissociation of the gaseous species proceeds via additional electron molecule collisions.

Research has also been done using NF_3 plasmas for etching dielectric materials. Both Dielman and Sanders (78) and Thornquist (80) studied plasma reactions using NF_3 to obtain selective Si_3N_4 over SiO_2 etching. Dielman (78) reported a selectivity of 8:1 using NF_3 and a selectivity increase to 10:1 using NF_3 mixed with 5% by volume CF_2Cl_2. Thornquist (80) added molecular oxygen to NF_3 to

increase the reaction selectivity of silicon nitride over silicon dioxide. Saia and Gorowitz (79) used a mixture of NF_3, argon and oxygen to etch tapered contact holes in silicon dioxide. The oxygen present in the plasma eroded the photoresist mask material. The gradual erosion of the mask provided a sloped profile of the SiO_2 feature.

Barkanic et al. (81) showed the etching characteristics of thermally grown silicon dioxide using reactive ion etching. In this work, low-pressure plasmas (25 to 50 millitorr) of NF_3–inert gas mixtures were generated. The silicon dioxide etch rate is shown in Figure 2.7.2 as a function of power density for a range of concentrations, pressures and diluent gases. The reaction rate of silicon dioxide has a strong linear dependence on input power. Further, the rate of etching silicon dioxide demonstrates minimal dependence on NF_3 concentration, pressure and inert gas diluent.

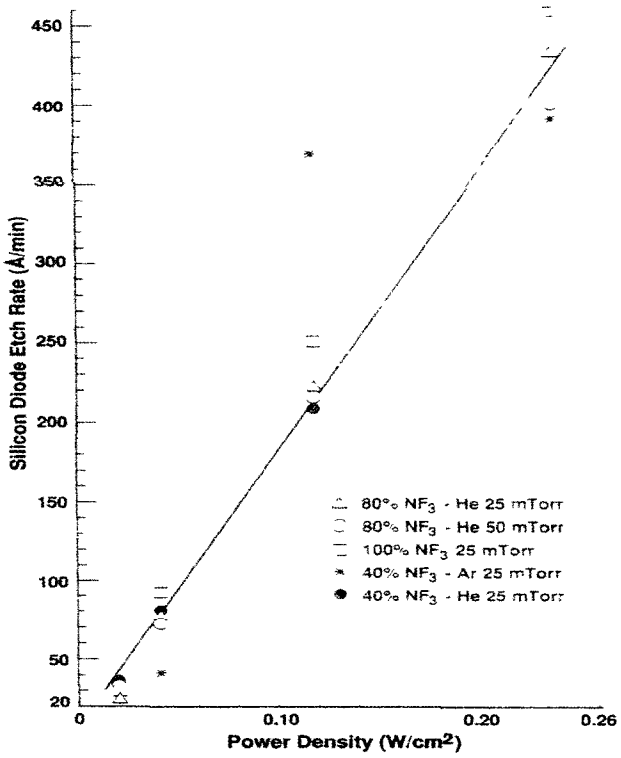

Figure 2.7.2 Silicon Dioxide Etch Rate as a Function of Power Density (81).

Sellamuthu et al. investigated the use of halocarbon additives to NF_3 (82). In this work, single crystal silicon was patterned using a mask of silicon dioxide. Mixtures of NF_3 with different chlorofluorocarbons (CF_3Cl, CF_3Br and CF_2Cl_2) were tested. In this investigation, anisotropy was studied without consideration for reaction selectivity. A scanning electron micrograph of a vertical

wall profile obtained using a mixture of 50% CF_3Br in NF_3 is shown in Figure 2.7.3. XPS analysis of the post-etched surface was performed. The authors suggest the halocarbon formed a sidewall passivation film via plasma polymerization.

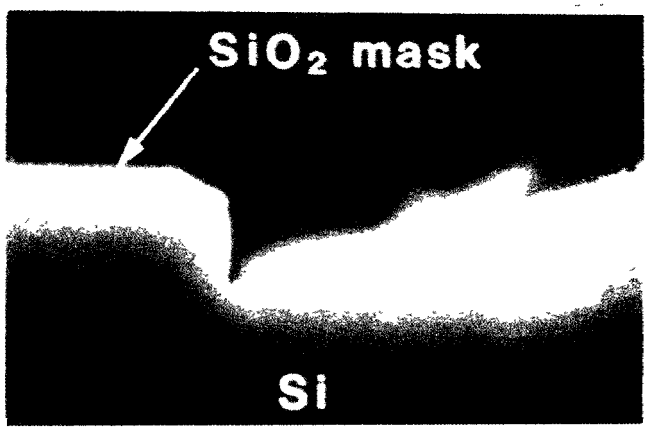

Figure 2.7.3 SEM of Silicon Etch Using NF_3 and CF_3Br (82).

More recently, Lin (83) developed a method of etching silicon to provide a tapered opening. The taper could be controlled between 60 and 85 degrees using a plasma consisting of nitrogen trifluoride mixed with hydrogen bromide.

Low temperature plasma etching of silicon has unique advantages. Tsujimoto et al. (84) conducted microwave plasma

etching using nitrogen trifluoride, sulfur hexafluoride and carbon tetrafluoride. In this work, the substrate was maintained at a constant temperature ranging between -150 and 30 °C. Lateral etch rates were minimized when the temperature was kept below -130 °C. As a result, anisotropic profiles could be obtained with high vertical etch rates and high reaction selectivity. This process provides ideal etch characteristics; however, the low temperature requirements are not consistent with existing manufacturing methods.

The thermal reaction of NF_3 with (110) silicon was studied over the temperature range of 300 to 1,200 Kelvin (85). In the study, laser and electron ionization mass spectrometry were used to analyze gaseous reaction products. The apparent activation energy for SiF_2 production was determined to be approximately 92.5 kJ/mol. No SiF was detected in the gaseous reaction products.

The interaction of silicon (100) with a nitrogen trifluoride ion beam was studied under controlled conditions (86). Presence of a Si-N-F moiety was identified using XPS. The F(1s) peak was shifted to

a higher binding energy relative to the peak observed with fluorine and silicon reacting. The authors believe that etching, nitridation and fluorination are proceeding simultaneously on the surface.

Researchers at Applied Materials, Inc. (87) identified conditions for optimizing a plasma process for cleaning surfaces. When a plasma of nitrogen trifluoride was diluted using molecular nitrogen, the etching rate of electronic material increased and the uniformity of etch rate across the chamber improved.

Most recently, Hsueh et al. (88) studied the ion energy distribution for an NF_3-based plasma used for cleaning surfaces. Plasma ion mass spectrometry was used to correlate ion energy with diluent gas and operating pressure in the plasma. Ion energies were minimized when operating at higher pressures using helium as the diluent gas.

Langan et al. (89) studied the role of diluent gases in an electronegative gas discharge. Argon, helium and nitrogen were

added to nitrogen trifluoride. Both silicon dioxide and silicon nitride were etched over a range of pressures and the etch rates were determined. Electrical measurements of the plasma were made and used to calculate actual power dissipation in the plasma. The authors propose that the dominant role of the diluent in the plasma is to control plasma electronegativity. Work in this area continued by Langan et al. (90) using electrical impedance measurements to analyze NF_3/Ar plasmas. Conditions were identified to maximize the etch rate of dielectric films for reactor cleaning applications.

2.8 Ellipsometry

Laser ellipsometry is a surface and film measurement technique often used in the analysis of semiconductor materials (91,92). The technique can be used for the determination of film thickness, refractive index and film composition. It is an extremely sensitive measurement and can differentiate between film thicknesses of only a few nanometers. The technique is based on optic principles established by Drude in 1889 (93). He studied the

optical properties of light reflected from a solid surface and established that the elliptical polarization of reflected light could be controlled by phase and amplitude adjustment of the incident light. In the research reported herein, ellipsometry was used to measure the change in film thickness of oxidized silicon on exposure to a reactive plasma environment.

In ellipsometry, the film to be measured is optically transparent to the laser light and the underlying substrate material is optically reflective. As the light passes through the film, the polarization state changes. The change in polarization of the light is then measured.

The fundamental equation of ellipsometry can be developed from consideration of first principles in optics. The incident field components are represented as E. The subscript **p** represents the parallel and the subscript **s** represents the perpendicular component of the field. Therefore,

$$E_p = E_{op} e^{i\alpha_p} \quad (1)$$

$$E_p = E_{os} e^{i\alpha_s} \quad (2)$$

The reflected field components can be represented in a similar fashion using R_p and R_s.

$$R_p = R_{op} e^{i\beta_p} \quad (3)$$

$$R_s = R_{os} e^{i\beta_s} \quad (4)$$

In these equations, α_p, α_s, β_p and β_s represent the respective phases for the incident and reflected fields.

The reflection coefficient can be introduced for an optical material to describe the relationship between the incident and reflected fields. The reflection coefficient ρ is:

$$\rho = \frac{\rho_p}{\rho_s} \tag{5}$$

$$\rho = \frac{R_{op}/E_{op}}{R_{os}/E_{os}} e^{i(\beta-\alpha)} \tag{6}$$

In this equation $\alpha = \alpha_p - \alpha_s$ and $\beta = \beta_p - \beta_s$. Each represents the phase angle of the incident and reflected light, respectively. One can also define the angle φ in such a way that

$$\tan\varphi = \frac{R_{op}/E_{op}}{R_{os}/E_{os}} \tag{7}$$

Using the phase angle Δ,

$$\Delta = \beta - \alpha \tag{8}$$

an equation can be presented that represents the reflection coefficient ρ.

$$\rho = \tan\varphi e^{i(\Delta)} \tag{9}$$

This is the fundamental equation of ellipsometry. Measuring φ, the change in the amplitude ratio, and Δ, the change in the phase, the reflection coefficient ρ can be determined. The reflection coefficient is a function of the film refractive index, extinction coefficient and thickness. The solution to the fundamental equation of ellipsometry relates the optical properties of the film and film thickness to the reflection coefficient (94).

2.9 X-ray Photoelectron Spectroscopy

XPS is a commonly used diagnostic tool for surface analysis in the semiconductor industry. Mayasumi et al. (95) used XPS to establish the cleaning effectiveness of different process chemistries on single crystal silicon.

Information regarding the chemical composition of solid surfaces and the nature of the chemical bonding on the surface is provided by XPS. Any consideration of the use of XPS for surface

analysis must first begin with a description of the relevant physical processes. What follows is a succinct review of the photoelectric effect. The remainder of this section is adapted from references 96-98.

The technique involves irradiating a solid surface with energetic x-rays in a vacuum. The x-ray radiation impinging on the solid surface has a narrow wavelength range and is often referred to as being monochromatic. In the photoionization process, high-energy photons interact with core-level electrons of an atom. Photoionization is ionization caused by an energetic photon. A core electron is emitted from the solid surface with a kinetic energy that is characteristic of that element.

$$M + h\nu \rightarrow M^{+} + e^{-}$$

In this equation, the photon energy is $h\nu$, the product of Plank's constant and the frequency of the radiation.

This technique is valuable in surface analysis because each element has a unique and characteristic spectrum. The electrons that escape the surface are subsequently sorted by their energy and are representative of the first few atomic layers of the solid. The photoelectrons produced during an XPS analysis have poor penetrating power and are incapable of passing through more than 1 to 5 nm of a solid. This limited electron escape depth is one reason why the technique is ideally suited for surface analysis. Core electron binding energies are shown in Table 2.9.1 for several elements (99).

Table 2.9.1. Core Electron Binding Energies (99).

Atomic Number	Element	Binding Energy (E_b), eV
3	Li	55
4	Be	111
5	B	188
6	C	284
7	N	399
8	O	532
9	F	686
10	Ne	867
11	Na	1072; 63
12	Mg	89
13	Al	74; 73
14	Si	100; 99
15	P	136; 135
16	S	165; 164
17	Cl	202; 200
19	K	297; 294
20	Ca	350; 347
21	Sc	407; 402
22	Ti	461; 455
23	V	520; 513
24	Cr	584; 575
25	Mn	652; 641
26	Fe	723; 710
27	Co	794; 779
28	Ni	872; 855
29	Cu	951; 931
30	Zn	1044; 1021
32	Ge	129; 122
47	Ag	373; 367
78	Pt	74; 70
79	Au	87; 83

The technique can be used to distinguish between atoms present in a solid. In the simplest model of the process, the kinetic energy of the emitted electron (E_k) is represented by the equation:

$$E_k = h\nu - E_b - \phi \qquad (10)$$

The energy of the x-ray photon is $h\nu$, E_b is the binding energy of the emitted core electron, and ϕ is the work function of the spectrometer. The excess energy found after the ionization process must appear as translational energy of the products. Because the kinetic energy of the emitted electron can be measured and the spectrometer work function and the photon-source energy are known, the binding energy can be calculated accurately. The binding energy of the electron is the ionization energy associated with an electron in a specific atomic shell of a specific atom. A schematic of the one-electron process is shown in Figure 2.9.2.

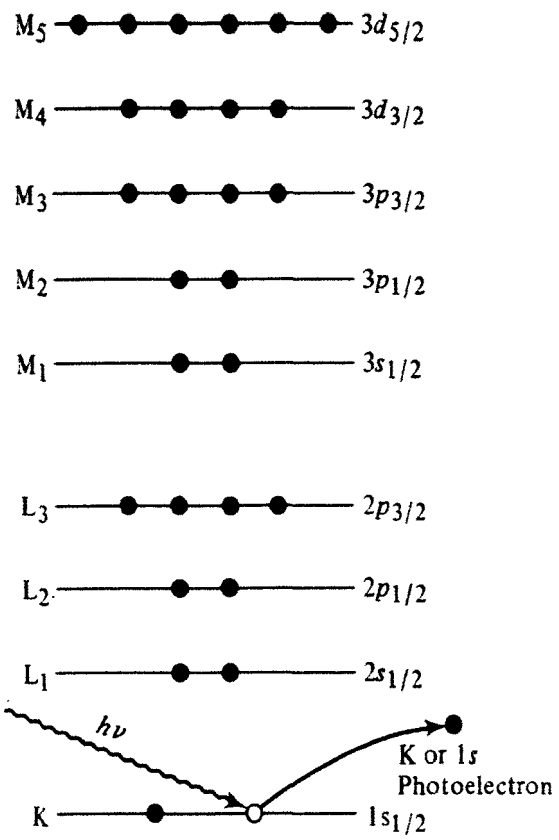

Figure 2.9.2. Diagram of the Photoelectric Process (99).

The technique can be used to establish the nature of the chemical bonding present in the solid. The binding energy of the emitted electron can be changed or shifted by changes in the chemical environment of the atom. For example, an atom bonded to one or more electronegative atoms will emit photoelectrons of a

slightly lower kinetic energy. The emitted electron has a slightly higher binding energy.

Broadening of the spectral peak can be associated with other phenomena as well. For example, the binding energy E_b of the photoelectron is uncertain. The energy distribution measured is a function of the lifetime of the initial and final states of the atom emitting the electron.

Spectral peaks can be broadened by inherent limitations of the instrument. These include the resolution of the energy analyzer used to sort the electrons by their kinetic energies and the energy distribution of the x-ray source.

Another physical phenomenon that can lead to changes in peak shape is electron inelastic collisions. If a photoelectron is involved in an inelastic collision between the time it is emitted and the time it is subsequently detected, a measurable loss of electron energy occurs. The reduction in the kinetic energy of the

photoelectron gives the appearance of a higher binding energy for the electron. Under these circumstances, the peak tails toward higher binding energy.

The XPS technique is useful for studying the nature of the bonding present in surface-treated organic polymers. Toshihura and Pavlath (100) fluorinated the surfaces of polyethylene, polypropylene, polystyrene and polymethyl-methacrytlate using glow discharges of several inorganic fluoride gases. The authors investigated plasma surface treatments using NF_3, SiF_4 and BF_3. Post-etch surfaces were analyzed using XPS. The carbon 1s peak was deconvoluted to establish the nature of the bonding. The C1s peak shifted from 285 eV for CH_2 to 294 eV for CF_3, depending on the plasma exposure.

2.10 Chemometrics

2.10.1 Design of Experiments (101, 102)

One of the key objectives of any statistical method is to identify and describe the relationship between influencing factors and a response. In the context of experimental design, these factors are identified as the exploratory variables. Correlations, whether strong, weak or non-existent, can be used to establish the relative influence of variables on an outcome and establish any dependence between the exploratory variables and the response variables.

Non-random variability in a response can be caused by many different factors. These factors, commonly referred to as lurking variables, need to be tightly controlled if meaningful correlations are to be established with a minimum of error. These parameters are held constant in the experimental design. For example, variations in material composition, thin film density, surface contamination and surface morphology can lead to variation in a response variable.

To further complicate the analysis, many confounding factors are associated with the plasma process itself. The reactivity of the plasma can be influenced by reactive gas composition, power density, ion energies, electron temperature, electron density, pressure, substrate temperature and gas diluent to name a few.

For this application, it is of paramount importance to use chemometrics to define parametric interactions and establish the dependence of response variables. The random effects of lurking variables can be minimized using a properly designed experimental matrix. This study requires a multifactorial design and multivariate analysis. The following tables contain a list of exploratory variables, response variables and lurking variables.

Table 2.10.1. Exploratory Variables

Power Density
Pressure
Reactive Gas Concentration
Gas Etchant

Table 2.10.2. Response Variables

Silicon Reaction Rate
Silicon Dioxide Reaction Rate
Etch Anisotropy

Table 2.10.3. Lurking Variables

Gas Flow Rate
Electrode Temperature
Electrode Spacing
Surface Area
Electrode Material
Excitation Frequency
Diluent Gas
Wafer Placement
Wafer Temperature
Gas Purity
Sample Pattern

2.10.2 Error Propagation and Analysis

The propagation of uncertainty in the reported data was determined using classical statistical methods (101, 103). For multiple measurements on a sample, the arithmetic sample mean was determined:

$$X = \frac{\sum x_i}{N} \qquad (11)$$

The individual measurements are represented by x_i and N represents the number of measurements. Variability in the measurement was determined by repeating the measurement N times and calculating the standard deviation S.

$$S = \sqrt{\frac{\sum (x_i - x)^2}{N-1}} \qquad (12)$$

The standard deviation was used as a representative measure of random error.

If measured data are used in mathematical calculations, errors can propagate. The basic premise for determining error in calculated values is that the total variance is the sum of the individual variances.

$$S^2 = \sum S_i^{\,2} \qquad (13)$$

For addition and subtraction, the total error e_T is determined by:

$$e_T = \sqrt{e_1^{\,2} + e_2^{\,2} + \ldots e_n^{\,2}} \qquad (14)$$

In this case e_1, e_2 through e_n represent the absolute errors associated with the measurements, reported as the standard deviations.

For multiplication and division, calculations of error propagation are based on the relative error, er_i, for measurement *i*.

$$er_i = \left(\frac{S_i}{X_i}\right) \times 100 \qquad (15)$$

Once relative errors are determined, the total error for the calculated value can be determined using:

$$e_T = \sqrt{(e_1\%)^2 + (e_2\%)^2 + \ldots (e_n\%)^2} \qquad (16)$$

Silicon

The silicon etch rate was determined using four measurements:

1. initial mass of the silicon sample m_i,
2. final mass of the silicon sample after plasma exposure m_f,
3. area of the silicon sample A,
4. time of plasma exposure t.

The initial and final mass measurements were made using a microbalance. The balance was zeroed before each set of mass measurements and checked for calibration after each set of mass

measurements. The standard deviation of seven measurements on the same sample was used to establish random error. The density of silicon was determined by measuring the mass for a measured volume of silicon wafer. Area was determined using the density of silicon and the measurement of wafer thickness using a micrometer. The area calculation was also done using a ruler having millimeter increments, readable to +/- 0.5 mm. Square samples were measured for length and width to establish the area. A typical plasma exposure time was five minutes. However, under many conditions, it took as long as 10 seconds to stabilize the plasma environment.

An example of a calculation of silicon etch rate follows:

$$R_{Si} = \frac{m_i - m_f}{\rho A t} \qquad (17)$$

where:

m = initial and final masses, g
ρ = density of silicon at 298 K, 2.33 g/cm^3
A = area of silicon sample, 2.25 cm^2
t = time of plasma exposure, 5 min.

$$= \frac{0.25318000(\pm 0.00000015) - 0.25296250(\pm 0.00000015)}{2.33 \times 2.25(\pm 0.10_6) \times 5.00(\pm 0.16_7)}$$

$= 8.30 \times 10^{-6}$ cm/min

$= 83.0(\pm 4.8)$ nm/min

The random error associated with the silicon etch rate is approximately 5.8%.

Silicon Dioxide

The reaction rates for silicon dioxide were determined using three measurements:

1. silicon dioxide thickness before plasma exposure,
2. silicon dioxide thickness after plasma exposure,
3. plasma exposure time.

Ellipsometry was used to determine the thickness of the SiO_2 layer. The instrument is extremely accurate (+/- 0.1 nanometer); however, the thickness of the initial oxide could vary as a result of the uniformity of the oxidation process. The post-etch SiO_2 thickness had added variability introduced by the possible non-uniformity of

the plasma exposure. Even though the samples are small, 1.5 cm by 1.5 cm, the non-uniformity of the etch rate can affect uniformity in the final film thickness. As in the case for etching silicon, stabilizing the plasma could take as long as 10 seconds.

An example calculation of the silicon dioxide etch rate is:

$$R_{SiO_2} = \frac{t_{initial} - t_{final}}{time} \qquad (18)$$

where $t_{initial}$ and t_{final} are the thicknesses of silicon dioxide in nanometers. Plasma exposure time is 5 minutes.

$$R_{SiO_2} = \frac{448.0(\pm 0.7) - 411.0(\pm 1.4)}{5.00(\pm 0.17)}$$

$$= 7.40(\pm 0.41) \text{ nm/min}$$

The error in the silicon dioxide etch rate measurement is approximately 5.5%.

Experimental data that seemed inconsistent was tested using a significance test (101) prior to being dropped from the data set. An analysis was made by calculating a test statistic using experimental measurements and comparing the test statistic with a critical "t" value from a student t-distribution. A one-tail test was performed using a 5% level of significance and one degree of freedom for two measurements.

In a specific example, the silicon dioxide etch rate was measured and the average of two measurements found to be 3.44 nm/min. A linear extrapolation through surrounding data points determined the SiO_2 etch rate should be 0.96 nm/min. The extrapolated value was used as the null hypothesis in the test. At a 5% level of significance, the critical "t" value is 6.314. The calculated test statistic is 18.2, well into the rejection region of the distribution. The data point could be dropped from the data set.

2.10.3 Response Surface Methodology (104, 105)

Response Surface Methodology (RSM) is a statistical method that involves using quantitative data from experiments to determine and simultaneously solve multivariant equations. The result of an analysis using RSM is a continuous mathematical function that relates the factors to the measured response. The technique is ideally suited for determining how a specific response variable is affected by changes in the levels of key factors.

In the experimental study, three factors (concentration, power and pressure) were investigated for each of the three gas compositions. For each factor, four or five levels were tested. This is a non-symmetrical experimental design since the factors are characterized using a different number of levels.

In developing a model, the change in the response variable y is described as a function of several independent variables x_i.

$$y = f(X_1, X_2, \ldots, X_n) \tag{19}$$

Presenting the dependence of y as an equation for two variables gives:

$$y = a_o + a_1 X_1 + a_2 X_2 + a_{12} X_1 X_2 \tag{20}$$

the coefficient a_{12} represents the effects of the possible interaction of the variables x_1 and x_2. These are typically referred to as confounding estimates. The results of k experiments can be used to estimate the coefficients a_n of the polynomial expression for the response variable y. In the equation, each term represents a main effect if there is only one variable. Each term represents an interaction effect if there is more than one variable. In this research, the surface responses were generated using Origin® from Microcal Software, Inc.

2.10.4 Linear Regression Analysis

Results of the investigation were plotted in two dimensions to illustrate the effect of variation of a single exploratory variable, x_i, on the response variable, y_i. In these cases, the data were plotted using a linear least squares regression analysis (106).

This method of statistical analysis is the most commonly used method for determining the best-fit line through experimental bivariate data (x_i, y_i). The criterion for measuring the fit of the line is established by calculating the sum of the squares of the deviations about the line. The summation is done using all of the bivariate data (x_1, y_1), (x_2,y_2), ..., (x_n,y_n).

$$\sum[y_i-(a+bx_i)]^2=[y_1-(a+bx_1)]^2+[y_2-(a+bx_2)]^2+\ldots \\ \ldots+[y_n-(a+bx_n)]^2 \qquad (21)$$

The line that provides the best fit to the data is the line that provides a minimum of the summation.

The determination of the best-fit line was done using the mathematical software program Origin® from Microcal Software, Inc. The software is used to calculate the best-fit line using the following equations:

$$y = a + bx \tag{22}$$

with b equal to the slope of the line and a equal to the y intercept. The slope of the line and intercept are calculated using n data points:

$$b = \frac{n\sum(x_i y_i) - \sum x_i \sum y_i}{n\sum x_i^{\,2} - \left(\sum x_i\right)^2} \tag{23}$$

$$a = \frac{\left(\sum y_i\right)}{n} - b\frac{\left(\sum x_i\right)}{n} \tag{24}$$

3. Experimental Details

3.1 Experimental Design

Several plasma chemistries were investigated using a parallel plate electrode reactor. Nitrogen trifluoride was used as the primary etch gas in a low-pressure reactive plasma. Single crystal silicon and silicon dioxide were etched using nitrogen trifluoride in argon or mixtures of nitrogen trifluoride with either dichlorodifluoromethane or molecular chlorine in argon. Plasma pressure, power density and the concentration of reactive gas in the argon diluent were varied and etching characteristics were determined. The experimental conditions used in the investigation are shown in Tables 3.1.1, 3.1.2 and 3.1.3.

Table 3.3.1 contains the experimental conditions using nitrogen trifluoride and argon. Experimental work done using mixtures of nitrogen trifluoride, dichlorodifluoromethane and argon is illustrated in Table 3.1.2. Mixtures of nitrogen trifluoride, chlorine and argon were also tested and the experiments are described in Table 3.1.3.

Table 3.1.1. Experimental Conditions for Nitrogen Trifluoride in Argon Plasmas

NF_3 in Ar	Power	Pressure
(vol %)	(watts)	(mtorr)
25	250	400
	250	600
	250	700
	250	800
	500	400
	500	800
	750	400
	750	800
	1000	400
	1000	600
	1000	700
	1000	800
50	625	600
75	250	400
	250	600
	250	700
	250	800
	1000	400
	1000	600
	1000	700
	1000	800

Table 3.1.2. Experimental Conditions for 25% Nitrogen Trifluoride, Dichlorodifluormethane in Argon Plasmas

CF_2Cl_2 (Volume %)	Power (watts)	Pressure (millitorr)
19	250	400
	250	600
	250	700
	250	800
	500	400
	500	800
	750	400
	750	800
	1000	400
	1000	600
	1000	700
	1000	800
31	625	600
62	250	400
	250	600
	250	700
	250	800
	500	400
	500	800
	750	400
	750	800
	1000	400
	1000	600
	1000	700
	1000	800

Table 3.1.3. Experimental Conditions for 25% Nitrogen Trifluoride, Chlorine in Argon Plasmas

Cl_2 (volume %)	Power (watts)	Pressure (millitorr)
19	250	400
	250	800
	1000	400
	1000	800
31	625	600
62	250	400
	250	800
	1000	400
	1000	800

Unpatterned silicon and silicon dioxide were etched in the first set of experiments. In these experiments, the goal was to establish reaction rates for both single crystal silicon and silicon dioxide. For each experiment, samples of both silicon and silicon dioxide were placed in the plasma reactor. Reaction selectivity was subsequently determined by calculating the ratio of the silicon etch rate to the silicon dioxide etch rate. Trends in etch rate and selectivity were then correlated with operating conditions. In a separate study, etch

profiles for patterned silicon were obtained using scanning electron microscopy (SEM). Pattern anisotropy trends for various plasma compositions and conditions were established. In the anisotropy study, sidewall passivation chemistry was investigated using XPS.

Chemometric techniques were used to establish the dependence of response variables on operating conditions of the plasma. A multi-factor, multi-level non-symmetric experimental design was used to investigate the effect of plasma operating parameters on the etch characteristics. Three factors were tested in the experimental design: the concentration of reactive gas in argon, the input power to the plasma and the plasma operating pressure. The experimental matrix had three concentration levels, five power levels and four pressure levels. For all experiments, the total gas flow rate was maintained at 16 standard cubic cm^3/min and the substrate temperature was maintained at 24°C (+/- 1°C). A typical sample was etched in the plasma for five minutes. The data were used to establish the dependence of the reaction rate and reaction selectivity on the operating parameters.

Investigations were also done on etching directionality obtained from the patterning process. Etch directionality or anisotropy was studied for various operating conditions of the plasma and types of etchant mixtures used. Etch profiles for patterned silicon were obtained using SEM. XPS was used with a 20 degree take-off angle to establish a correlation between sidewall passivation film composition and etch anisotropy.

In the anisotropy study, several plasma parameters were investigated as independent variables. The effect on anisotropy was then measured. The reactive gas compositions used were nitrogen trifluoride in argon or nitrogen trifluoride mixed with dichlorodifluoromethane in argon. The plasma power input was varied between 250 and 1000 watts. The halogen-bearing gas concentration was varied between 25 to 87 volume percent. Plasma pressure was varied between 400 and 800 millitorr. In the investigation, single crystal silicon with a <111> crystallographic

orientation was etched. The silicon was masked with two μm wide parallel aluminum lines using a process described in Chapter 3.2. The spacing between the lines was five μm.

3.2 Sample Preparation

Samples of p-type single crystal silicon wafers, boron doped to a density of 10^{19} atoms/cm^3, were obtained from Virginia Semiconductor, Fredericksburg, VA. The wafers were three inches in diameter and the crystallographic orientation was either <100> or <111>.

The wafers were cleaned prior to processing using the standard RCA clean (34). The cleaning process involves using a 5:1:1 ratio of deionized water to 30% hydrogen peroxide to 29% ammonium hydroxide (cleaning solution #1) to remove organic contamination. The cleaning process further involves using a 5:1:1 ratio of deionized water to 30% hydrogen peroxide to 37% hydrogen chloride (cleaning solution #2) to remove ionic contamination. All

chemicals were electronic grade and supplied by J.T. Baker Chemical Corporation. The wafers were immersed in RCA cleaning solution #1 at 75 °C for five minutes, rinsed using 18.3 megaohm-centimeter deionized water, immersed in RCA cleaning solution #2 for five minutes at 65 °C, rinsed using 18.3 megaohm-centimeter water, immersed in a dilute 10:1 solution of water to 49% hydrofluoric acid, rinsed in deionized water and spun dry.

For the silicon dioxide etch rate determination, three-inch diameter p-type <100> silicon wafers were oxidized to a thickness of approximately 0.40 μm in an atmosphere of steam at 1100 °C. The oxidation was done using a four-inch diameter Centigrade Systems, Inc. furnace with a flat zone of approximately one foot. The oxidation took approximately 30 minutes. A gaseous stream of nitrogen saturated with water vapor was generated and introduced into the furnace. Air Products high-purity nitrogen was fed through a glass bubbler filled with 18.3 MΩ-cm deionized water heated to 80°C. The nitrogen was generated from the boil-off of a liquid

nitrogen cryogenic dewar and fed to the bubbler at a flow rate of two l/min.

The silicon wafers and oxidized silicon wafers were then backside scribed using a diamond scribe and broken into 1.5 cm by 1.5 cm square pieces to be used in the plasma reactor. The surface area being etched has an effect on the reaction rate in the plasma (16). The larger the surface area, the lower the reaction rate. As a result, the surface area of the samples used in this investigation was maintained at a constant value.

The backsides of the samples were then labeled using a diamond scribe. Immediately prior to etching, the silicon and silicon dioxide samples were cleaned using J.T. Baker Electronic Grade acetone, rinsed in 18.3 MΩ-cm deionized water and blown dry using high purity 4.8 grade nitrogen from BOC Group, Inc.

Surface contamination of silicon during storage and surface cleaning chemistry was recently studied using GC/MS and IR

spectroscopy (35). Samples of silicon were RCA cleaned and exposed to either a clean room environment or stored in a polypropylene container. The researchers showed that low boiling organic contaminants tend to adhere almost immediately to a cleaned surface of silicon. Acetone was shown to be an effective solvent for the removal of contamination accumulated during storage.

For etch anisotropy determinations, samples of silicon were prepared using standard wet chemical etching to obtained parallel lines two μm wide with five μm spaces (36). Samples of p-type single crystal <111> silicon were prepared for anisotropy studies using an aluminum mask. Figure 3.2.1 shows a flow diagram of the necessary steps required to obtain the final image on the silicon wafers. In each step, a cross-sectional view of the surface of the silicon wafer is presented.

Twelve three-inch diameter wafers were positioned on a planetary platform of the Indel electron beam evaporator. The evaporation chamber was pumped using a cryogenic pump to

3 x 10^{-7} torr and the wafers were coated with approximately 500 nm of aluminum. The evaporation was done with an electron beam generated using a 7,000-volt filament bias. The aluminum deposition rate was approximately 1.0 nm/sec for approximately eight minutes.

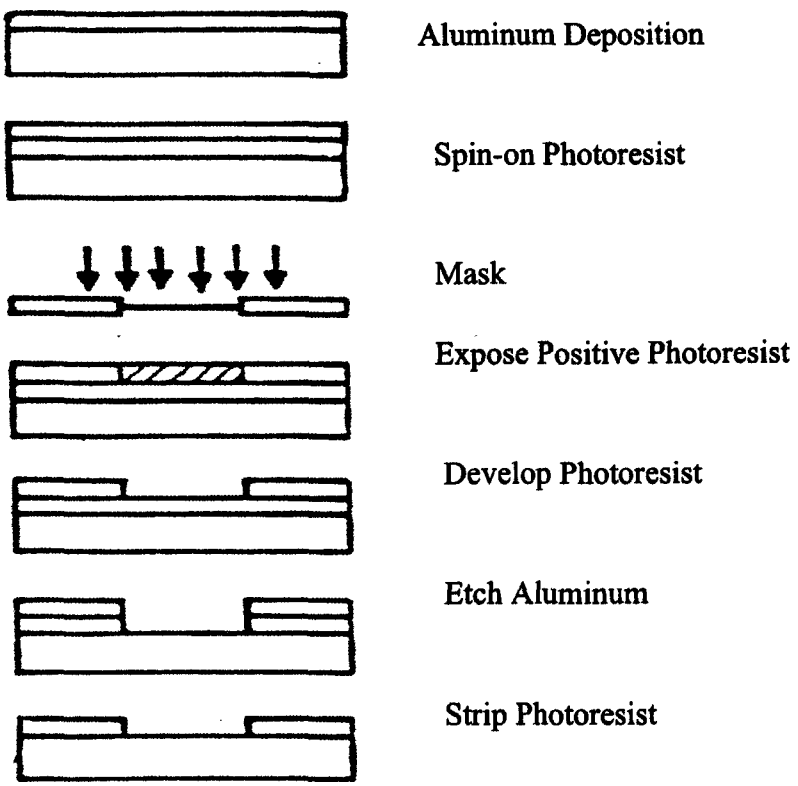

Figure 3.2.1. Flow Chart for Anisotropy Sample Preparation

The aluminum coated silicon wafers were then patterned using photolithography. The wafers were vapor primed using a mixture of 50% hexamethyldisilazine in xylene and coated with Olin Corporation OCG 825 positive photoresist. The photoresist was applied using a spin applicator at 5,000 rpm for 40 seconds. The wafers were then soft baked for 30 min at 100°C. Optical exposure of the photoresist was done using a contact printer manufactured by Karl Suss, Inc., Waterbury, VT. The exposure was for 3.5 seconds at approximately 25 mJ/sec. The image of parallel lines and spaces was developed in Olin Chemical developing solution. The wafers were then rinsed in deionized water, spun dry and hard baked for 30 minutes at 125 °C.

The aluminum was then patterned with lines and spaces running parallel on the surface. An aluminum etch solution, consisting of a 16:1:1:2 ratio of 85% phosphoric acid: 50% acetic acid: 68% nitric acid: water, was used for patterning. The aluminum was etched at a temperature of 46°C for approximately 2 minutes.

After a deionized water rinse, J.T. Baker PR3000 photoresist strip was used to remove the photoresist pattern.

The samples of patterned aluminum on silicon were then broken into 1.5 cm by 1.5 cm square pieces to be used in plasma etch experiments. The samples were exposed to various plasma conditions for a sufficient time period to determine the degree of undercut of the mask. After exposure to the plasma, the samples were cross-sectioned perpendicular to the aluminum line pattern using a back-side diamond scribe. The post-etched, cross-sectioned samples were then mounted on a sample holder for inspection in the SEM.

3.3 Plasma Reactor

All plasma experiments were done using a Plasma-Therm, Inc. reactor. Model number PK-2440 has 22-inch diameter electrodes and a parallel plate electrode configuration, as shown in Figure 3.3.1. The vacuum chamber and electrode assembly are constructed

of aluminum alloy 6061. The reactor has gases flowing radially from a gas distribution ring at the outer perimeter to the exhaust port located in the center of the lower electrode. The wafer support electrode is fitted with a recessed plate to position the wafers securely on the electrode.

The plasma reactor is pumped using an Alcatel rotary vane vacuum pump. The pump capacity is 17 standard ft^3/min. The pump is suitable for use with oxidizing gases and is charged with Fomblin™ brand perfluorinated lubricating oil. The chamber pressure is controlled using an automatic throttling valve on the exhaust line. The pressure controller was manufactured by Vacuum General, Inc. Vacuum in the chamber was measured using a baratron pressure transducer. All process gases were metered using MKS Instruments, Inc. mass flow controllers. All reactor purge gases were metered using Aalborg rotometers.

The reactor can be operated with either the upper or lower electrode powered. The upper electrode was powered throughout this investigation. This is commonly referred to as plasma etching

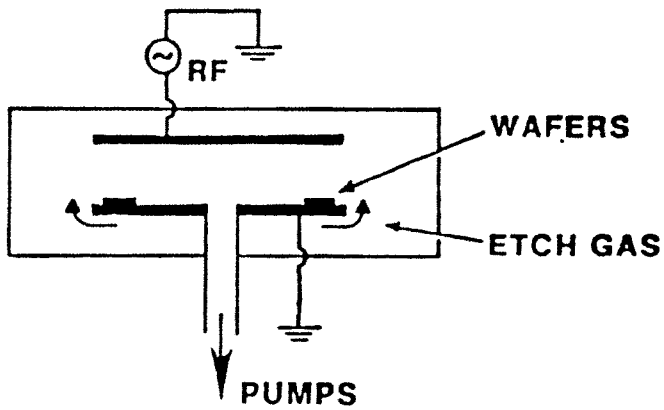

Figure 3.3.1. Schematic of Radial Flow Plasma Reactor

mode. Power is transmitted to the electrodes from a 13.56 Mhz radiofrequency generator. The power supply has a maximum output of 3,000 watts of forward power. The power is coupled capacitively to the load using an automatic matching network. The matching network consists of variable tuning and loading capacitors. Throughout the experiments, the spacing between the electrodes was maintained constant at one cm. The electrode temperature was controlled using a closed-loop refrigeration unit, charged with a solution of 50% ethylene glycol in water. The upper and lower electrode temperatures were maintained between 23 and 25 °C.

3.4 Scanning Electron Microscopy (SEM)

The scanning electron micrographs for this study were typically taken at two levels of magnification. At 4,000X magnification, multiple etched features could be observed. At higher magnification, 10,000X, only one etched surface feature could be observed. The higher magnification was used in all cases to calculate the etch bias for different experimental conditions.

Cross-sections of post-etch patterned silicon were examined for profile variations as a function of the plasma operating conditions. A Philips SEM model XL30 was used for the majority of the microscopy work. A JOEL, Ltd. SEM model JSM-6300F was periodically used throughout the study to evaluate surface etching characteristics.

Typical samples of silicon were patterned with aluminum. All samples were mounted on a vertical aluminum sample holder using conductive carbon tape. The 8 mm wide tape was purchased from Ted Pella, Inc. Samples were typically examined using 20 to 25 kV electron gun voltage. The filament current was saturated at approximately 8 μamps. A typical working distance from the sample was 10 mm and operating pressure for the SEM chamber was 2 X 10^{-5} mbar. Sample magnification was either 4,000 or 10,000.

Samples periodically had to be sputter coated to minimize sample charging. For these samples, approximately 1.5 to 3.0 nm of

precious metal was sputter deposited onto the sample surface. The Polaron Model E5100 Sputter Coater was used for this operation using a gold-palladium source. Argon gas was used to purge the vacuum chamber to a base pressure of 0.040 torr. Typically, a source voltage of -2.5 kV was used, which generated a current of about 5 mamp. The coating was deposited for approximately 30 seconds.

3.5 Ellipsometry

Ellipsometry was used throughout the study to determine the thickness of silicon dioxide before and after exposure to the plasma environment. A Rudolph Research, Inc. ellipsometer, Model Auto EL shown in Figure 3.5.1, was used with automatic null location (37).

The measurement involves using a collimated beam of polarized, monochromatic visible light incident on a transparent surface. The incident light is generated using a low power helium-neon laser with an optical output wavelength of 632.8 nm. The laser

is positioned at a fixed angle of incidence of 70° to the surface being analyzed. Figure 3.5.2 is a schematic of a typical laser ellipsometer (37).

Prior to each set of measurements, a sample of known thickness was run to check the instrument accuracy and the sample mounting stage was leveled using an optical leveling system. For each silicon dioxide sample, two measurements of film thickness were made and the average of the measurements is reported.

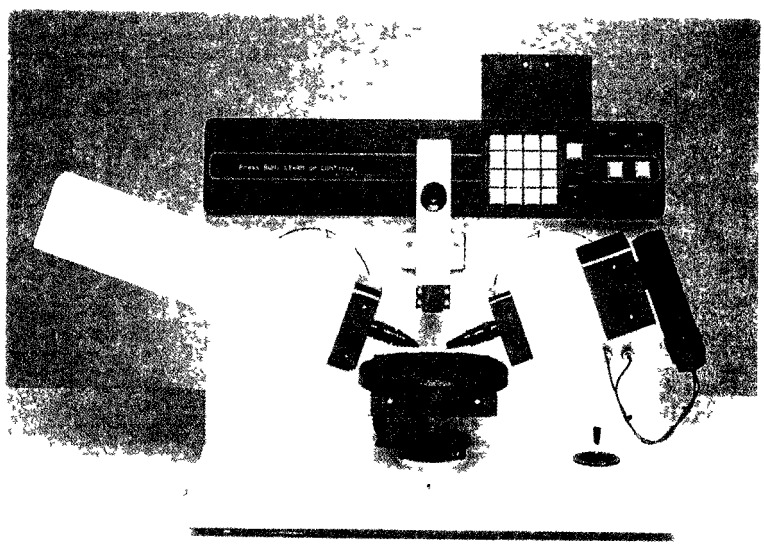

Figure 3.5.1. Rudolph Research Ellipsometer (37)

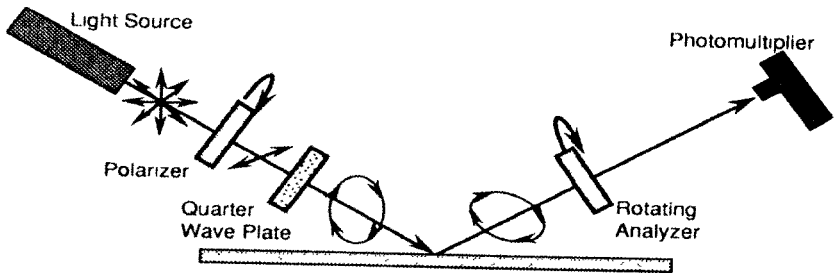

Figure 3.5.2. Schematic View of Ellipsometer (37)

3.6 Profilometry

Etch rates of silicon for selected plasma conditions were confirmed using step height measurements or profilometry using a Tencor Instruments profilometer. Measurements were taken before and after plasma exposure and the difference in step height was used to establish the reaction rate of silicon.

Prior to each use, the calibration of the Tencor Alpha Step Model 200 was checked using an 82.4 nm standard purchased from VLSI Standards, San Jose, CA. The step height measurement technique uses an extremely sensitive 12 μm stylus and drags the stylus over the surface. As the stylus moves across the surface,

contours and discontinuities of the surface are recorded. Three measurements were made for each sample, and the average step height was used to calculate silicon etch rate.

3.7 X-ray Photoelectron Spectroscopy

XPS was used to establish correlations between etch anisotropy and the composition of the post-etch film on the surface. The surface analysis was done using the Scienta ESCA-300 spectrometer. Measurements from the XPS instrument were used to establish the nature of the bonding in the surface layers after exposure to the plasma.

The system has a water-cooled aluminum anode that rotates at approximately 10,000 rpm. The instrument source is a narrow energy distribution of Al K-alpha x-rays obtained using a monochromator. The beam is focused on an area of approximately 40 mm^2. The take-off angle can be varied between 0 and 90° so angle-resolved measurements can be made.

For each sample, a survey scan was taken initially, followed by a high-resolution scans. The scans were taken using transmission lens mode and sweep acquisition mode. Survey scans took 5.5 minutes and used one sweep in 1 electron-volt steps at a rate of 0.30 sec/step and a pass energy of 300 electron-volts. High resolution scans took 17 minutes and used ten sweeps in 0.05 electron-volt steps at a rate of 0.30 seconds per step and a pass energy of 150 electron-volts.

3.8 Microbalance

Mass measurements were made before and after etching the silicon samples. The difference in mass was used to determine the etch rate. All mass measurements were made using a Mettler Corporation microbalance model number M5. Prior to and immediately following a set of measurements, the balance was calibrated using a 200 mg standard purchased from Christian Becker Corporation, New York, NY. Each silicon mass was measured twice and the average mass used to calculate etch rate.

4. Results and Discussion

4.1 Plasma Etching Using Nitrogen Trifluoride in Argon

Figure 4.1.1 is a response surface of reaction selectivity using a plasma of 25% NF_3 in argon. The response surface is a plot of the silicon to silicon dioxide reaction selectivity as a function of power and pressure. The correlation is shown for input powers ranging from 250 to 1,000 watts and operating pressures ranging from 400 to 800 millitorr.

At a low pressure of 400 millitorr, a power increase from 250 to 1,000 watts decreases reaction selectivity. At an operating pressure of 800 millitorr a similar trend is observed. Silicon to silicon dioxide reaction selectivity decreases as the power input increases. Selectivity values range from 10 to 30 at low pressure and from 10 to 85 at high pressure.

In Figure 4.1.1, there is a strong positive correlation between reaction selectivity and operating pressure. An increase in selectivity from 30 to 85 occurs on increasing the operating pressure from 400 to 800 millitorr at fixed power. Reaction selectivity is least sensitive to pressure increases at high power densities. At 1,000 watt power input, the increases in silicon and silicon dioxide etching rates are comparable as the pressure is increased.

At low power and high pressure, ion bombardment is minimized. Operating at low power minimizes the plasma potential and the degree of ion enhanced etching. The high pressure reduces the mean free path in the plasma. As a result, ion collisions further reduce ion energies. At a high power of 1,000 watts, reaction selectivity remains fairly constant. The etching occurs with a significant ion enhanced component, thereby minimizing losses associated with collision events. A more detailed analysis of reaction selectivity is obtained by examining the silicon and silicon dioxide response surfaces separately.

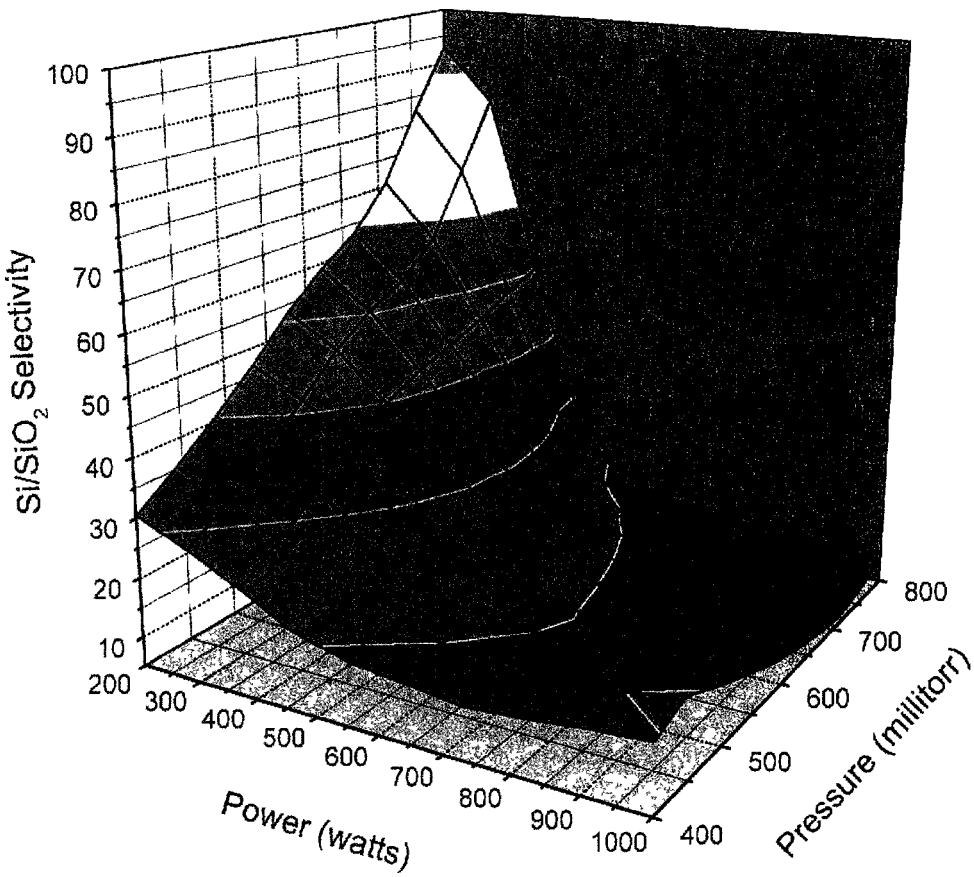

Figure 4.1.1. Reaction Selectivity Response Surface for Nitrogen Trifluoride in Argon

Figure 4.1.2 is a response surface of the silicon etch rate as a function of power and pressure for a 25% NF_3 in argon plasma. At a power input of 250 watts, the etch rate of silicon increases from 40 to 90 nm/min as the pressure is increased from 400 to 800 millitorr. At a fixed pressure of 400 millitorr, the silicon etch rate increases from 40 to 100 nm/min as the power is increased from 250 to 1,000 watts. At high power density, the etch rate of silicon is relatively insensitive to increases in pressure.

For 25% nitrogen trifluoride in argon, a low power input of 250 watts generates a plasma that is etch rate responsive to increases in pressure. The higher pressure increases the number density of fluorine atoms and other reactive species in the plasma. As a result, a doubling of pressure presents a near doubling of the silicon etch rate.

A trend of increasing silicon etch rate is also evident as power is increased at a fixed pressure of 400 millitorr. An increase in

power from 250 to 1,000 watts results in further dissociation and ionization of the plasma. The increased dissociation presents a

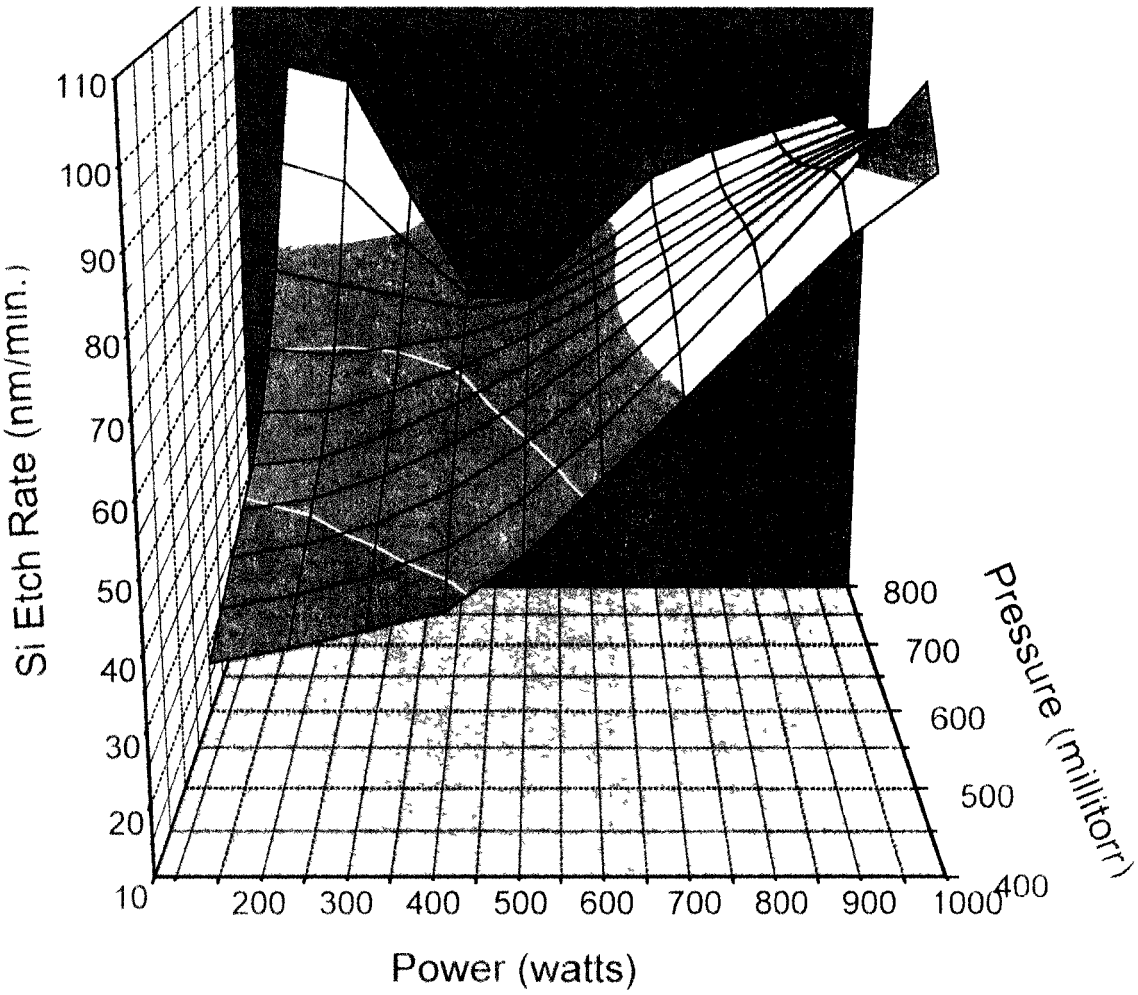

Figure 4.1.2. Response Surface for Silicon Etch Rate for Nitrogen Trifluoride in Argon

higher concentration of reactive species to the surface. The higher power input also provides higher ion energies, which further enhance the removal rate of silicon.

Figure 4.1.3 is a response surface of the silicon dioxide etch rate using 25% nitrogen trifluoride in argon. The silicon dioxide etch rate is plotted as a function of input power and operating pressure. At low input power, the silicon dioxide etch rate is minimally dependent on pressure. At 250 watts, the silicon dioxide etch rate is less than 1 nm/min at pressures ranging from 400 to 800 millitorr.

The correlation between silicon dioxide etch rate and power input is strong and positive. At both low and high operating pressures, an increase in power results in a substantial increase in silicon dioxide etch rate. At 800 millitorr, SiO_2 etch rates increased from 1 to 10 nm/min on increasing the power from 250 to 1,000 watts. The silicon dioxide etch rates increased from 1 to 8 nm/min when the operating pressure was maintained at 400 millitorr.

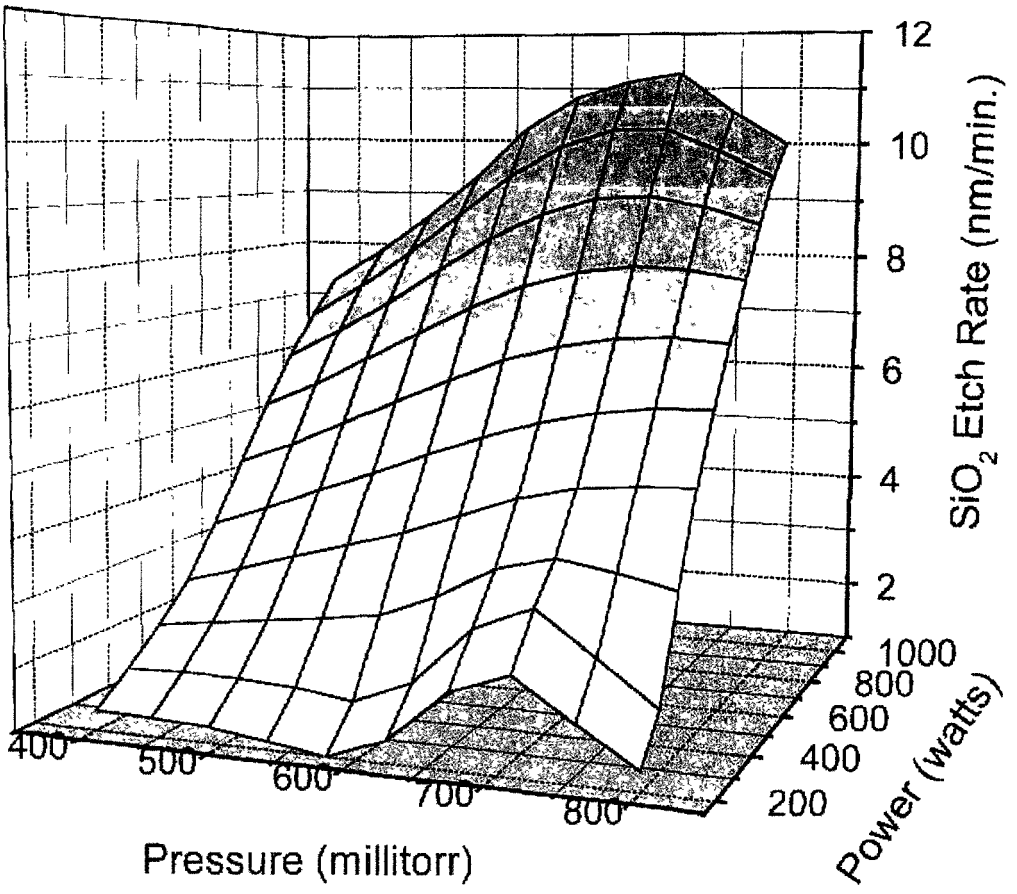

Figure 4.1.3. Response Surface for Silicon Dioxide Etch Rate for 25% Nitrogen Trifluoride in Argon

At low power, regardless of pressure, the etch rate of silicon dioxide is low. Under these conditions, ion energies are low. Silicon dioxide is a relatively hard material compared to silicon. High ion energies are needed to assist in etching. The higher power input levels result in both increased dissociation and higher ion energy levels. The minimum silicon dioxide etch rates occur at low power. In contrast with silicon, high etch rates occur at low power and high pressure. As a result, the highest reaction selectivity occurs under these conditions.

Figure 4.1.4 is a response surface of the silicon to silicon dioxide reaction selectivity at a fixed input power of 250 watts. The selectivity is shown as a function of volume percent nitrogen trifluoride and pressure. At low concentrations of 25% NF_3 in argon, the reaction selectivity increases from 40 to 100 as the pressure is increased from 400 to 800 millitorr. Higher concentrations of NF_3 in argon are not as responsive to increases in operating pressure. A trend of decreasing reaction selectivity is observed as the nitrogen trifluoride concentration is increased. Selectivity decreases

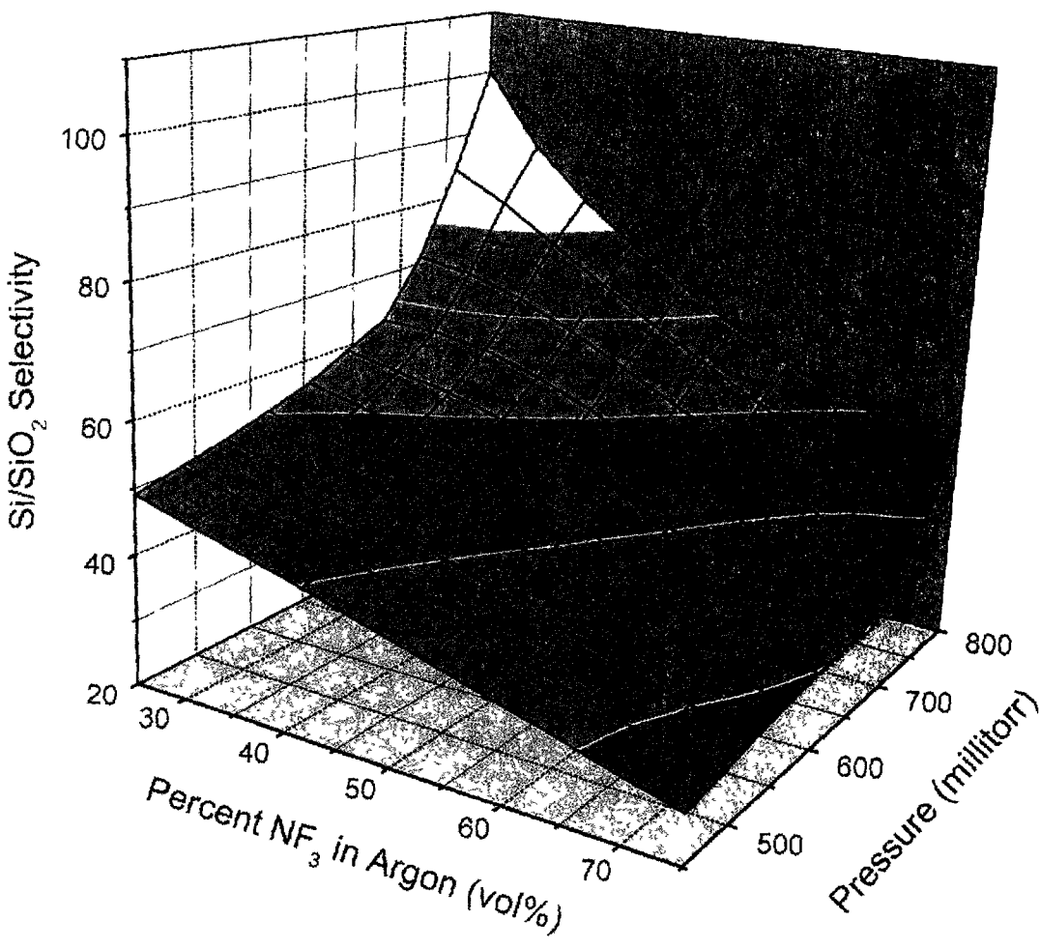

Figure 4.1.4. Reaction Selectivity Response Surface for Nitrogen Trifluoride in Argon

from 100 to 50 as the concentration of NF_3 is increased from 25 to 75% at 800 millitorr. A decrease of lesser magnitude is observed as the NF_3 concentration is decreased at a pressure of 400 millitorr.

Higher concentrations of reactive gas in the plasma should result in higher reaction rates. The increased concentration of NF_3 in the feed gas can provide a higher density of monatomic fluorine atoms for etching. The etching of both silicon and silicon dioxide would increase as a result. The etching may be influenced by another reaction.

Complete dissociation of nitrogen trifluoride may be difficult at high concentrations. In this study, a plasma could not be generated when using NF_3 concentrations higher than 80%. Halogen atoms are electronegative and an electron scavenger. At high concentrations of NF_3, electron loss mechanisms dominate making plasma generation difficult. At low concentrations of NF_3, argon is present in high concentrations. An ionization event with an argon

atom results in the generation of an additional electron. As a result, stable plasmas can be formed more easily. A partial dissociation of NF_3 would make available other nitrogen-fluorine reactive species in the plasma. For example,

$$NF_3 + e^- \rightarrow NF_2 + F + e^-$$

The difluoroamine could react preferentially with silicon dioxide to form a gaseous reaction product.

$$NF_2 + SiO_2 \rightarrow NOF_2 + Si$$

Figure 4.1.5 is a response surface of the silicon dioxide etch rate at a fixed power of 250 watts. The silicon dioxide etch rate is shown as a function of volume percent nitrogen trifluoride and operating pressure. As the pressure is increased for the 25% nitrogen trifluoride in argon mixture, the silicon dioxide etch rate increases from 1 to 3 nm/min. Using 75% nitrogen trifluoride in argon, the silicon dioxide etch rate increased from 7 to 10 nm/min

over the same pressure range. In general, as the concentration of nitrogen trifluoride increases, the silicon dioxide etch rate increases.

At low power inputs, the degree of dissociation of the parent etch gas is minimized. A higher concentration of NF_3 would likely result in a lesser degree of dissociation. The reaction rate increases with increases in pressure. Dissociation at higher pressure would be more difficult. Another possibility for the increased silicon dioxide etch rate is an increase in cationic bombardment of the surface. This is unlikely since the degree of ion bombardment would decrease as the pressure in the plasma increased.

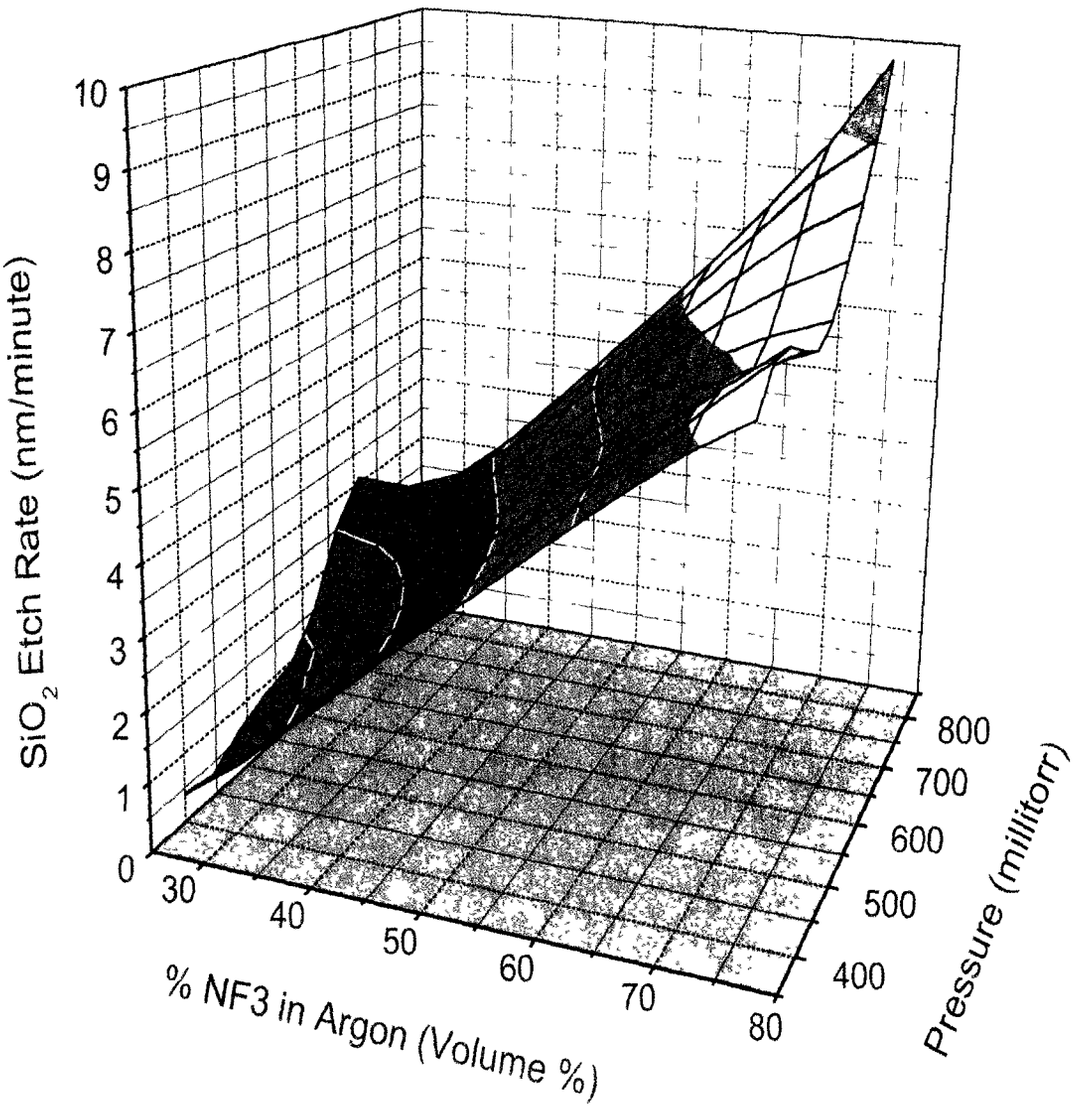

Figure 4.1.5. Response Surface for Silicon Dioxide Etch Rate for Nitrogen Trifluoride in Argon

Silicon and silicon dioxide etch rate data are illustrated graphically in Figure 4.1.6. The silicon dioxide etch rates are presented in blue and the silicon etch rates are presented in black. Data are shown for both 25 and 75% nitrogen trifluoride in argon at a power input of 1,000 watts. The etch rates are shown as a function of operating pressure of the plasma.

For a plasma of 25% NF_3 in argon, changes in pressure have a minimal effect on the etch rate of silicon dioxide. At pressures from 400 to 800 millitorr, the rates varied between 5 to 6 nm/min. The silicon etch rate has a stronger dependence on operating pressure of the plasma. For 25% NF_3 in argon at 1,000 watts, the same increase in pressure increased the silicon etch rate from 100 to 140 nm/min.

As the concentration of nitrogen trifluoride in argon was increased to 75%, the effect of increasing pressure became more pronounced. At low pressure, the etch rate of silicon was approximately 200 nm/min. At a pressure of 800 millitorr, the etch

rate increased to 850 nm/min. Over the same pressure range, the silicon dioxide etch rate increased from 15 to 50 nm/ min.

The etch rate of silicon increases with increasing pressure and concentration of nitrogen trifluoride. The rate increases are consistent with theory. As the pressure is increased, the number density of fluorine atoms in the plasma increases. The increase in partial pressure of reactive atoms results in an increase in the reaction rate of silicon. As the concentration of nitrogen trifluoride is increased, the potential for fluorine atom generation increases. Higher concentrations of fluorine atoms result in an increase in the reaction rate of silicon.

Silicon dioxide etch rates are strongly dependent on the degree of ionic bombardment of the surface. Maxima in the silicon dioxide etch rate are typical under conditions that favor a high degree of radiation enhanced chemistry, low pressure and high power. For 25% NF_3 in argon, the etch rate of silicon dioxide is nearly independent of operating pressure. In this operating regime,

the etch rate is sensitive to increases in ion bombardment. At 75% NF_3 in argon, the etch rate of silicon dioxide increases over three fold as the pressure increases from 400 to 800 millitorr. Although fluorine atoms are known to react spontaneously with silicon dioxide at room temperature, the etch rate enhancement is larger than is expected using the model developed by Flamm et al. (51). An alternative mechanism may be involved in etching the silicon dioxide.

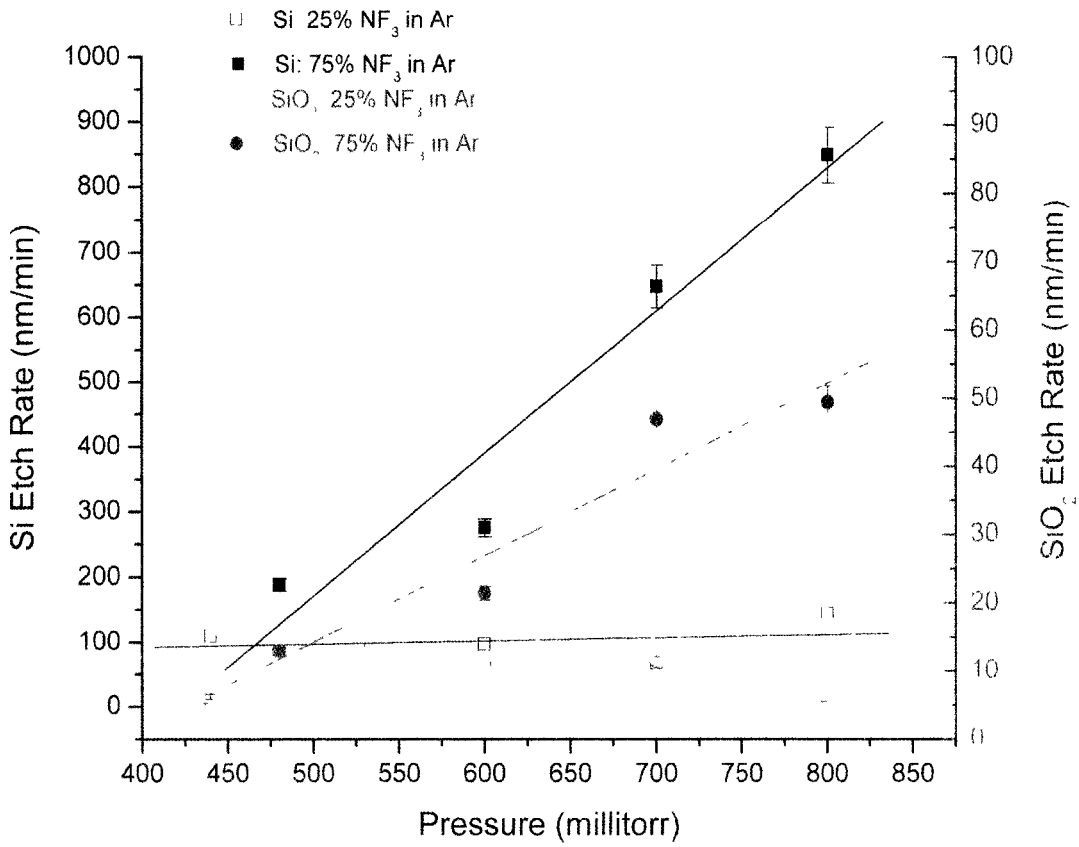

Figure 4.1.6. Silicon and Silicon Dioxide Etch Rates as a Function of Pressure for Nitrogen Trifluoride in Argon

4.2 Plasma Etching Using 25% Nitrogen Trifluoride-Dichlorodifluoromethane-Argon Mixtures

A response surface for silicon to silicon dioxide reaction selectivity using a mixture of 25% nitrogen trifluoride, 19% dichlorodifluoromethane and argon is shown in Figure 4.2.1. Selectivity is shown as a function of power input and operating pressure of the plasma. Power input ranged between 250 and 1,000 watts and pressure ranged between 400 and 800 millitorr.

Reaction selectivity ranged from 57 at low power and high pressure to 3 at low power and low pressure. For higher power input, 1000 watts, the reaction selectivity was maintained in a fairly narrow range. Reaction selectivity varied between 9 and 20 over the range of operating pressures.

Reaction selectivity is maximized under conditions that minimize ion bombardment of the surface. Low power input reduces ion energy and concentration. High pressure reduces ion energy through inelastic collisions. Under these conditions, the extent of

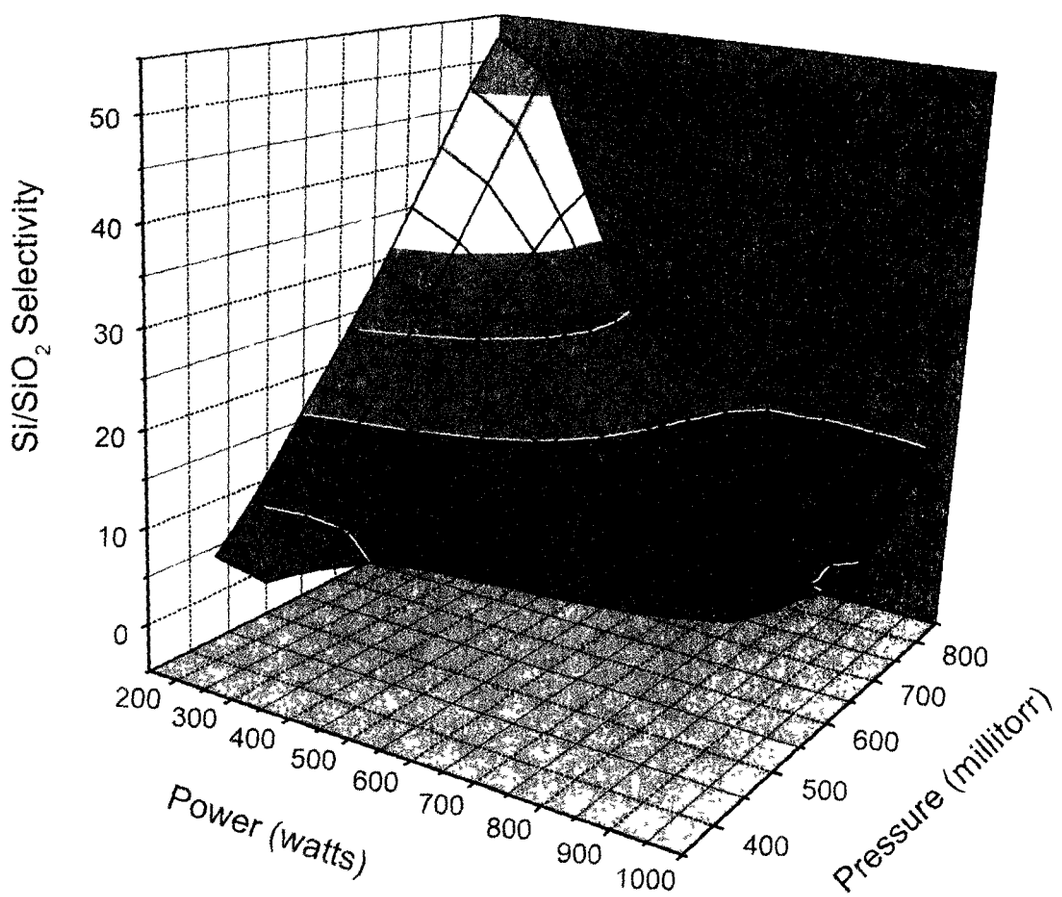

Figure 4.2.1. Reaction Selectivity Response Surface using 25% Nitrogen Trifluoride-19% Dichlorodifluoromethane-Argon

polymer film formation on the surface is likely minimal. As a result, minimal ion clearing is required to etch the surfaces.

A response surface for the silicon etch rate is shown in Figure 4.2.2. The etch rate of silicon is shown as a function of power and pressure for a gas mixture using 25% NF_3, 19% CF_2Cl_2 in argon. At 250 watts, the etch rate of silicon increases from 20 to 480 nm/min as the pressure increases from 400 to 800 millitorr. As the power increases, the etch rate increases to a lesser extent with increasing pressure. At 1000 watts, the etch rate increases from 280 to 400 nm/min.

A maximum silicon etch rate occurs using conditions of low power and high pressure. Under these conditions, polymer film formation is not likely. The formation of a thin layer of polymeric material would probably inhibit the etching rate of silicon. Further, under conditions of low power, the degree of ionization and ion

energy are both at a minimum. As a result, the potential for ion clearing of a polymeric film is minimal.

The silicon dioxide response surface is shown in Figure 4.2.3. Silicon dioxide etch rate is shown as a function of power and pressure for the 25% NF_3, 19% CF_2Cl_2 in argon gas mixture. The silicon dioxide etch rate ranges from 5 to 22 nanometers per minute. The etch rate of silicon dioxide is nearly independent of operating pressure over the range of 400 to 800 millitorr. The power input has a large effect on the silicon dioxide etch rate. At low power, 250 watts, the etch rate varies between 5 to 8 nanometers per minute. As the power is increased to 1000 watts, the silicon dioxide etch rate increases to between 19 and 22 nanometers per minute.

Under conditions of high power, the silicon dioxide etch rate is maximized. At high power levels, two separate mechanisms can contribute to the increased silicon dioxide etch rate. First, high power levels result in high ion concentrations and ion energy. The

increased ion bombardment of the silicon dioxide is believed to enhance reaction rates. The second mechanism for silicon dioxide etching involves the formation of fluorocarbon radicals. Conditions of high input power are more likely to generate difluorocarbene radicals. Difluocarbene radicals are known to react with silicon dioxide, forming volatile reaction products (53,54).

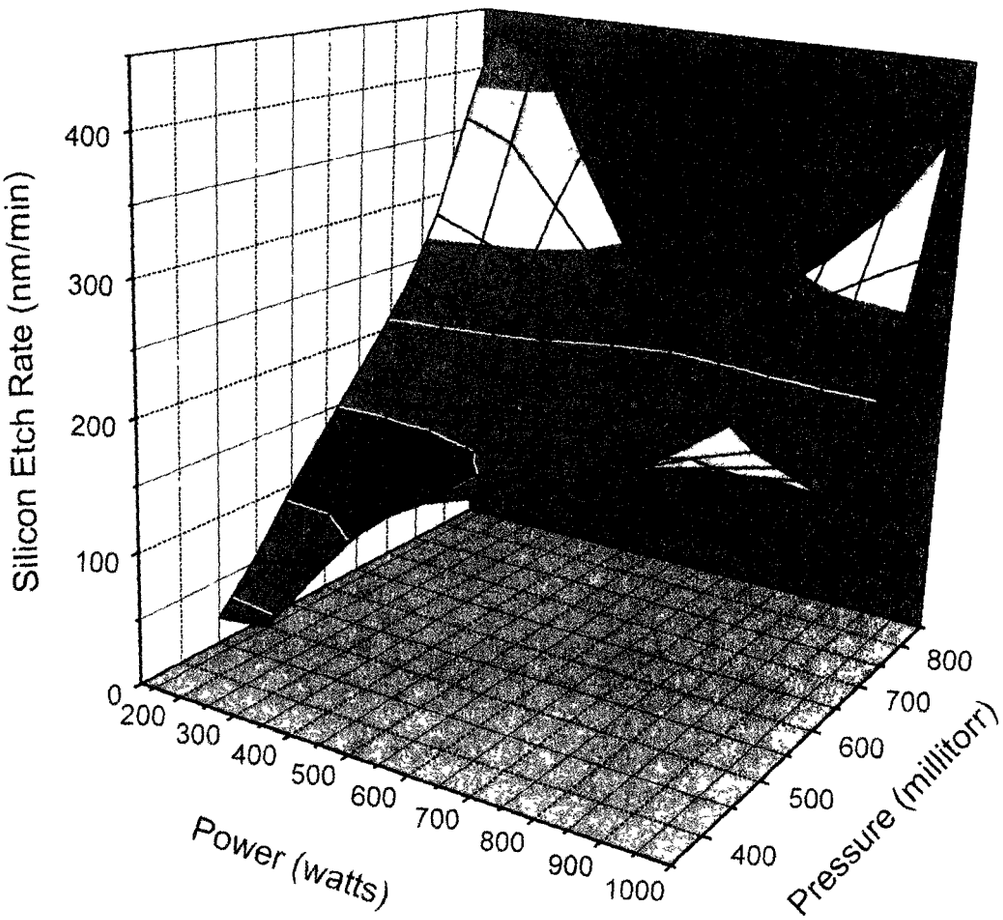

Figure 4.2.2. Silicon Etch Rate Response Surface Using 25% Nitrogen Trifluoride-19% Dichlorodifluoromethane-Argon

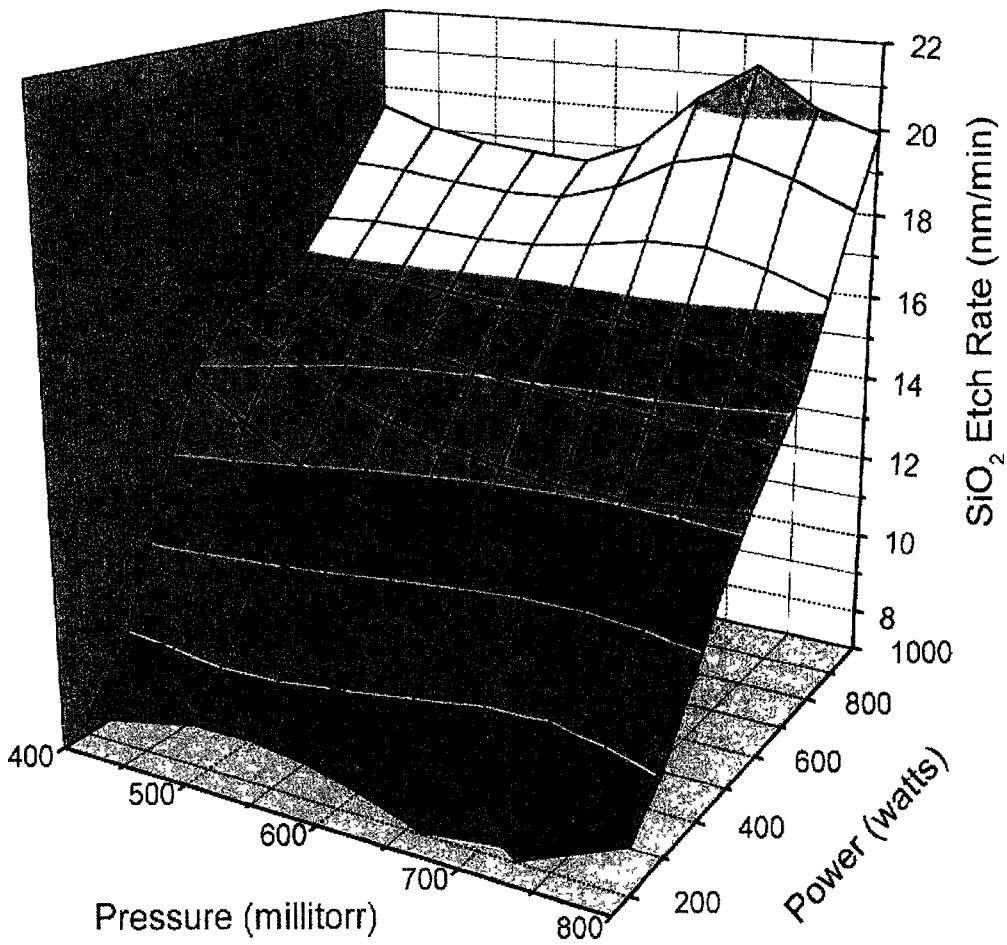

Figure 4.2.3. Silicon Dioxide Etch Rate Response Surface Using 25% Nitrogen Trifluoride-19% Dichlorodifluoromethane-Argon

Silicon etch rates are shown in Figure 4.2.4 as a function of power. The experiment was done using mixtures of 25% NF_3 and varying percentages of CF_2Cl_2 in argon. Etch rate data are shown for concentrations of 19 and 62% CF_2Cl_2 at 400 millitorr and 19% CF_2Cl_2 at 800 millitorr. Least squares regression analysis was used to fit the linear data and a second-order polynomial function was used to fit the nonlinear data.

For a plasma using a 25% NF_3, 19% CF_2Cl_2, argon mixture and a pressure of 400 millitorr, a strong positive linear correlation is observed as a function of power. Etch rates of silicon increase from approximately 20 nm/min at 250 watts to over 250 nm/min at 1,000 watts. At higher operating pressure, a nonlinear correlation with increasing power is evident. At 250 watts, 800 millitorr, the silicon etch rate increased to more than 450 nm/min. As power was increased, the etch rate decreased to a minimum of approximately 250 nm/min. As the power was further increased to 1,000 watts, the etch rate increased to approximately 400 nm/min.

For 19% dichlorodifluoromethane, 25% nitrogen trifluoride in argon at 250 watts, a substantial effect arises due to increased operating pressure of the plasma. On increasing the pressure from 400 to 800 millitorr, the silicon etch rate increases from 20 to nearly 480 nm/min. There was a less substantial effect at other operating concentrations and powers. For 1,000 watts and 19% dichlorodifluoromethane the dependence on pressure was smaller. The silicon etch rate increased from 280 to 400 nm/min as the pressure was increased from 400 to 800 millitorr.

Figure 4.2.5 is a graph of the silicon dioxide etch rate as a function of input power. Data are presented for 25% NF_3, 19% CF_2Cl_2 in argon at 400 and 800 millitorr and 25% NF_3, 62% CF_2Cl_2 in argon at 800 millitorr. For the mixtures using 19% CF_2Cl_2 at a power input of 250 watts, the silicon dioxide etch rate is approximately 7 nm/min. As power input increases to 1,000 watts, the silicon dioxide etch rate increases linearly to approximately 15 to 20 nm/min.

For a plasma of 25% NF_3, 62% CF_2Cl_2 in argon at 800 millitorr, etch rates of silicon dioxide increase linearly as the input power to the plasma increases. The etch rates increase from 15 to 30 nm/min as the power increases from 500 to 1,000 watts.

Under the conditions of low power input, the SiO_2 etch rate is not sensitive to operating pressure. The etch rate of silicon dioxide is likely limited by polymer film formation. The protective layer that forms on the surface is difficult to clear under conditions of low ion bombardment. At high power input, the silicon dioxide etch rate dependence on pressure and dichlorodifluoromethane concentration is more apparent. The increase in power results in an increase in ion energy and an increase in clearing of the surface film. Under conditions of high power, an increase in pressure or dichlorodifluoromethane concentration results in an increase in silicon dioxide etch rate. A higher partial pressure of etchant species accounts for the increased rates.

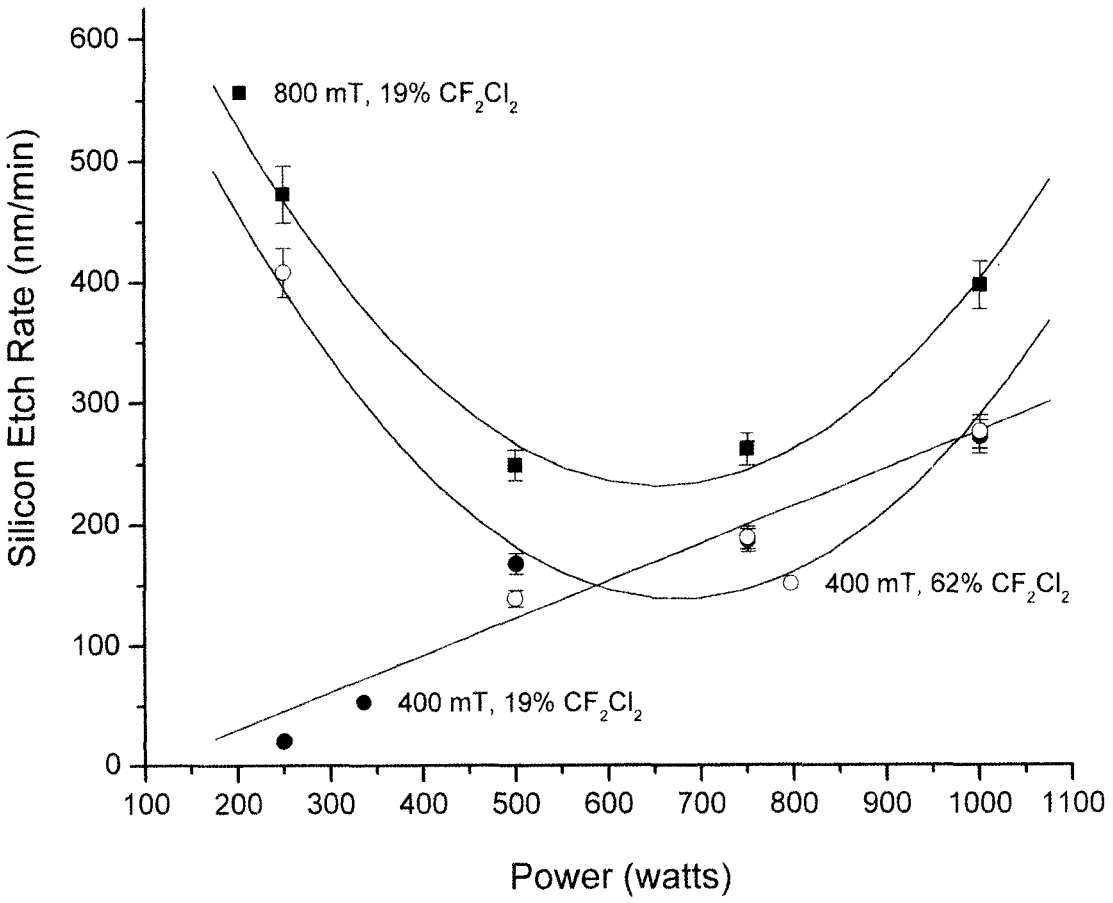

Figure 4.2.4. Silicon Etch Rate as a Function of Power for Dichlorodifluoromethane- 25% Nitrogen Trifluoride-Argon

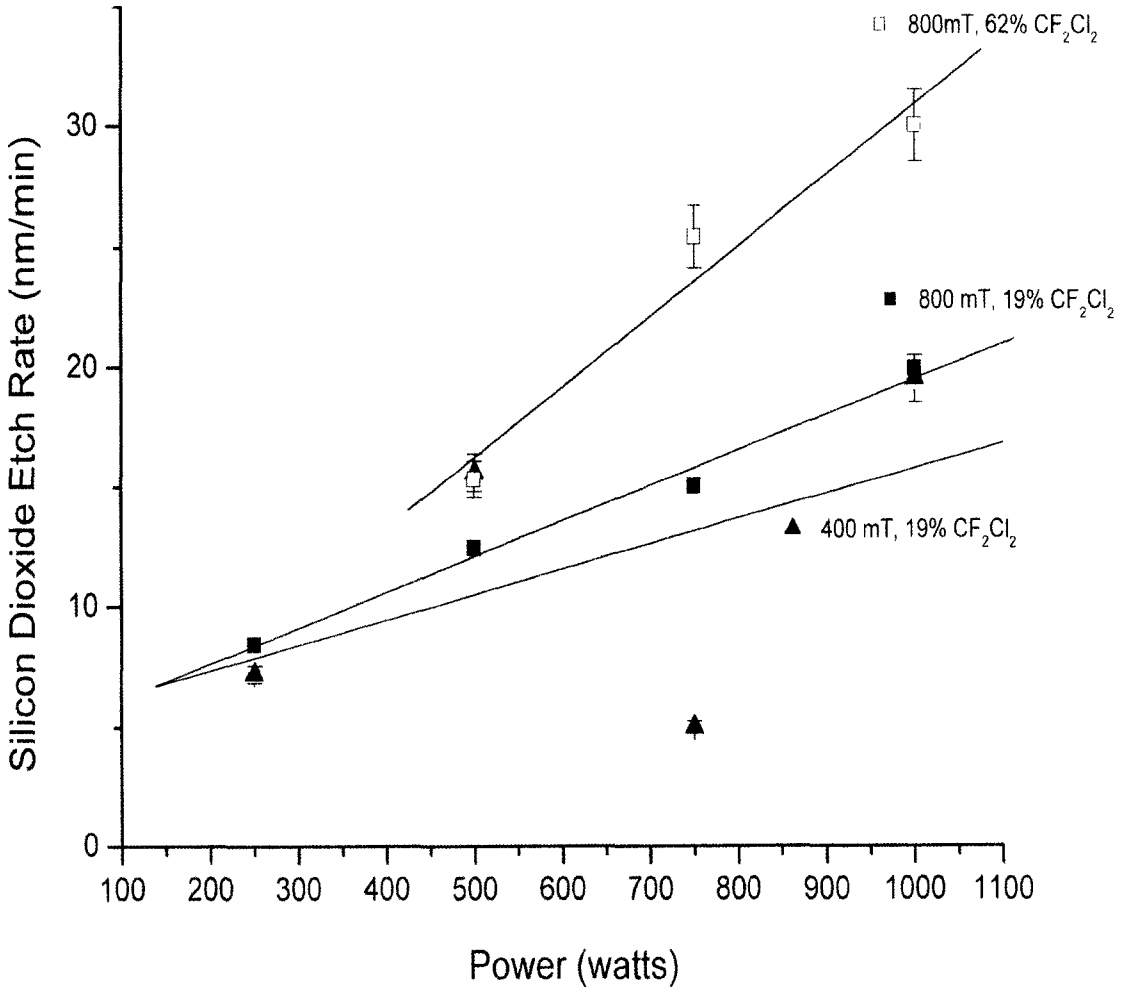

Figure 4.2.5. Silicon Dioxide Etch Rate as a Function of Power for Dichlorodifluoromethane-25% Nitrogen Trifluoride-Argon Mixtures

4.3 Plasma Etching Using Chlorine-Nitrogen Trifluoride-Argon Mixtures

Silicon and silicon dioxide etch rates and silicon to silicon dioxide reaction selectivities are presented in Table 4.3.1. Data are presented for mixtures of 25% nitrogen trifluoride, 19 and 62% chlorine and argon. The etching results are shown for several input powers, pressures and concentrations of chlorine.

As shown in the table, reaction selectivity is highest when the plasma is operated under conditions of low power and high pressure. The highest reaction selectivity, 83, was obtained using 19% chlorine, 25% nitrogen trifluoride in argon operating at 250 watts and 800 millitorr.

These findings are consistent with results reported in Chapter 4.1.1. The highest values of reaction selectivity occur under conditions of minimum ion bombardment. This is a result of the silicon dioxide etch rate sensitivity to radiation enhanced etching.

Selectivity is highest under conditions of minimum ion bombardment.

Silicon etch rates are shown in the table for a 62% chlorine mixture at 800 millitorr. The silicon etch rate shows a substantial increase from 90 to 350 nm/min as the power was increased from 250 to 1,000 watts. Data are also shown for the 62% chlorine

Table 4.3.1. Selectivity and Reaction Rates for Chlorine, Nitrogen Trifluoride and Argon

Cl_2	Power	Pressure	Si Etch Rate	SiO_2 Etch Rate	Selectivity
(vol %)	(watts)	(mtorr)	(nm/min)	(nm/min)	-
62	1000	800	350	21	17
62	1000	420	210	17	12
62	250	800	90	2	54
19	1000	800	220	12	18
19	250	800	330	4	83

mixture at 1,000 watts. The silicon etch rate increased from 210 nm/min at 420 millitorr to 350 nm/min at 800 millitorr.

The silicon etch rate is sensitive to increases in operating pressure and power. Higher pressure provides more reactive gas in the plasma. The higher density of reactive neutral species increases the reaction rate of silicon. At higher power levels, two factors can impact the reaction rate. The increase in power provides a higher electron energy distribution and an increase in dissociation reactions. The increased dissociation provides higher concentrations of reactive species and higher reaction rates. Additionally, the increased power generates higher ion energies. As a result, there can be a substantial increase in radiation enhanced etching of the surface.

Silicon dioxide etch rate depends minimally on plasma operating pressure between 420 and 800 millitorr. For the 62% chlorine mixture at 1,000 watts, the silicon dioxide etch rate increased from 17 to 21 nm/min. The silicon dioxide etch rate is

also shown as a function of input power. For both 19 and 62% chlorine mixtures with nitrogen trifluoride and argon, the silicon dioxide etch rate increases as power increases. The 62% chlorine mixture results in a higher silicon dioxide etch rate compared to the 19% chlorine mixture. The etch rate increases from 12 to 21 nm/min on increasing the chlorine concentration while maintaining the pressure at 800 millitorr and the power at 1,000 watts.

Under these plasma conditions, the silicon dioxide etch rate increases as the density of reactive gas increases. This observation is similar to that of etching silicon. Increases in operating pressure and reactive gas concentration both increase the reaction rate of silicon dioxide.

4.4 Etch Anisotropy using Nitrogen Trifluoride in Argon Plasmas

Figure 4.4.1 is a 400 X optical micrograph of the post-patterned aluminum lines on single crystal silicon.

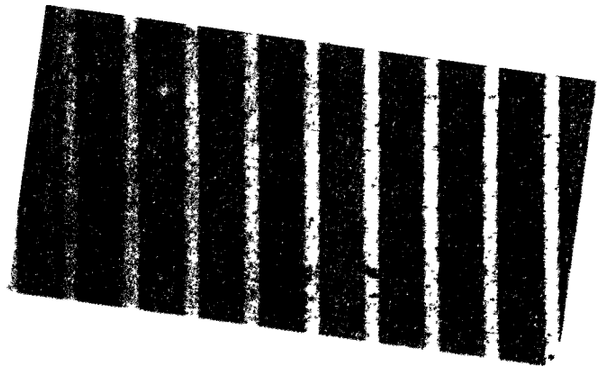

Figure 4.4.1. Optical Micrograph (400X) of Patterned Aluminum on Silicon

Figure 4.4.2 is a 10,000 X scanning electron micrograph of an under-etched silicon sample. The sample is tilted to approximately 80 degrees from the ground plane to more clearly see the aluminum line pattern.

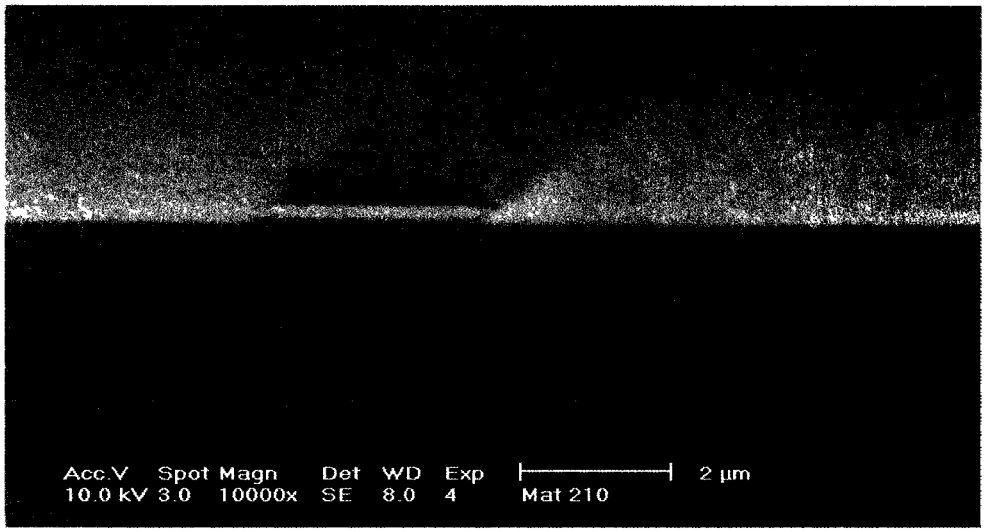

Figure 4.4.2. Under-etched silicon showing aluminum pattern

Experimentation started with a concentration of 25 percent nitrogen trifluoride by volume in argon diluent. The micrographs shown in Figures 4.4.3 and 4.4.4 illustrate an etch profile in single crystal silicon at 4,000 and 10,000 X respectively. An input power of 250 watts and a pressure of 400 millitorr were used. The etch bias was measured and the percent under-cut was calculated to be 74%.

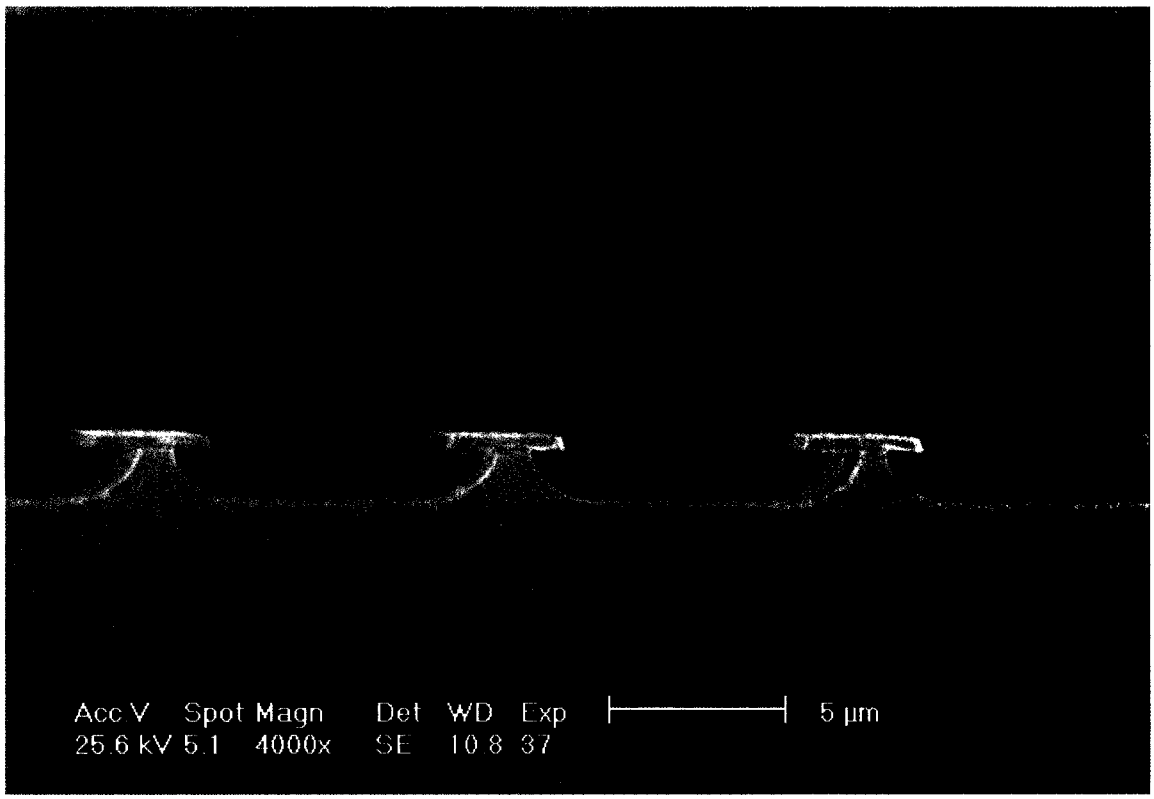

Figure 4.4.3. SEM of etched silicon at 4,000X using 25% NF_3 in argon, 250 watts, 400 millitorr.

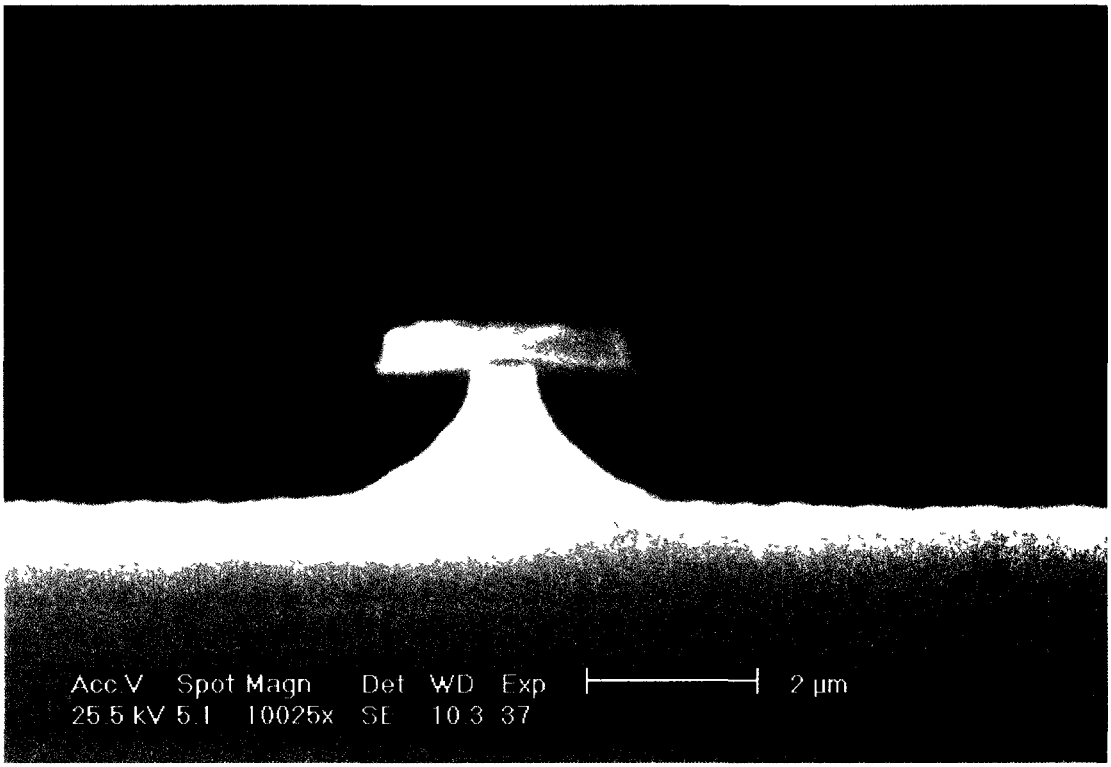

Figure 4.4.4. SEM of etched silicon at 10,025X using 25% NF_3 in argon, 250 watts, 400 millitorr.

Under plasma conditions using 25% NF_3 in Ar, 250 watts and 400 milltorr, atomic fluorine concentrations are likely low. The silicon etch rate under these conditions is only 96 nm/min. The low power input results in a low plasma potential, low ion energy and a low degree of radiation enhanced surface chemistry. The etching occurs in both the lateral and vertical directions at an equal rate. Interestingly, the etching rate is independent of crystallographic

orientation. The vertical etch is in the (111) and the horizontal etch is in several planes (100, 010, 001...,). The etch profile is isotropic.

The micrographs shown below in Figures 4.4.5 and 4.4.6 represent etch profiles for patterned silicon exposed to a plasma of 25% nitrogen trifluoride in argon. The micrographs were taken at 4,000 and 10,000 X magnification, respectively. For these experiments, input power was increased to 1,000 watts. The plasma pressure was maintained constant at 400 millitorr.

The effect of increasing plasma power density is illustrated in the figures. The silicon surface has a channel or notch etched adjacent to the aluminum mask. A channel runs parallel and adjacent to the etched feature. Etch bias was measured and undercut was calculated to be approximately 41%.

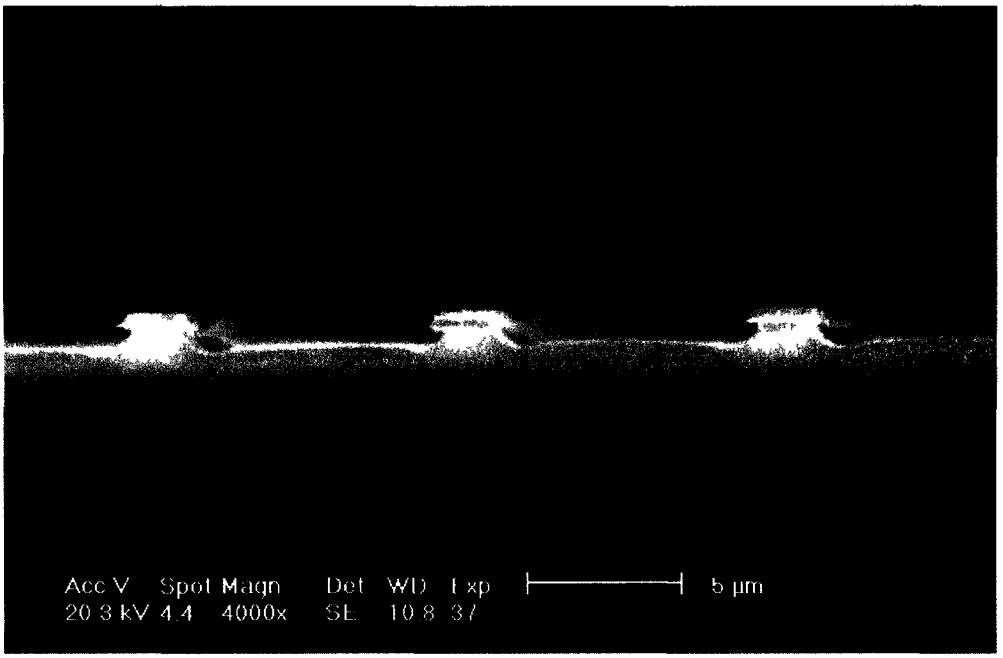

Figure 4.4.5. SEM of etched silicon at 4,000 X using 25% NF_3 in argon, 1,000 watts, 400 millitorr.

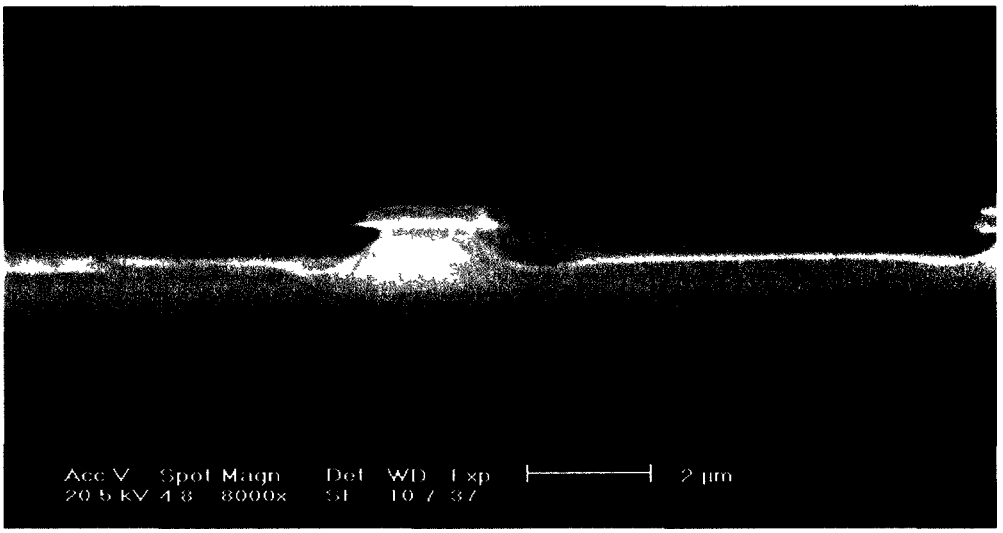

Figure 4.4.6. SEM of etched silicon at 8,000 X using 25% NF_3 in argon, 1,000 watts, 400 millitorr.

For a plasma using 25% NF_3 in argon, 1,000 watts and 400 millitorr, the degree of anisotropic etching is increased. The higher power input affects two plasma characteristics. Both the degree of dissociation and ionization increase. There is an increase in neutral and cation densities in the plasma. As a result of a higher plasma potential, the degree of ion assisted etching increases, thereby increasing anisotropy.

The effect of increasing plasma pressure is shown in the micrograph in Figure 4.4.7. In this case, the pressure was increased to 800 millitorr while the input power was maintained at 1,000 watts. The concentration of NF_3 in argon was maintained at 25% by volume.

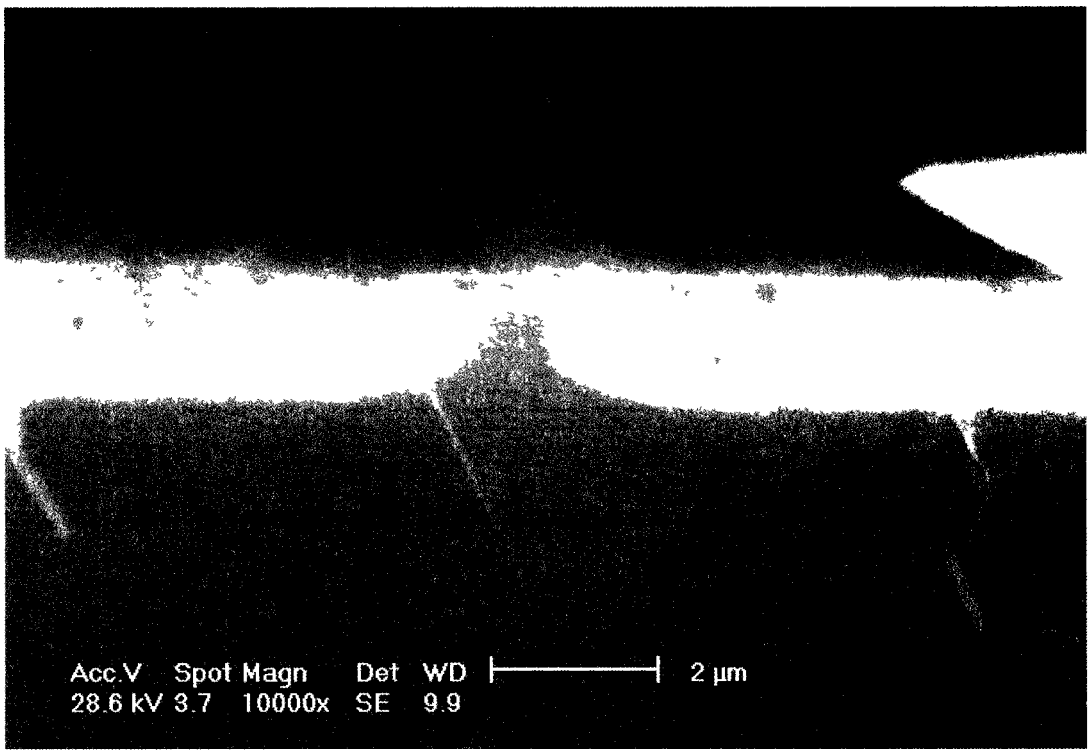

Figure 4.4.7. SEM of etched silicon at 10,000 X using 25% NF_3 in argon, 1,000 watts, 800 millitorr.

For the high power density (1,000 watt) low pressure (400 millitorr) conditions, the etch bias was measured at 0.75. The high power density, high-pressure condition (800 millitorr) provided an etched feature 43% under-cut. The micrograph is also free from any channels or notches running parallel to the etched feature.

Increasing the pressure to 800 millitorr increases the mask under-cut. The higher pressure results in a reduced mean free path and a corresponding increase in collision frequency. The higher frequency of collisions with the feature sidewall results in an increase in lateral etching. At higher pressure, ions that are accelerated through the sheath are less likely to traverse without collisions. Further, higher pressures also result in higher concentrations of fluorine atoms.

A plasma using a higher concentration of nitrogen trifluoride in argon was also tested. Figure 4.4.8 is a micrograph of etched silicon using 75% nitrogen trifluoride by volume in argon. The power and pressure were maintained at 250 watts and 400 millitorr, respectively. Under these conditions, the percent under-cut was calculated to be 15%.

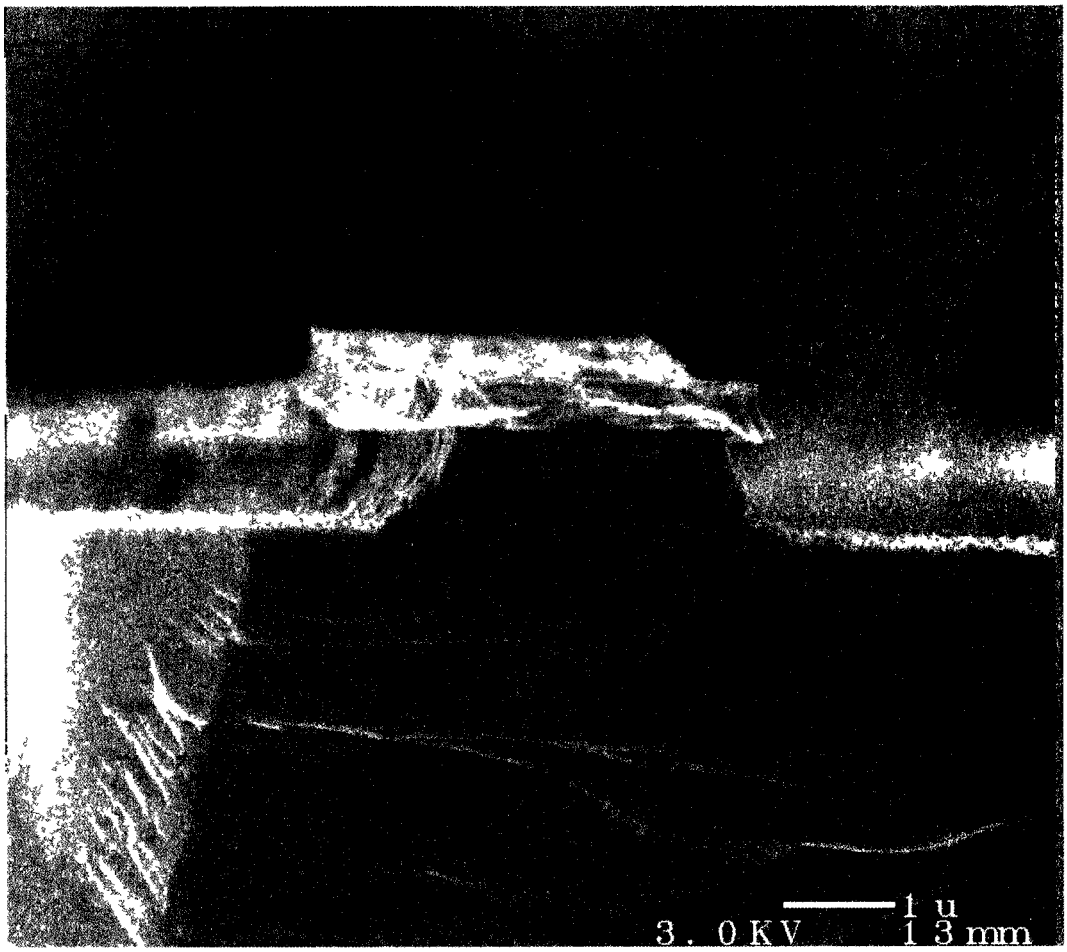

Figure 4.4.8. SEM of etched silicon at 10,000 X using 75% NF_3 in argon, 250 watts, 400 millitorr.

The following table summarizes the anisotropy results using nitrogen trifluoride and argon mixtures.

Table 4.4.1. Summary of Anisotropy Data for NF_3 - Argon

% NF_3 in Ar	Power (watts)	Pressure (millitorr)	Under-cut (%)
25	250	400	74
25	1000	400	41
25	1000	800	43
75	250	400	15

In a plasma, purely chemical etching would occur in all directions at a equal rate. The plasma acts as a source of reactive species and little or no radiation enhanced etching occurs. In the case of completely isotropic etching with a non-erodible aluminum mask, the etch profile is shaped in a semicircular pattern. Isotropic etching is most likely to occur under conditions of high pressure and low power.

Damage induced, anisotropic etching typically occurs at low pressure. Anisotropic profiles are promoted by positive ion bombardment (11). Ion enhanced etching provides a high yield of substrate atoms per incident ion. Ions accelerated towards the substrate in the plane normal to the surface increase the reaction rate. The ions can damage the silicon lattice, increase the surface area, add energy to the surface through thermalization and increase the reaction rate. Anisotropic profiles are more likely to occur at low pressure and high power.

4.5 Anisotropy Using NF_3-CF_2Cl_2-Argon Plasmas

Admixtures of nitrogen trifluoride with dichlorodifluoromethane and argon were studied to determine the effects of plasma parameters and composition on etching anisotropy. The initial experiments using 62% CF_2Cl_2, 25% NF_3 in argon resulted in isotropic profiles in the single crystal silicon. Figure 4.5.1 is an 8,000 X micrograph of silicon etched at 250 watts and 400 millitorr for fifteen minutes. The etch bias was measured and the under-cut calculated to be 61%.

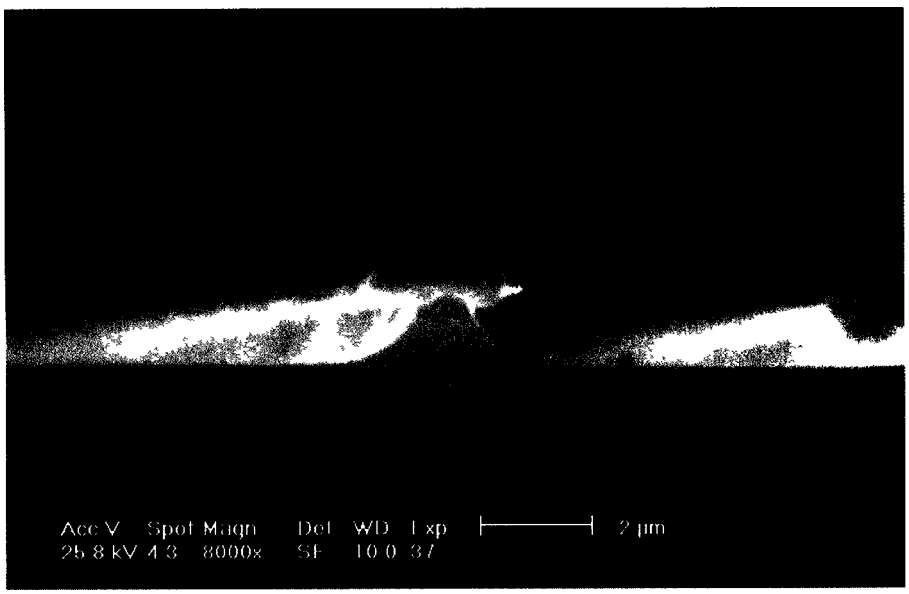

Figure 4.5.1. SEM of silicon at 8,000 X using 62% CF_2Cl_2, 25% NF_3 in argon, 250 watts, 400 millitorr.

In the experiments using admixtures of NF_3, CF_2Cl_2 and Ar, the dichlorodifluormethane acts as a polymer forming gas. The mechanism by which anisotropy is obtained involves sidewall passivation. Because the undercut shown in Figure 4.5.1 is substantial, the degree of polymer formation and ion enhanced etching are minimal. The low applied power of 250 watts generates a low plasma potential and a low degree of ion bombardment. The post-etch SEM has a relatively smooth silicon surface with a minimal amount of damage.

Polymer formation is strongly linked to the concentration of CF_2 radicals (63, 65). At low power density, the amount of difluorocarbene radical formation is minimized. For these experimental conditions, the silicon etch rate is high at 410 nm/min. This is further evidence there is no polymer layer inhibiting the reaction with silicon.

Figures 4.5.2 and 4.5.3 are scanning electron micrographs of etched single crystal silicon shown at 4,000 and 8,000 X

respectively. The etching was done using an admixture of 62% CF_2Cl_2, 25% NF_3 in argon at 1,000 watts power and 800 millitorr operating pressure. The under-cut was calculated to be 29%.

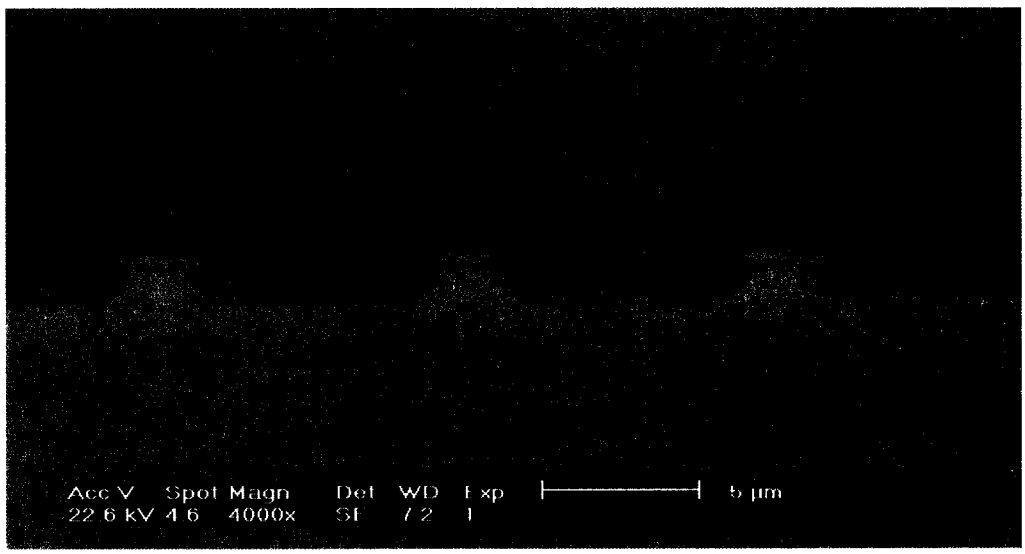

Figure 4.5.2. SEM of etched silicon at 4,000 X using 62% CF_2Cl_2, 25% NF_3 in argon, 1,000 watts, 800 millitorr.

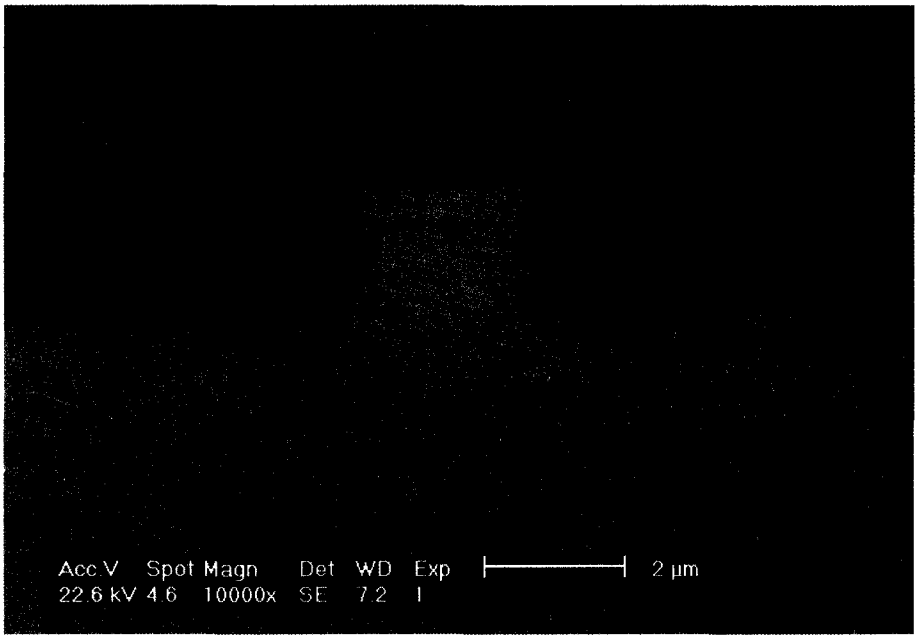

Figure 4.5.3. SEM of etched silicon at 10,000 X using 62% CF_2Cl_2, 25% NF_3 in argon, 1,000 watts, 800 millitorr.

As the power and pressure are increased to 1,000 watts and 800 millitorr respectively, the etch profile becomes more anisotropic (less rounded). The increase in power provides a higher degree of ion enhanced etching. Further, higher power input promotes a higher degree of dissociation in the plasma. Higher concentrations of polymer forming species and higher pressures tend towards a higher rate of polymer deposition on the surface. Under these plasma conditions, the etch rate of silicon is 370 nm/min. This is a decrease from the rate of 410 nm/min observed using 250 watts and 400 millitorr. The reduced silicon etch rate can be explained by the formation a polymeric inhibiting layer on the surface of the silicon.

Figures 4.5.4 and 4.5.5 are scanning electron micrographs of etch silicon at 4,000 and 8,000 X respectively. For this experiment, the plasma composition was maintained at 62% CF_2Cl_2, 25% NF_3 in argon. The power input was 1,000 watts and the pressure was held at 400 millitorr. Under these conditions, etch under-cut was not measurable.

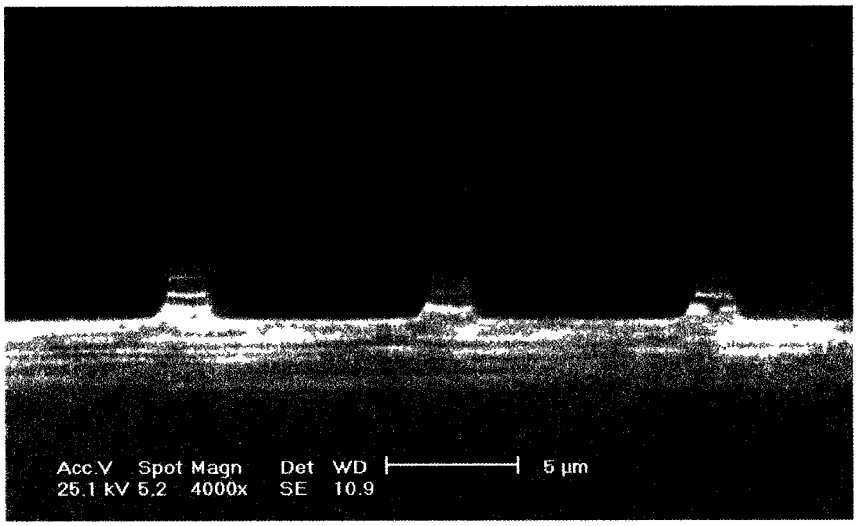

Figure 4.5.4. SEM of etched silicon at 4,000 X using 62% CF_2Cl_2, 25% NF_3 in argon, 1,000 watts, 400 millitorr.

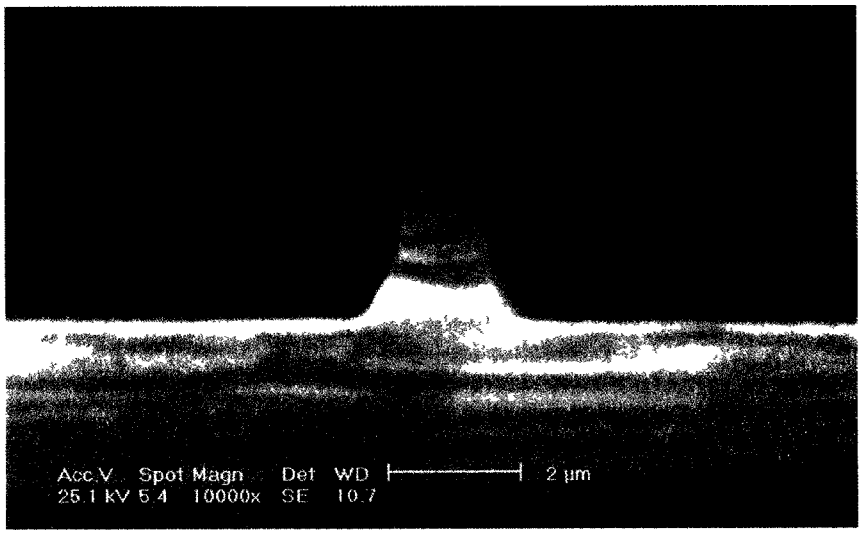

Figure 4.5.5. SEM of etched silicon at 10,000 X using 62% CF_2Cl_2, 25% NF_3 in argon, 1,000 watts, 400 millitorr.

As the pressure is reduced to 400 millitorr, the undercut is minimized and the etch bias approaches unity. At 62% CF_2CL_2 and 1000 watts, a reduction in pressure increases the degree of ion assisted vertical etching. At low pressure, there is little etching of the sidewall protective layer. Etching proceeds in the vertical direction as polymeric material is removed from surface with the assistance of ion bombardment.

Figures 4.5.6 and 4.5.7 are scanning electron micrographs of etch silicon using 31% CF_2Cl_2, 25% NF_3 in argon. The etching was done using 1,000 watts power input and 400 millitorr operating pressure. Under these conditions, the under-cut was not measurable.

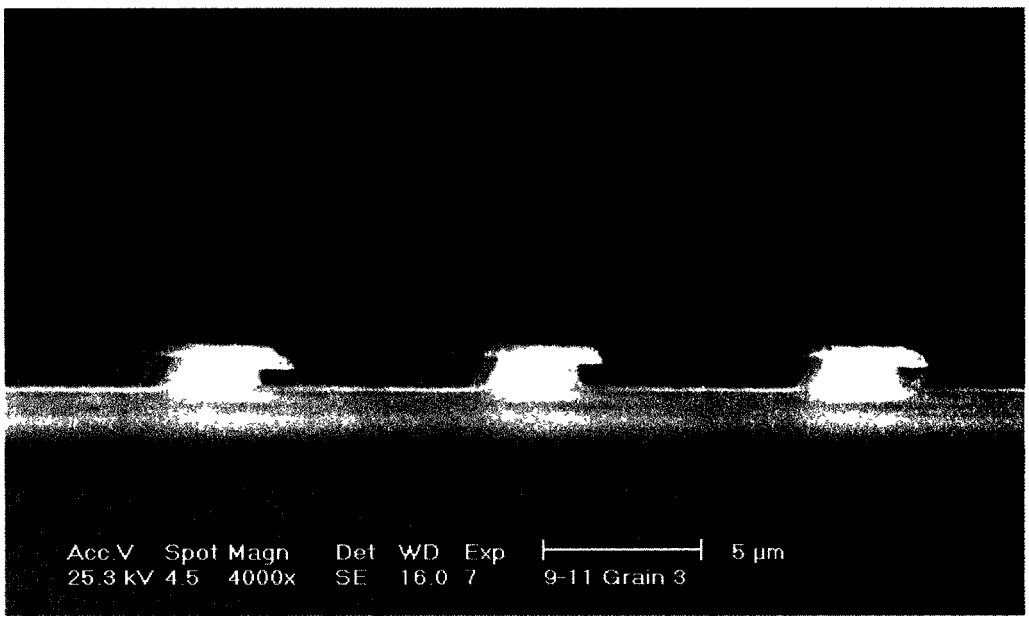

Figure 4.5.6. SEM of etched silicon at 4,000 X using 31% CF_2Cl_2, 25% NF_3 in argon, 1,000 watts, 400 millitorr.

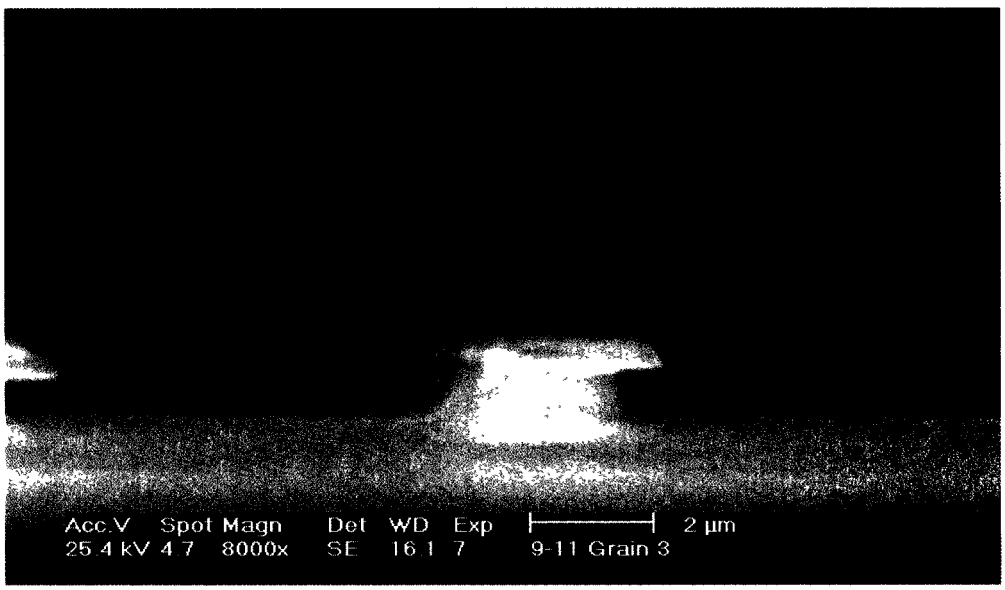

Figure 4.5.7. SEM of etched silicon at 8,000 X using 31% CF_2Cl_2, 25% NF_3 in argon, 1,000 watts, 400 millitorr.

For a plasma using 31% CF_2Cl_2, under-cut of the mask was minimized, however the profile is sloped or directional. The lower concentration of polymer forming gas will decrease the concentration of difluorocarbene in the plasma. The rate of polymer deposition will likely be lower and less of a protective layer will develop on the silicon surfaces.

XPS was performed on a sample of silicon masked by aluminum. The silicon sample was exposed to a plasma of 62% dichlorodifluoromethane, 25% nitrogen trifluoride in argon at 400 millitorr and 1000 watts. The sample was etched until the total vertical etch depth was two microns. The etch time was ten minutes.

The sample was then cross-sectioned, mounted and analyzed using scanning electron microscopy. A 10,000 X micrograph of the etched silicon sample is shown in Figure 4.5.8. On inspection of the micrograph, a thin film of material can be seen on the surface of the aluminum and the feature sidewall.

The sample was then analyzed using XPS. The sample was mounted horizontally on a stage and the XPS system was set-up to measure at a 20° take-off angle. The take-off angle minimized the analysis of the base of the etched feature. The angle was determined using an etch depth of two microns and a space width between features of five microns. A survey scan from 0 to 1100 electron-volt (eV) was taken initially. The survey spectrum is shown in Figure 4.5.9. Subsequently, a high resolution carbon 1s scan was taken from 280 to 296 eV. The carbon 1s spectrum is shown in Figure 4.5.10. A high resolution spectrum of the fluorine 1s region is shown in Figure 4.5.11.

The survey spectrum has peaks for silicon (99, 151 eV), aluminum (73, 118 eV), oxygen (23, 531, 978, 999, 1013 eV), fluorine (30, 685, 832, 858, 877 eV), chlorine (199, 201, 271 eV) and carbon (285 eV).

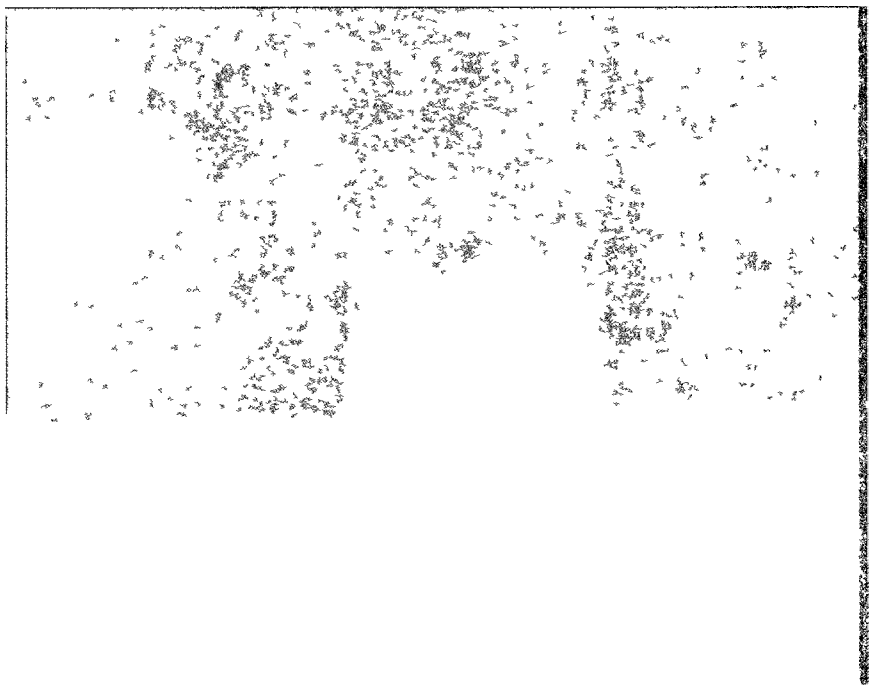

Figure 4.5.8. Cross-sectional SEM of Etched Feature Showing Polymer Film

The high resolution spectrum of the carbon 1s region was resolved into four peaks having a guassian distribution using deconvolution software provided by Scienta, Inc. Hydrocarbon surface contamination on silicon has a small peak at 284.7 eV. Adventitious hydrocarbon on the aluminum surface is the large peak at 286.3 eV. There are two small peaks at 288 and 291.3 eV. The peak at 288 eV is likely material having C-H-O bonding positioned on the aluminum surface. The peak at the highest

binding energy of 291.3 ev is possibly due to carbon-fluorine bonding.

The large peak, centered at 286.3 eV, is hydrocarbon contamination on the surface of aluminum. At a 20° take-off angle, a large percentage of the surface being analyzed is aluminum. The peak shift to the binding energy of 291.3 eV indicates the carbon is bonded to a halogen (100). The CF_2 bonding environment has a binding energy in the region of 291 eV. The results of the XPS analysis are not conclusive. The distinction between carbon polymer deposited on the silicon side-wall versus the horizontal aluminum surface is not clear. The presence of silicon in the survey spectrum is evidence that silicon may be mixed in with the polymeric over-layer or the analysis is taken at a location where the polymeric film is not continuous. Aluminum in the survey spectrum is further evidence of a discontinuous film since the aluminum does not participate in an etching reaction.

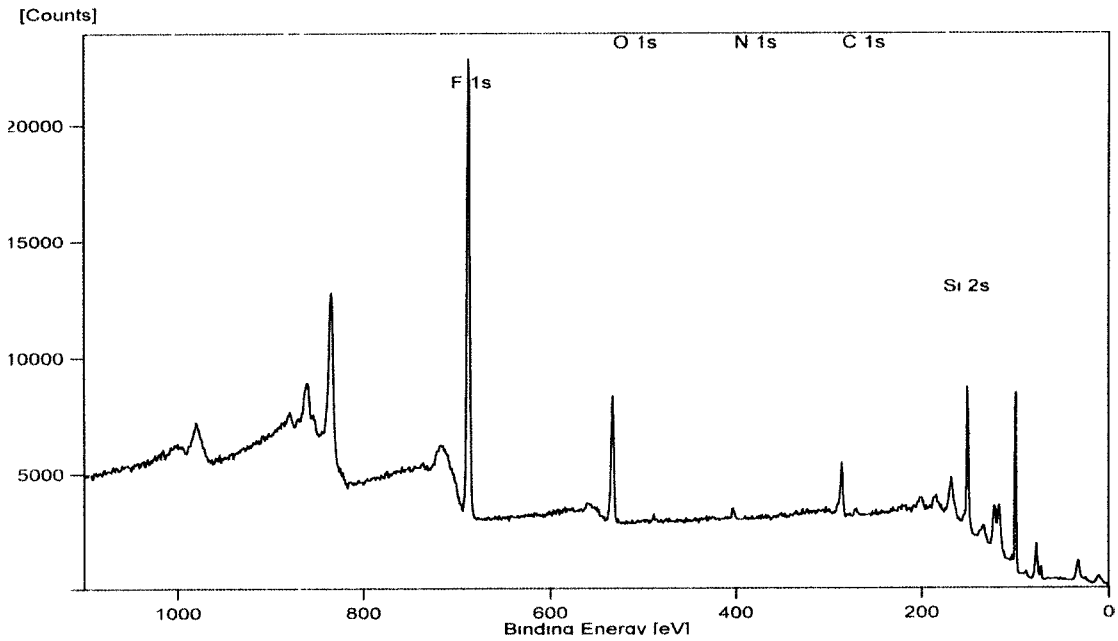

Figure 4.5.9. XPS Survey Spectrum of Etched Silicon

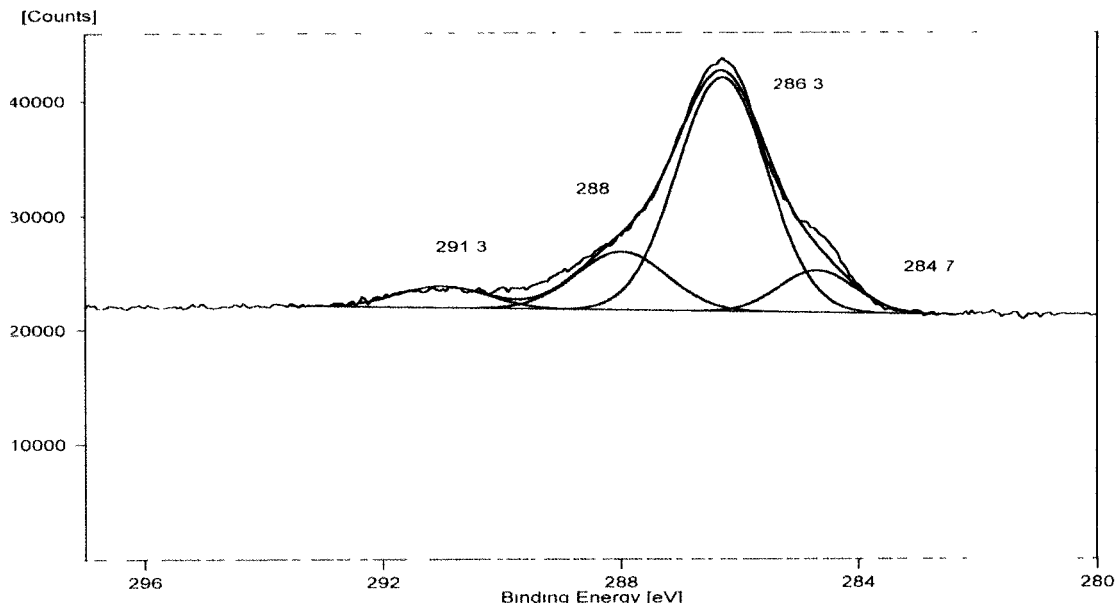

Figure 4.5.10. XPS High Resolution Carbon 1s Spectrum

Figure 4.5.11 is a high resolution XPS spectrum of the F1s region. The small peak at 687 eV is assigned to an Al-F-O bonding environment. The large peak at 688.6 eV is Al-F bonding. The large peak is expected because the analysis was performed at a 20° take-off angle. The peak at 690.5 eV is likely a result C-F-H bonding. The peak positioned at 692 eV is consistent with a CF_2 bonding environment (98). Again, due to the nature of the material analyzed, it not clear whether the carbon is on the silicon or the aluminum.

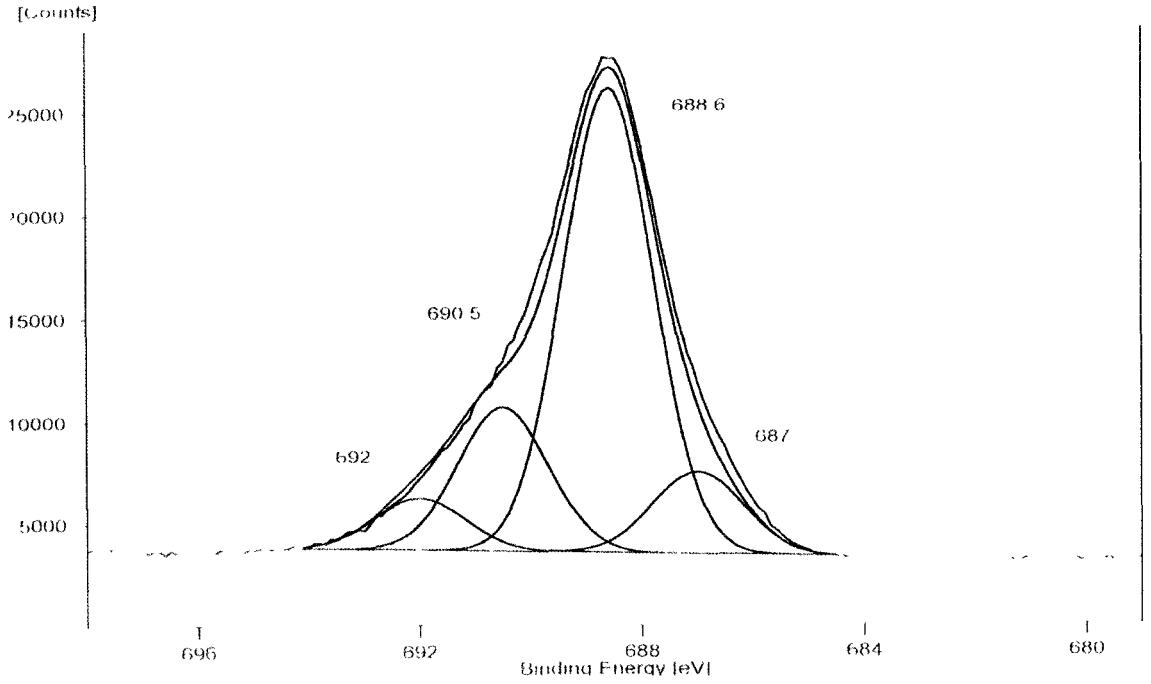

Figure 4.5.11. XPS High Resolution Fluorine 1s Spectrum

5. Conclusions

Silicon to silicon dioxide reaction selectivity was determined for mixtures of nitrogen trifluoride in argon. The sensitivity of the silicon dioxide etch rate to ion bombardment is directly linked to lowering the reaction selectivity. Selectivity was found to be highest under processing conditions that minimize cationic bombardment of the surfaces. Selectivity approaching 90:1 was obtained for a plasma of 25% nitrogen trifluoride in argon at 250 watts power and 800 millitorr. The reaction rate of silicon dioxide was found to be most sensitive to increases in input power. At increased power levels, cation density and bombardment energy are high.

Reaction selectivity was also found to be a function of concentration and pressure. Selectivity was highest for conditions of high pressure and low concentration. The silicon dioxide etch rate was determined to be sensitive to increases in nitrogen trifluoride concentration. At high concentrations of NF_3, the etch rate of silicon dioxide increased, decreasing reaction selectivity. The reaction of

difluoroamine with silicon dioxide is suggested as an alternative reaction pathway to higher etch rates.

In the operating window investigated, plasmas could not be generated using concentrations of NF_3 greater than 80% in diluent argon. The electronegativity of halide species results in rapid electron attachment reactions. Since electron loss reactions dominate under these conditions, generating a stable plasma through electron impact reactions is difficult. The rates of recombination reactions exceed those of electron generation reactions.

Trends in anisotropy were established using mixtures of nitrogen trifluoride in argon. Over the range of power and pressure investigated, completely anisotropic etch profiles in silicon could not be obtained. The silicon used for the anisotropy experiments had a (111) crystallographic orientation. Etching the silicon in the vertical direction etches the (111) crystal plane. For plasma conditions having minimal radiation enhancement, etching occurred

in the vertical and horizontal directions (100, 010, 001,.... planes) at equal rates. The observation leads to the conclusion that fluorine atoms, under conditions of minimal ion bombardment, etch without preference to crystallographic orientations. For a mixture of 25% nitrogen trifluoride in argon, etch anisotropy was improved for conditions of high ion bombardment. High power and low pressure conditions provided the highest degree of etch anisotropy. For 75% nitrogen trifluoride in argon, etch anisotropy was highest for conditions of low power and low pressure.

Mixtures of nitrogen trifluoride, dichlorodifluoromethane and argon were investigated. Both reaction selectivity and anisotropy were studied under conditions of varying power, pressure and gas composition. In general, silicon to silicon dioxide reaction selectivity was lower for gas mixtures containing dichlorodifluoromethane. The highest selectivity of 50:1 was obtained for conditions of low power and high pressure. Under these conditions, ion bombardment is minimal. It is also suspected that polymer formation is minimal under these conditions.

For mixtures using dichlorodifluoromethane, the reaction selectivity decreases are a result of two factors. As with the nitrogen trifluoride and argon mixtures, increases in ion bombardment increase the reaction rate of silicon dioxide, thereby decreasing reaction selectivity. The difluorocarbene also plays a role in etching silicon dioxide. As the concentration of difluorocarbene increases, the reaction rate of silicon dioxide increases and the reaction selectivity decreases.

For mixtures of nitrogen trifluoride, dichlorodifluoromethane and argon, the anisotropy improved as the degree of ion bombardment increased. Low power density plasmas generated undercut of the mask and isotropic etching. Anisotropic profiles in etched silicon were obtained using 62% CF_2Cl_2, 25% NF_3 in argon at high power and low pressure. Etching with a mixture of 31% CF_2Cl_2, 25% NF_3 in argon resulted in a sloped profile in etched silicon without mask under-cut.

An acceptable patterning process is feasible using an admixture of nitrogen trifluoride and dichlorodifluoromethane. For gas mixtures using NF_3 in argon, high reaction selectivity is obtained, but mask under-cut occurs. The use of a polymer forming chemistry with NF_3 provides a method of improving etch anisotropy while keeping the reaction selectivity at acceptable levels of approximately 20:1.

6. Suggestions for Future Research

The work presented in this dissertation represents a culmination of nearly twenty years of experience in the field of semiconductor processing. Over the past two decades, the science associated with microchip manufacturing has undergone incredible transformations. Progress has been made in statistical methods for process control, analytical chemistry for process diagnosis, thin film metrology, deposition and etching chemistry, reliability analysis and environmentally benign manufacturing processes. With all that has been accomplished, many areas remain to be explored and many basic issues need to be resolved.

The use of plasma chemistry for pattern transfer has a strong position in the industry. Further work must be performed to define the impact of the plasma state interaction with the electronic materials on film properties and reliability. The impact of metallic contamination resulting from the use of corrosive materials must be defined. As microdevice thin films continue to shrink, carrier

lifetime depletion will become increasingly important. The sources and solutions for metallic contamination are ill-defined.

Contamination, in general, has been a pre-occupation of many of the process chemists in the industry, yet establishing the limits of influence for individual contaminants has been elusive. Particulates continue to remain a focal point for contamination reduction. The dynamics of particle transport are becoming clearer. However, the chemistry associated with the formation of particulates in the plasma state must be better understood.

Beacause control of anisotropy is of paramount importance in pattern transfer, this issue will remain critical for many generations of devices. A more thorough understanding of wall profile variability must be developed and correlated with variability in dopant concentration and micro-loading effects. As the area of material being patterned varies, the reproducibility and uniformity of a process across the surface must meet tighter tolerances. A more developed understanding of the passivation mechanism must be

established. Additional research in anisotropy should use plasma diagnostics and XPS to study the surface chemistry.

Plasma polymerization chemistry should be studied further. The mechanics of both side-wall passivation and particle formation in the plasma are plasma polymerization phenomena. As a result, investigations using difluorocarbene and dichlorocarbene could be beneficial in better understanding their role in thin film pattern transfer.

The area of chemometrics has many opportunities. Beacause the coupling of statistical analysis with chemistry is a relatively new field, semiconductor manufacturers can benefit from expanding the scope of applications in this field. Additional work must be pursued using chemometrics for optimization. The Simplex methodology, and optimization theory in general, have seen little use in this area and will be required if yields are to be maintained as the wafer diameter is scaled larger.

Another area where additional work must be done is in modelling. The use of models for inferential analysis becomes critical as semiconductor device dimensions shrink. The inherent expense associated with trial-and-error processing and the pace at which the industry changes forces this issue. The coupling of modelling, analytical chemistry and chemometrics will be at the helm of future developmental endeavors.

The industry must look for alternative etchant gases that have a minimal impact on our environment. Research has been initiated in this area at the Massachusetts Institute of Technology. The goal of this initiative is to develop new process chemistries that use gases that are not as long-lived in the atmosphere. Over the next twenty years, pattern transfer for manufacturing integrated circuits must steadily progress to more environmentally benign process technologies.

References

1. Sematech Annual Report, 2000.

2. Sematech Semiconductor Industry Technology Roadmap,1997.

3. Gordon Moore, One Component, 64, 1965.

4. Intel Developer Forum, Santa Clara, CA, September 1997.

5. Bowles, S., Edwards, R., Understanding Capitalism, Second Edition, Harper Collins College Publisher, 1993.

6. Meieran, Eugene, " 21st Century Manufacturing Capabilities," Intel Technology Journal, 4, 1998.

7. TMSC Corporation press release dated December, 2000.

8. Mautz, K.E., Semiconductor International, 7, 112(2000).

9. Coclaser. R.A., Microelectronics Processing and Device Design J. Wiley and Sons, Inc., 1980.

10. Sze, S.M., VLSI Technology, McGraw-Hill Company, New York, NY, 1983.

11. Einspruch, N.G., Brown, D. M., VLSI Electronics, Plasma Processing for VLSI, Academic Press, New York, NY, 1984.

12. Semicon West Conference Proceedings, May 2003.

13. Sze, S.M., ibid, page 307.

14. Semicon West Conference, 2003.

15. Sze, S.M., ibid, page 328.

16. Mogab C.J., " The Loading Effect in Plasma Etching," J. Electrochem. Soc., 124,1262(1977).

17. Einspruch, N.G., Brown, D.M., ibid, page 447.

18. Whyte, W., Clean Room Design, Second Edition, J. Wiley and Sons, Inc., 1999.

19. Personal communication, Eugene Karwacki, Manager of Research in Electronic Gases.

20. Durham, J.A., Steinbruchel, Ch., "Particles Generated in a Plasma Reactor: Source Material, Plasma Chemistry and Process Effects," Plasma Processing, Volume 90-14, page 207, The Electrochemical Society, Pennington, N.J., 1990.

21. Petrucci, J.L., Steinbruchel, Ch., "Particles Generated in a Plasma Reactor: Excitation Frequency and Etch Rate Effects," Plasma Processing, Volume 90-14, page 219, The Electrochemical Society, Pennington, N.J., 1990.

22. Heyns, M., Hasenack, C., DeKeersmaecker,R., Falster, R., "The impact of Si-surface characteristics on MOS device yield," Semiconductor Cleaning Technology, Volume 90-9, page 293, The Electrochemical Society, Pennington, N.J., 1990.

23. Meuris, M., Heyns, M., Mertens, P., Verhaverbeke, S., Philipossian, A., "The Combined Effect of Silicon Surface Roughness and Metal Impurity Contamination on Gate Oxide Integrity," Cleaning Technology in Semiconductor Device Manufacturing, Volume 92-12, page 144, The Electrochemical Society, Pennington, N.J., 1992.

24. Atsumi, J., Ohtsuka, S., Munehira, S., Kajiyama, K., Semiconductor Cleaning Technology, Volume 90-9, page 59, The Electrochemical Society, Pennington, N.J., 1990.

25. Meier, P.C., Zund, R.E., Statistical Methods in Analytical Chemistry, J. Wiley and Sons, Inc., 1993.

26. Sze, S.M., ibid, page 324.

27. Hansen, J.I., Fung, A., Lacis, D., Rind, S., Lebedeff, R., Ruedy, G., Russel and Stone, P., J. Geophys. Res., 93, 9341(1988).

28. Hansen, J.I., www.giss.nasa.gov/research/observe/surftemp/2001fig1.gif.

29. NASA Goddard Institute forSpaceScienceURL:www.giss.nasa.gov.

30. Hansen,J., Makiko, S., Ruedy, R., Lacis, A., Oinas, V., " Global Warming in the Twenty-first Century: An Alternative Scenario," PNAS Early Edition, June 16, 2000.

31. Environmental Science and Technology, 11/01/99, Volume 33, Issue 21, page 447A, 1/9P.

32. "Greenhouse Gases and Global Warming Potentials," excerpt from the *Inventory of U.S. Greenhouse Emissions and Sinks: 1990-2000,* Office of Atmospheric Programs, U.S. Environmental Protection Agency, April, 2002.

33. "The U.S. Greenhouse Gas Inventory," Office of Air and Radiation, U.S. Environmental Protection Agency, EPA 430-F-02 -008, April, 2002.

34. Kern, W., Puotinen, D.A., "Cleaning Solutions Based on Hydrogen Peroxide for Use in Silicon Semiconductor Technology," RCA Rev.,31, 187(1970).

35. Sugimoto F., Okamura S., "Adsorption Behavior of Organic Contaminants on a Silicon Wafer Surface," J. Electrochem. Soc., 146(7) 2725-2729 (1999).

36. Coclaser, R.A., ibid, page 22.

37. Rudolf Research, Inc., Ellipsometer Product Literature.

38. Irving, S.M., "A Plasma Oxidation Process for Removing Photoresist Films," Solid State Technology, 14(6), 47(1971).

39. Chapman, B., Glow Discharge Processes, J. Wiley and Sons, Inc., New York, N.Y., page 38, 1982.

40. Coburn, J., American Vacuum Society, Educational Committee.

41. Barkanic, J.A., Reynolds, D.M., Jaccodine, R.J., Stenger, H.G., Vedage, H., "Plasma Etching Using NF_3: A Review," Solid State Technology, 32(4), 109 (1989).

42. Hickman, W.M., Fox, R.E., J. Chem. Phys., 25, 642(1956).

43. Chapman, B., "Glow Discharge Processes," J. Wiley and Sons, Inc., New York, NY, page 49, 1980.

44. T.J. Chuang, J. Appl. Phys., 51(5), 2614(1980).

45. Flamm D.L., Donnelly V.M., Mucha J.A., J. Appl. Phys., 52(5), 3633(1981).

46. Gerlach-Meyer U., Coburn J.W., Kay E., Surface Science, 103, 177(1981).

47. Coburn J.W., Winters H.F., J. Appl. Phys., 50(5), 3189(1979).

48. Srivastava, R.D., Heterogeneous Catalytic Science, CRC Press, 1988.

49. Donnelly, V.M., Flamm, D.L., J Appl. Phys., 55(1), 244(1984).

50. Flamm, D.L., Donnelly, V.M., Mucha, J.A., J. Appl. Phys., 52(5), 3633(1981).

51. Flamm D.L., Mogab C.J., Sklaver E.R., J. Appl. Phys., 50, 6211(1979).

52. Einspruch, N. G., ibid, page 69.

53. Flamm D.L., Mogab C.J., Sklaver E.R., J. Appl. Phys., 50, 6211(1979).

54. Langan J.G., Shorter J.A., Xin X., Joyce S.A., Steinfeld J.I., Surface Science, 207, 344(1989).

55. McFeely F.R., Yarmoff J.A., Taleb-Ibrahimi A., Beach D.B., Surface Science, 206, 371(1988).

56. Joyce S., Langen J.G., Steinfeld J.I., J. Chem. Phys., 88,2027 (1988).

57. Ho P., Johannes J.E., Buss R. J., Meeks E., J. Vac. Sci. Technol. A: Vacuum, Surfaces and Films, 19(5), 2344(2001).

58. Coburn, J.W., "Plasma and Reactive Ion Etching," American Vacuum Society Educational Committee.

59. Sze, S.M., ibid, page 320.

60. Zarowin C.B., J. Vac. Sci. Technol., A, 2(4), 1537(1985).

61. Zarowin C. B., J. Appl. Phys., 57(3), 929(1985).

62. Bruce, R.H., Solid State Technology, "Anisotropy Control in Dry Etching," 10, 64(1981).

63. Flamm D.L., Plasma Chemistry and Plasma Processing, 1,11, 37(1981).

64. Sellamuthu, R., Barkanic, J., Jaccodine, R., J. Vac. Sci and Technol., B5(1), 342(1987).

65. Millard M., Kay E., J. Vac. Sci. Technol., 18(2), March (1981).

66. Plumb, I.C., Ryan, K.R., "Plasma Chemistry and Plasma Processing," 6(1), 11(1986).

67. Cunge, G., Inglebert, R. L., Joubert, O., Vallier, L., Sadeghi, N., J. Vac Sci. and Technol., B 20(5), 2137(2002).

68. Coburn J.W., Winters H.F., J. Vac. Sci. Technol., 16(2),391(1979).

69. Stoffels E., Stoffels W.W., Vender D., Kroesen G.M.W., deHoog F.J., J. Vac. Sci. Technol., A 13(4), 2051(1995).

70. Stoffels W.W., Stoffels E., Havelag M., Kroesen G.M.W., deHoog F.J., J. Vac. Sci. and Technol., A 13(4), July/Aug, 1995, 2058.

71. Eisele, K.M., "Plasma Etching of Silicon with Nitrogen Trifluoride," Proceedings from Symposia on Plasma Etching, J. Electrochem. Soc., 174, (1981).

72. Barkanic J.A., Hoff A., Stach J., Golja B., "Dry Etching using NF_3/Ar and NF_3/He Plasmas," in Silicon Processing, ASTM STP 850, Philadelphia, PA , 1984.

73. Korman C.S., Chow T.P., Bower D.H., " Etching Characteristics of Polysilicon, SiO_2 and $MoSi_2$ in NF_3 and SF_6 Plasmas," Solid State Technology, vol. 26(1), page 115, (1983).

74. Bower D.H., "Planar Plasma Etching of Polysilicon using CCl_4 and NF_3," J. Electrochem. Soc., vol. 129(4), page 795, (1982).

75. Barkanic J.A., Reynolds D.M., Jaccodine R.J., Stenger H.G., Parks J., Vedage H., "Plasma Etching Using NF_3: A Review," Solid State Technology, vol. 4, page 109, (1989).

76. Donnelly V.M., Flamm D., "Anisotropic Etching of SiO_2 in Low Frequency CF_4-O_2 and NF_3-Ar Plasmas," J. Appl. Phys., vol. 55(1), page 242 (1984).

77. Greenberg K.E., Verdeyen J.T., "Kinetic Processes of NF_3 Etchant Gas Discharges," J. Appl. Phys., vol. 57(5), page 1596 (1985).

78. Dielman J., Sanders F.H.M., "Method of Manufacturing a Semiconductor Device by Means of Plasma Etching," European Patent Application No. 0109706, May 30, 1984.

79. Saia R.J., Gorowitz B., "Dry Etching of Tapered Contact Holes in Multilayer Resist," J. Electrochem. Soc., 132(8), 1954(1985).

80. Thornquist S.C., "Selective Plasma Etching of Silicon Nitride in The Presence of Silicon Oxide," U.S. Patent No. 4,568,410, February, 4, 1986.

81. Barkanic, J.A., Reynolds, D.M., Jaccodine, R.J., Stenger, H.G., Vedage, H., "Plasma Etching Using NF3: A Review," Solid State Technology, 32(4), 109 (1989).

82. Sellamuthu R., Barkanic J.A., Jaccodine R., ibid. page 345.

83. Lin, J., "Method for forming a tapered opening in silicon," U.S. Patent 5,651,858, issued July 29, 1997.

84. Tsujimoto, K., Okudaira, S., Tachi, S., "Low temperature microwave plasma etching of crystalline silicon," Japanese Journal of Applied Physics, Part 1, 30(12A), 3319-3326 (1991)

85. Squire, D.W., Dagata, J.A., Hsu, D.S.Y., Dulcey, C.S., Lin, M.C., "Thermal reaction of fluorine and nitrogen trifluoride with silicon (110) studied by laser ionization mass spectrometry," J. Phys. Chem.,92(10), 2827-2834 (1988).

86. Little, T.W., Ohuchi, F.S., " Chemical interaction of NF_3 ion beams and plasmas with Si (Part I): x-ray photoelectron

spectroscopy studies," Surface Science, 445(2-3), 235-242 (2000).

87. Baslish, K., Nowak, T., Tanaka, T., Beals, M., "Method and apparatus fore cleaning parts of a deposition system or etching wafers," European Patent Application 1,148,533, November 24, 2001.

88. Hsueh, H., McGrath, R.T., Ji, B., Langan, J.G., Karwacki, E.J., "Ion energy distributions and optical emission spectra in NF_3 based process chamber cleaning plasmas," J. Vac. Sci. Technol. B, 19 (4), 1346-1357 (2001).

89. Langan, J.G., Beck, S.E., Felker, B.S., Rynders, S.W., "The role of diluents in electronegative fluorinated gas discharges," J. Appl. Phys., 79(8-1), 3886-3894 (1996).

90. Langan, J.G., Rydners, S.W., Felker, B.S., Beck, S.E., "Electrical Impedance analysis and etch rate maximization in NF_3/Ar discharges," J. Vac. Sci. and Technol. A, 16(4), 2108-2114 (1998).

91. Thompkins, H., A User's Guide to Ellipsometry, Academic Press, 1992.

92. Reidling, K., Ellipsometry for Industrial Applications, Springer-Verlag, 1988.

93. Drude, P., Ann. Phys. Chem., 36,532,865 (1889).

94. Collett E., Polarized Light Fundamnetals and Applications, Marcel Dekker, Inc., 1993, page 528.

95. Mayasumi M., Imai M., Takahashi J., Kawada K., Ohmi T., " A

Study of Surface Treatment of Silicon Wafer using Small Angle Incident X-ray Photoelectron Spectroscopy," J. Electrochem. Soc., 146(6) 2235-2238 (1999).

96. Briggs, D., Seah, M.P., Practical Surface Analysis; Auger and XPS, J. Wiley and Sons, New York, NY, 1990.

97. Powell, C.J., Seah, M.P., J. Vac. Sci. Technol., A8, 735(1990).

98. Smith, G.C., Surface Analysis by Electron Spectroscopy," Plenum Press, New York, NY, 1994.

99. Gosh, P.K., Introduction to Photoelectron Spectroscopy, Chemical Analysis Series, Volume 67, J. Wiley and Sons, New York, NY, 1983.

100. Toshiharu, Y., Pavlath, A. E., Journal of Applied Polymer Science, Applied Polymer Symposium 38, *Plasma Polymerization and Plasma Treatment,* H.K. Yasuda, editor, John Wiley and Sons, 215-223,1984.

101. Bluman A., Elementary Statistics, McGraw-Hill Company, 2003.

102. Atkinson, A.C., Donev, A.N., Optimum Experimental Designs, Oxford University Press, Oxford, 1992.

103. Kenkel, J., Analytical Chemistry for Technicians, Third Edition, Lewis Publishers, 2003.

104. Meier, P.C., Zund, R.E., ibid.

105. Myers, R.H., Montgomery, D.C., Response Surface Methodology, Second Edition, J. Wiley and Sons, Inc., 2002.

106. Devore, J., Peck, R., Introductory Statistics, Second Edition, West Publishing Company, New York, NY, 1994

VITA

John Anthony Barkanic was born on February 24, 1956 in Hazleton, Pennsylvania. After the completion of twelve years of Catholic schooling, he attended The Pennsylvania State University, Hazleton Campus and studied Chemical Engineering. He completed his Bachelor of Science degree in Chemical Engineering from Penn State University in 1979.

Subsequently, he had the opportunity to work for Air Products and Chemicals in the Industrial Gas Division for approximately seven years. In that time, he pursued a graduate degree in Chemical Engineering and focused on research and development for the semiconductor industry. In 1985, he was awarded a Master of Science degree in Chemical Engineering from The Pennsylvania State University for his work in the area of thin film processing.

Over the past sixteen years, he has run a small engineering and consulting company. As an independent, he has been involved in hundreds of projects dealing with manufacturing, environmental

science and the chemistry of material processing. He currently works with small to medium sized Pennsylvania based manufacturing companies to promote the use of environmentally benign process chemistry. He has published more than fifty technical papers and presentations in the area of thin film processing for the semiconductor industry. The majority of the work is plasma chemistry for pattern transfer and thin film deposition. He holds several patents for his work in this area.